

Rehabilitation of Prestressed Concrete Bridge Components by Non-Electrical (Conventional) Methods

PUBLICATION NO. FHWA-RD-98-189

FEBRUARY 1999



PB99-148975



U.S. Department of Transportation
Federal Highway Administration

Research and Development
Turner-Fairbank Highway Research Center
6300 Georgetown Pike
McLean, VA 22101-2296

REPRODUCED BY: **NTIS**
U.S. Department of Commerce
National Technical Information Service
Springfield, Virginia 22161

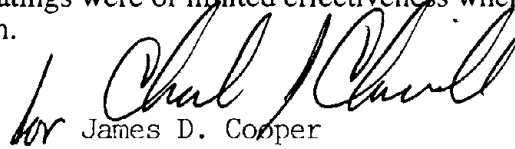


FOREWORD

This report will be of interest to engineers concerned with corrosion-induced repair of prestressed concrete highway structures using conventional repair techniques. The report will also be of interest to owners, inspectors, design firms, and highway bridge construction contractors.

A technology review was conducted for corrosion-induced and other deterioration in prestressed bridge structures. In addition, detailed field corrosion surveys were carried out on 12 prestressed concrete bridges. A technology review and field survey findings are published in an interim report.

In a laboratory program, prestressed and post-tensioned specimens were exposed to a salt solution designed to simulate both deicer applications and marine exposures. Corrosion was accelerated by application of anodic current to prestressing strands and reinforcing steel. Concrete was then removed from preselected deteriorated areas on each test specimen and repairs were made to these areas. Specimens were then re-exposed to chloride environments. Significant deterioration of coatings applied to prestressing strand and reinforcing steel occurred over the 4 years of severe exposure. Corrosion was observed on the interior surfaces of the individual strands, so it is likely that chloride ions penetrated into the interstices of the strand bundles and initiated corrosion prior to the repairs. Penetrating sealers and coatings were of limited effectiveness when applied to specimens undergoing active corrosion.



for James D. Cooper
Acting Director, Office of Engineering
Research and Development

NOTICE

This document is disseminated under the sponsorship of the Department of Transportation in the interest of information exchange. The United States Government assumes no liability for its contents or use thereof. This report does not constitute a standard, specification, or regulation.

The United States Government does not endorse products or manufacturers. Trade and manufacturers' names appear in this report only because they are considered essential to the object of the document.

1. Report No. FHWA-RD-98-189		2. Government Accession No.		3. Recipient's Catalog No.	
4. Title and Subtitle Rehabilitation of Prestressed Concrete Bridge Components by Non-Electrical (Conventional) Methods				5. Report Date February 1999	
				6. Performing Organization Code	
7. Author(s) D. Whiting, H. Tabatabai, B. Stejskal, M. Nagi				8. Performing Organization Report No. M 10018	
9. Performing Organization Name and Address Construction Technology Laboratories, Inc. 5420 Old Orchard Road Skokie, Illinois 60077				10. Work Unit No. (TRAIS) 3D4CO622	
				11. Contract or Grant No. DTFH61-91-C-00045	
12. Sponsoring Agency Name and Address Office of Engineering R & D Federal Highway Administration 6300 Georgetown Pike, McLean, VA 22101-2296				13. Type of Report and Period Covered Final Report Oct. 1991-Sept. 1998	
				14. Sponsoring Agency Code	
15. Supplementary Notes Contracting Officer's Technical Representative (COTR): Y. P. Virmani, HNR-10					
16. Abstract This report describes a technology review, field surveys, and laboratory investigations into the corrosion of prestressed concrete (PS/C) highway bridge elements and conventional repair methods used for these structures. Details of the technology review and field surveys are given in an Interim Report (FHWA-RD-95-041). Subsequent to completion of the field surveys, a laboratory program designed to evaluate corrosion performance of conventional concrete repair materials was initiated. Test specimens were precorroded by application of anodic current while exposed to chloride solutions. In order to study conventional concrete repairs, it was necessary to remove concrete from preselected areas on each purposely corroded test specimen and replace the chloride-contaminated/deteriorated original concrete with repair materials. Materials evaluated included conventional portland cement concrete, latex-modified fiber-reinforced patching mortar, and silica fume concrete containing either organic or inorganic corrosion inhibitors. Specimens where concrete was not removed were used to study the effects of sealers and coatings applied on concrete surfaces to mitigate ongoing corrosion. All specimens were exposed for approximately 200 weeks to a 15% solution of sodium chloride after repair. At the conclusion of exposure, patches were removed from repair specimens and the steel and the applied coatings were examined. In many of the specimens, significant deterioration of the coatings applied to prestressing strands and reinforcing steel had occurred over the 4 years of severe exposure. The distress was greater for the steel coated with liquid epoxy coating than the companion area of steel coated with a zinc-rich product. Typically, there was more disruption of coating and corrosion of base steel in areas where latex-modified mortar had been used as a repair material than where conventional concrete or silica fume concretes were used. Corrosion was observed in repair areas where bulk chloride ion contents were below commonly accepted threshold levels. When tendon bundles were cut and pulled apart, corrosion was observed on the interior surfaces of the individual strands. It is likely that chloride ions penetrated into the interstices of the strand bundles while the specimens were precorroded, and prior to the repairs. Penetrating sealers and coatings were of limited effectiveness when applied to the surface of concrete specimens undergoing active corrosion.					
17. Key Words Chlorides, concretes, corrosion, patching, prestressed concrete, rehabilitation, sealers			18. Distribution Statement No original distribution by the sponsoring agency. This document is available to the public through the National Technical Information Service, Springfield, VA 22161.		
19. Security Classif. (of this report) Unclassified		20. Security Classif. (of this page) Unclassified		21. No. of Pages 129	22. Price

SI* (MODERN METRIC) CONVERSION FACTORS

APPROXIMATE CONVERSIONS TO SI UNITS

APPROXIMATE CONVERSIONS FROM SI UNITS

Symbol	When You Know	Multiply By	To Find	Symbol	When You Know	Multiply By	To Find	Symbol
LENGTH				LENGTH				
in	inches	25.4	millimeters	mm	millimeters	0.039	inches	in
ft	feet	0.305	meters	m	meters	3.28	feet	ft
yd	yards	0.914	meters	m	meters	1.09	yards	yd
mi	miles	1.61	kilometers	km	kilometers	0.621	miles	mi
AREA				AREA				
in ²	square inches	645.2	square millimeters	mm ²	square millimeters	0.0016	square inches	in ²
ft ²	square feet	0.093	square meters	m ²	square meters	10.764	square feet	ft ²
yd ²	square yards	0.836	square meters	m ²	square meters	1.195	square yards	yd ²
ac	acres	0.405	hectares	ha	hectares	2.47	acres	ac
mi ²	square miles	2.59	square kilometers	km ²	square kilometers	0.386	square miles	mi ²
VOLUME				VOLUME				
fl oz	fluid ounces	29.57	milliliters	mL	milliliters	0.034	fluid ounces	fl oz
gal	gallons	3.785	liters	L	liters	0.264	gallons	gal
ft ³	cubic feet	0.028	cubic meters	m ³	cubic meters	35.71	cubic feet	ft ³
yd ³	cubic yards	0.765	cubic meters	m ³	cubic meters	1.307	cubic yards	yd ³
NOTE: Volumes greater than 1000 l shall be shown in m ³ .								
MASS				MASS				
oz	ounces	28.35	grams	g	grams	0.035	ounces	oz
lb	pounds	0.454	kilograms	kg	kilograms	2.202	pounds	lb
T	short tons (2000 lb)	0.907	megagrams (or "metric ton")	Mg (or "t")	megagrams (or "metric ton")	1.103	short tons (2000 lb)	T
TEMPERATURE (exact)				TEMPERATURE (exact)				
°F	Fahrenheit temperature	5(F-32)/9 or (F-32)/1.8	Celsius temperature	°C	Celsius temperature	1.8C + 32	Fahrenheit temperature	°F
ILLUMINATION				ILLUMINATION				
fc	foot-candles	10.76	lux	lx	lux	0.0929	foot-candles	fc
fl	foot-Lamberts	3.426	candela/m ²	cd/m ²	candela/m ²	0.2919	foot-Lamberts	fl
FORCE and PRESSURE or STRESS				FORCE and PRESSURE or STRESS				
lbf	poundforce	4.45	newtons	N	newtons	0.225	poundforce	lbf
lbf/in ²	poundforce per square inch	6.89	kilopascals	kPa	kilopascals	0.145	poundforce per square inch	lbf/in ²

* SI is the symbol for the International System of Units. Appropriate rounding should be made to comply with Section 4 of ASTM E380.

TABLE OF CONTENTS

<u>Chapter</u>	<u>Page</u>
1. INTRODUCTION.....	1
PROBLEM STATEMENT.....	1
OBJECTIVES.....	1
SCOPE OF WORK AND STUDY APPROACH.....	1
2. TECHNOLOGY REVIEW AND FIELD SURVEYS.....	3
TECHNOLOGY REVIEW.....	3
Types of Corrosion.....	3
Susceptibility to Corrosion.....	3
Corrosion Studies.....	3
Case Histories.....	4
FIELD SURVEYS.....	4
Pre- and Post-Tensioned Beams in Marine Environments:	
Findings and Recommendations.....	5
Pretensioned I-Beams Exposed to Deicing Environments:	
Findings and Recommendations.....	6
Pretensioned Box Beams Exposed to Deicing Environments:	
Findings and Recommendations.....	7
Post-Tensioned Beams Exposed to Deicing Environments:	
Findings and Recommendations.....	8
CONCLUSIONS FROM TECHNOLOGY REVIEW AND FIELD SURVEYS.....	8
3. SPECIMEN PREPARATION AND TREATMENT.....	11
INTRODUCTION.....	11
Guidance Available From Technology Review and Field Surveys.....	11
Selection of Structural Elements for Testing.....	11
Environmental Exposures.....	12
DESIGN AND PREPARATION OF TEST SPECIMENS.....	13
Pre-Tensioned Concrete Beams.....	13
Pre-Tensioned Concrete Slabs.....	13
Pre-Tensioned Concrete Piles.....	16
Multi-Strand Post-Tensioned Elements.....	16
Threadbar Post-Tensioned Elements.....	16
Specimen Preparation.....	20
INITIATION OF CORROSION.....	21
Specimen Exposures.....	21
Acceleration of Corrosion.....	26
REPAIR PROCEDURES.....	35
Test Plan and Materials.....	35
Repair Applications.....	37

4. RESULTS	43
CATEGORY A - CONCRETE REMOVAL/REPLACEMENT	43
Slab Repairs.....	43
Beam Repairs.....	61
Pile Repairs	76
CATEGORY B - COATINGS AND SEALERS.....	89
Pretensioned Slabs.....	89
Pretensioned Beams	95
Pretensioned Piles	99
5. SUMMARY, CONCLUSIONS, AND RECOMMENDATIONS.....	113
SUMMARY	113
CONCLUSIONS	116
RECOMMENDATIONS.....	117
REFERENCES.....	119

LIST OF FIGURES

Figure	Page
1. Design details for pretensioned concrete beam specimens	14
2. Design details for pretensioned concrete slab specimens.....	15
3. Design details for pretensioned concrete piles.....	17
4. Design details for multi-strand post-tensioned concrete beam specimens	18
5. Design details for threadbar post-tensioned concrete beam specimens	19
6. Arrangement of test specimens in laboratory	22
7. Splash system for exposure of soffits of AASHTO beams and pretensioned slabs.....	23
8. Spray applications of sodium chloride solutions at beam ends	24
9. Tanks for simulation of marine tidal exposure for pretensioned piles	25
10. Average chloride contents measured on specimens after electrical acceleration.....	29
11. Repair area details for pretensioned beam specimens.....	31
12. Repair area details for pretensioned slab specimens	32
13. Elevation view of repair area details for pretensioned pile specimens	33
14. Plan view of repair area details for pretensioned pile specimens.....	34
15. Average half-cell potentials in slab repair areas over 100 cycles of testing.....	46
16. Crack map for slab 1 at 100 cycles of exposure.....	47
17. Crack map for slab 2 at 100 cycles of exposure.....	48
18. Crack map for slab 3 at 100 cycles of exposure.....	49
19. Appearance of north repair area, slab 1, after 100 exposure cycles.....	50
20. Appearance of north repair area, slab 2, after 100 exposure cycles	50
21. Chloride contents measured on slab repair specimens.....	51
22. Comparison of chloride contents measured at center and near edges of slab repair patches.....	53
23. Appearance of uncovered tendons and reinforcing steel in north repair area, slab 1, after 100 exposure cycles	54

24.	Appearance of uncovered tendons and reinforcing steel in south repair area, slab 1, after 100 exposure cycles.....	54
25.	Appearance of interior of tendon bundle in north repair area, slab 1, after 100 exposure cycles	55
26.	Appearance of interior of tendon bundle in south repair area, slab 1, after 100 exposure cycles	55
27.	Appearance of uncovered tendons and reinforcing steel in north repair area, slab 2, after 100 exposure cycles.....	56
28.	Appearance of uncovered tendons and reinforcing steel in south repair area, slab 2, after 100 exposure cycles.....	56
29.	Appearance of interior of tendon bundle in north repair area, slab 2, after 100 exposure cycles	58
30.	Appearance of interior of tendon bundle in south repair area, slab 2, after 100 exposure cycles	58
31.	Appearance of uncovered tendons and reinforcing steel in north repair area, slab 3, after 100 exposure cycles.....	59
32.	Appearance of uncovered tendons and reinforcing steel in south repair area, slab 3, after 100 exposure cycles.....	59
33.	Appearance of interior of tendon bundle in north repair area, slab 3, after 100 exposure cycles	60
34.	Appearance of interior of tendon bundle in south repair area, slab 3, after 100 exposure cycles	60
35.	Average half-cell potentials in beam repair areas over 100 cycles of testing	62
36.	Crack map for beam 1 at 100 cycles of exposure	64
37.	Crack map for beam 2 at 100 cycles of exposure	65
38.	Crack map for beam 3 at 100 cycles of exposure	66
39.	Chloride contents measured on beam repair specimens	68
40.	Comparison of chloride contents measured at center and near edges of beam repair patches.....	69
41.	Appearance of uncovered tendons and reinforcing steel in north repair area, beam 1, after 100 exposure cycles	71
42.	Appearance of uncovered tendons and reinforcing steel in south repair area, beam 1, after 100 exposure cycles	71
43.	Appearance of interior of tendon bundle in north repair area, beam 1, after 100 exposure cycles	72

44.	Appearance of interior of tendon bundle in south repair area, beam 1, after 100 exposure cycles	72
45.	Appearance of uncovered tendons and reinforcing steel in north repair area, beam 2, after 100 exposure cycles	73
46.	Appearance of uncovered tendons and reinforcing steel in south repair area, beam 2, after 100 exposure cycles	73
47.	Appearance of interior of tendon bundle in north repair area, beam 2, after 100 exposure cycles	74
48.	Appearance of interior of tendon bundle in south repair area, beam 2, after 100 exposure cycles	74
49.	Appearance of uncovered tendons and reinforcing steel in north repair area, beam 3, after 100 exposure cycles	75
50.	Appearance of uncovered tendons and reinforcing steel in south repair area, beam 3, after 100 exposure cycles	75
51.	Appearance of interior of tendon bundle in north repair area, beam 3, after 100 exposure cycles	77
52.	Appearance of interior of tendon bundle in south repair area, beam 3, after 100 exposure cycles	77
53.	Average half-cell potentials in pile repair areas over 215 weeks of tidal cycling	79
54.	Chloride contents measured on pile repair specimens	81
55.	Appearance of uncovered tendons and reinforcing steel in north repair area, pile 1, after 215 weeks of tidal cycling	82
56.	Appearance of uncovered tendons and reinforcing steel in south repair area, pile 1, after 215 weeks of tidal cycling	82
57.	Appearance of interior of tendon bundle in north repair area, pile 1, after 215 weeks of tidal cycling	83
58.	Appearance of interior of tendon bundle in south repair area, pile 1, after 215 weeks of tidal cycling	83
59.	Appearance of uncovered tendons and reinforcing steel in north repair area, pile 2, after 215 weeks of tidal cycling	85
60.	Appearance of uncovered tendons and reinforcing steel in south repair area, pile 2, after 215 weeks of tidal cycling	85
61.	Appearance of interior of tendon bundle in north repair area, pile 2, after 215 weeks of tidal cycling	86

62.	Appearance of interior of tendon bundle in south repair area, pile 2, after 215 weeks of tidal cycling	86
63.	Appearance of uncovered tendons and reinforcing steel in north repair area, pile 3, after 215 weeks of tidal cycling	87
64.	Appearance of uncovered tendons and reinforcing steel in south repair area, pile 3, after 215 weeks of tidal cycling.....	87
65.	Appearance of interior of tendon bundle in north repair area, pile 3, after 215 weeks of tidal cycling	88
66.	Appearance of interior of tendon bundle in south repair area, pile 3, after 215 weeks of tidal cycling	88
67.	Macrocell currents in coated slab specimens over 118 cycles of testing	90
68.	Half-cell potentials in coated slab specimens over 118 cycles of testing	92
69A.	Appearance of surface of north half of slab 4 after 118 weekly salt ponding cycles.....	93
69B.	Appearance of surface of south half of slab 4 after 118 weekly salt ponding cycles.....	93
70A.	Appearance of surface of north half of slab 5 after 118 weekly salt ponding cycles.....	94
70B.	Appearance of surface of south half of slab 5 after 118 weekly salt ponding cycles.....	94
71.	Chloride contents measured on slab specimens prior to and after 118 weeks of exposure.....	96
72.	Macrocell currents in coated beam specimens over 118 cycles of testing	97
73.	Half-cell potentials in coated beam specimens over 118 cycles of testing.....	98
74A.	Appearance of surface of north half of beam 4 after 118 weekly salt ponding cycles	100
74B.	Appearance of surface of south half of beam 4 after 118 weekly salt ponding cycles	100
75A.	Appearance of surface of north half of beam 5 after 118 weekly salt ponding cycles	101
75B.	Appearance of surface of south half of beam 5 after 118 weekly salt ponding cycles	101
76.	Chloride contents measured on beam specimens prior to and after 118 weeks of exposure.....	102
77.	Half-cell potentials measured on north face of piling no. 4.....	103
78.	Half-cell potentials measured on south face of piling no. 4.....	104
79.	Half-cell potentials measured on north face of piling no. 5	105
80.	Half-cell potentials measured on south face of piling no. 5.....	106
81.	Appearance of surface of north face of pile 4 after 3080 tidal cycles	108

82.	Appearance of surface of south face of pile 4 after 3080 tidal cycles	109
83.	Appearance of surface of north face of pile 5 after 3080 tidal cycles	110
84.	Appearance of surface of south face of pile 5 after 3080 tidal cycles	111
85.	Chloride contents measured on pile specimens prior to and after 3080 tidal cycles.....	112

LIST OF TABLES

<u>Table</u>	<u>Page</u>
1. Mix proportions used for precast concretes (yd ³ basis)	20
2. Strength of precast concretes	21
3. Assignment of repair materials to test specimens	36
4. Assignment of coatings/sealers to test specimens	36
5. Properties and proportions for conventional concrete mixture used for category A repairs	38
6. Properties and proportions for silica fume concrete mixture with inorganic corrosion inhibitor used for category A repairs.....	39
7. Properties and proportions for silica fume concrete mixture with organic corrosion inhibitor used for category A repairs.....	40
8. Application rates of coatings/sealers to test specimens	41
9. Half-cell potentials measured on slab 1 after four wet/dry cycles	44
10. Half-cell potentials measured on slab 2 after four wet-dry cycles.....	44
11. Half-cell potentials measured on slab 3 after four wet/dry cycles	45
12. Half-cell potentials measured on beam 1 after four wet/dry cycles.....	61
13. Half-cell potentials measured on beam 2 after four wet/dry cycles.....	63
14. Half-cell potentials measured on beam 3 after four wet/dry cycles.....	63
15. Half-cell potentials measured on pilings after 12 weeks of tidal cycling	78

CHAPTER 1. INTRODUCTION

PROBLEM STATEMENT

Of the 576,000 bridges in the National Bridge Inventory, 65,000 have prestressed concrete (PS/C) support structures. These may be either pretensioned or post-tensioned systems. As prestressed elements are under significant mechanical stress, corrosion is more of a concern than in conventional reinforced-concrete structures. In prestressed elements, loss of a significant amount of cross section of the prestressing steel can lead to overload and failure of the remaining section. If this occurs on a large number of tendons in a member, then sudden and catastrophic failure may occur. Therefore, potential corrosion problems in PS/C bridges need to be identified, and long-term rehabilitative methods need to be developed to repair those structures already exhibiting corrosion so that their serviceability may be maintained without resort to costly replacement.

OBJECTIVES

The objectives of this study were: (1) to perform a detailed review of technology relating to corrosion-induced and other deterioration in PS/C bridges; (2) to identify a set of PS/C bridges located in various adverse environments and carry out field condition surveys and laboratory analyses on samples obtained from the selected structures; (3) to identify the causes for corrosion in PS/C structures based on analysis of collected field and laboratory data; and (4) to evaluate the effectiveness of rehabilitation techniques commonly used to extend the service life of PS/C bridges.

SCOPE OF WORK AND STUDY APPROACH

A technology review was conducted in the area of corrosion-induced and other deterioration in PS/C structures. The review included types of corrosion encountered in such structures, susceptibility of various types of prestressing systems to corrosion, previous laboratory and field studies of corrosion in PS/C structures, and case histories of corrosion-induced failures in PS/C bridge structures. The review was intended to reflect current knowledge in the area. Extensive references to previously published reviews and surveys were included.

Prestressed concrete bridges exhibiting ongoing corrosion were identified through consultation with State authorities. Field sites were identified in Connecticut, Florida, Illinois, Michigan, North

Dakota, Oregon, and Rhode Island. Detailed field surveys were carried out on 12 PS/C bridges in these states.

Based on the results of the surveys and technology review, specific adverse environments were recognized. Portions of PS/C bridges susceptible to corrosion in such environments, including specific elements and configurations, were identified.

Results of these first two phases of the study were published by the Federal Highway Administration (FHWA) in 1993 in an interim report.⁽¹⁾ Papers based on this report are also available in an American Concrete Institute (ACI) publication.^(2,3) A synopsis of the work and pertinent findings is included in Chapter 2 of this report. Readers requiring more detailed information on the technology review and field surveys are urged to obtain the interim report.

Model structural members representing most commonly used PS/C beams, slabs, and pilings were constructed for evaluation of the performance of PS/C repair systems. The members were stressed to levels typical of those used in actual construction. The specimens were then subjected to accelerated corrosive environments in order to induce corrosion on the embedded reinforcing steel and prestressing systems. Materials typical of those used for field repair of a variety of PS/C structural members were identified. These included repair concretes, as well as the application of penetrating sealers and coatings, where no concrete removal operations are needed. Penetrating sealers and coatings were applied to one set of specimens. For the second set of specimens, concrete was removed from portions of the test specimens and replaced with repair materials. These included a mix typical of those used for conventional concrete repairs, a polymer (latex)-modified repair material, and a repair material utilizing both silica fume and corrosion-inhibiting admixtures. Prestressing and reinforcing steel in the repair areas was coated with either a liquid-applied epoxy coating or a liquid-applied zinc-rich coating. The repaired specimens were then re-subjected to accelerated corrosive environments for a period of approximately 4 years. At the end of this exposure period, repair concrete was sampled for penetration of chloride ions, and the condition of the embedded steel in the repair areas was evaluated.

CHAPTER 2. TECHNOLOGY REVIEW AND FIELD SURVEYS

TECHNOLOGY REVIEW

The review of technology in the area of corrosion of PS/C bridges was included as Chapter 2 of the interim report published by FHWA. In this technology review, types of corrosion and recent theories explaining stress corrosion and hydrogen embrittlement were presented. Susceptibility of prestressing steel to corrosion in prestressed and post-tensioned concrete structures was discussed. Factors such as concrete materials, prestressing steel, and environments that may influence corrosion were categorized. Laboratory and field studies dealing with a variety of corrosion issues in pretensioned and post-tensioned concrete were summarized. These issues include the development and improvement of grout materials for bonded tendons in post-tensioned concrete members, use of epoxy-coated prestressing wires, and corrosion of unbonded tendons under severe exposure. Selected case histories and field evaluation of concrete bridges subjected to corrosion were also included in the review. This review gives an overview of corrosion problems in prestressed concrete members and will assist engineers in diagnosing the causes of corrosion and selecting the right methods and materials to be used for rehabilitation as well as in new construction. A brief synopsis in the form of an outline is presented in this report. For further details the reader should consult the interim report⁽¹⁾:

Types of Corrosion

- Pitting Corrosion — effects of chlorides, carbon dioxide.
- Stress Corrosion — anodic stress corrosion, cathodic stress corrosion, effects of hydrogen embrittlement.

Susceptibility to Corrosion

- Pretensioned Structures — quality of concrete, properties of prestressing steels, environmental effects.
- Post-Tensioning — structural types, concrete quality, environmental effects, post-tensioning and anchorage systems, sheaths and ducts, grouts, joints.

Corrosion Studies

- Laboratory Studies — "in vitro" studies, studies in concrete environments, long-term exposure studies, recent FHWA investigations.
- Field Studies — Treat Island exposure studies, FHWA bridge surveys, MnDOT surveys.

Case Histories

- Prestressed Box Beams — F.G. Gardiner Expressway, Toronto, Canada.
- Segmental Post-Tensioned Bridge — River Afan, South Wales, U.K.
- Prestressed Concrete Bridge — Schmargendorf, Germany.

FIELD SURVEYS

Twelve pre- and post-tensioned bridges built between 1954 and 1967 were surveyed to determine their overall condition and exposure to corrosive environments. Average original construction date for the bridges selected was 1960, making them, on average, 32 years old at the time of the survey. Bridges were located across the United States in both marine and inland areas and were exposed to salt water spray or deicer applications. Samples of concrete were obtained from the bridges during the field surveys and subjected to petrographic examination and chloride analyses in the laboratory. The following twelve bridges were included in the study:

- The Old Sunshine Skyway Bridge, Tampa, Florida.
- U.S. 23 over BR U.S. 23, Ann Arbor, Michigan.
- Astoria Bridge over the Columbia River, Astoria, Oregon.
- I-90 over Des Plaines River Road, Chicago, Illinois.
- I-90 over Mannheim Road, Chicago, Illinois.
- 32nd Street over U.S. 131, Grand Rapids, Michigan.
- Devil's Elbow Slide Viaducts, U.S. 101, Florence, Oregon.
- The Gandy Bridge, Tampa, Florida.
- Wolcott Avenue (Bissell Bridge) over the Connecticut River, Windsor, Connecticut.
- I-94 over I-29, Fargo, North Dakota.
- I-94 over U.S. 81, Fargo, North Dakota.
- I-195 (Washington Bridge) over Seekonk River, Providence, Rhode Island.

Detailed field surveys were carried out on these bridges using the following techniques:

- Visual examinations.
- Cover surveys.
- Delamination surveys.
- Half-cell (electrical potential) surveys.
- Corrosion rate (linear polarization) measurements.
- Chloride sampling.
- Petrographic analyses.

The 12 structures surveyed were grouped into 3 categories for the purposes of defining exposure conditions, causes of distress, and recommendations for avoiding future distress in structures representative of this type. The categories are listed below and include:

- Pre- and post-tensioned beams exposed to marine environments.
- Pre-tensioned I-beams exposed to deicing environments.
- Pre-tensioned box beams exposed to deicing environments.
- Post-tensioned beams (and other elements) exposed to deicing environments.

Pre- and Post-Tensioned Beams in Marine Environments: Findings and Recommendations

Marine environments represent a spectrum of severity of exposure, ranging from structures located in temperate climate bays and estuaries where exposure to brackish water is relatively indirect, to bridges over tropical waters exposed to direct saline spray. In the present study, the bridges in Astoria and Florence, Oregon were representative of the former type of exposure; the bridges in Tampa, Florida were representative of the latter type of exposure. In more temperate climates away from direct sea spray, there is a slow accumulation of chloride within the concrete. In post-tensioned structures, attack on the strands themselves in this type of environment is much more difficult, provided that ducts are intact and a high-quality grout has been used. If anchorage pockets are well protected by good quality mortars, there is little likelihood of corrosion of post-tensioned members in these types of environments. For pretensioned members, the Oregon experience indicates that the production of high-quality concrete of a low water-to-cement (w/c) ratio and permeability should significantly reduce the ingress of atmospheric chloride into these members.

Tropical marine environments represent a much more severe type of exposure. This may include direct continuous exposure to tidal action, such as for prestressed pilings, as well as intermittent exposure to wind-driven salt spray. Year-round warm temperatures help foster both the rate of ingress of the chlorides as well as the rate of corrosion itself. In the worst case, such as the beams of the Old Sunshine Skyway bridge in Tampa, Florida lying close to the water line, there is almost daily wetting of the elements by saline spray. Conventional repair methods, consisting of removal of deteriorated concrete and replacement with concrete, mortar, or shotcrete, are largely ineffective, as chlorides are easily able to remigrate through the repair concretes and again attack the prestressing steel. For pretensioned members to be durable over the long term in such environments, it may be necessary to invest in very high-quality concretes having extremely

low permeability to chloride ions, such as those prepared at low w/c ratios using silica fume and fly ash admixtures. Inclusion of a chemical corrosion inhibitor as additional protection may also be advisable in some cases. For post-tensioned members, use of non-corroding ducts (such as polyethylene ducts) would help to halt the progress of chlorides towards the strand; however, care must also be taken to protect the anchorage areas, otherwise salt solutions can enter the ducts at the anchorage and migrate longitudinally through the grout along the tendons. It may be necessary to encapsulate the anchorage in impermeable material or otherwise prevent chloride salts from entering the sealed ducts.

Pretensioned I-Beams Exposed to Deicing Environments: Findings and Recommendations

All of the structures of this type included in the field surveys (i.e., the Ann Arbor, Michigan and Chicago, Illinois structures) showed susceptibility to corrosion at localized points on the structure. This was either at end expansion joints separating the deck slab from the approach slab, or at joints separating the spans along the length of the bridge. The actions of traffic and environment eventually lead to joint failure, which allows deicer solutions to pass through the joint onto the pier caps and beam ends. Almost all the deterioration associated with inland I-beam structures is confined to beam ends. Another pathway for intrusion is from deteriorated drains, or gaps in bridge railings that allow deicing salts to flow off the deck and onto the beams. This is less common than the simple case of deteriorated joints. Obviously, to prevent seepage of deicing solutions into the concrete, the design of the structure must be changed so that deicers cannot run onto the beams, or they must be guided away from the beams. Use of one or more of the following approaches should enable the bridge designer to greatly reduce the potential for corrosive attack of pre-tensioned I-beam structures:

- Minimize exposure of beam ends to deicing salts running off the deck. This can be done by running beams through diaphragms over piers at the center of the bridge (offering opportunity for making the beams continuous), or running beam ends into concrete abutments at the ends of the bridge.
- Install and maintain a functional gutter and drainage system using large-capacity gutters and wide drainage pipes to carry water off the deck and into proper drainage facilities. Designing the proper slope into the deck will aid in preventing ponding of water on the deck.

- Install rigid concrete overlays on the deck to prevent leakage of water through the deck onto the superstructure. This will also help to protect the plain reinforcement in the deck from corrosion.
- Implement a joint maintenance program to ensure that deteriorating deck joints are replaced by the most effective designs and materials. Armored elastomeric compression seals offer the most positive means of preventing leakage through the expansion joints.
- Minimize the number of joints in the deck. Bridges up to 820 m (2695 ft) have been constructed without joints (except at abutments).

Pre-Tensioned Box Beams Exposed to Deicing Environments: Findings and Recommendations

Only one structure falling into this category (Grand Rapids, Michigan bridge) was included in this survey; however, conclusions reached concerning the mode of corrosive attack are almost identical to those observed in previous cases. The box beams are subjected to the same exposures as the I-beams at their ends. In addition to these similarities, the box structures suffer from an additional pathway for chloride intrusion through the longitudinal spaces between the beams. This subjects a much larger length of the beam to potentially corrosive conditions. Box beams are usually covered by asphaltic wearing surfaces when the top flange of the beams is not reinforced by a concrete deck slab. Eventually, the asphaltic wearing course ages, and cracks reflect through these spaces allowing salt solutions to penetrate along the entire length of the beam. A number of design features would help to eliminate this avenue of ingress. These could include the following:

- Installation of protective membrane systems on the top flange of the beam.
- Installation of a rigid wearing course or composite deck slab (provided the structure could accommodate the additional dead load).
- Transverse post-tensioning of the beams to hold beam faces together.
- Design of proper slope and drainage details so that dwell time of deicer solutions on the deck surface is held to a minimum.

Post-Tensioned Beams Exposed to Deicing Environments: Findings and Recommendations

Four of the structures included in this survey (the Wolcott Avenue bridge in Windsor, Connecticut; the two Fargo, North Dakota bridges; and the Washington Bridge in Providence, Rhode Island) were representative of this category of structural type and exposure. In spite of the severity of exposure (with the exception of the anchorage zones where plates and other hardware were observed to be corroded to varying degrees), post-tensioning rods and tendons fully grouted into metallic ducts performed extremely well, with little sign of serious corrosion. It is very important that the grout fully encapsulate the tendons within the ducts, and that no potentially corrosive substances be added to the grouts. By following similar design, jointing, and drainage details as recommended for the pretensioned structures, it should be possible to keep salts away from the anchorage zones and prevent the occurrence of corrosion of anchorage hardware in these areas as well. It appears that the frequency of corrosion of post-tensioned members is much lower than for structures utilizing pretensioned I- and box beams. If care can be taken with regards to grouting and minimizing exposure to deicer run-off, post-tensioned elements would appear to offer a high potential for long-lasting corrosion-free bridges in inland deicing locations.

CONCLUSIONS FROM TECHNOLOGY REVIEW AND FIELD SURVEYS

Based on information developed from the technology review and results of the field surveys on PS/C bridges carried out under this and previous studies, the following conclusions regarding performance of PS/C bridges in adverse environments can be drawn:

- Both chloride-induced pitting and stress-corrosion occur in prestressing steels. Quenched and tempered steel is more susceptible to stress corrosion and hydrogen embrittlement than cold-drawn stress-relieved prestressing wire. Therefore, the use of quenched and tempered steel should be avoided in PS/C construction.
- The anchorage zone in post-tensioned members is especially vulnerable to corrosion damage. Field performance, as well as laboratory studies, indicate that if anchorage recesses are not sealed and completely protected, moisture and chloride ions will penetrate to the prestressing wires and cause corrosion.
- Properly grouted, bonded post-tensioned systems offer high resistance to corrosion. Recent developments include the use of grout modifiers and silica fume to improve the

placement and durability of grouts used to fill post-tensioning ducts. The use of coated or polymeric ducts can also afford increased protection to tendons.

- In the vast majority of instances, performance of PS/C bridges in adverse environments has been excellent. There are only a handful of documented cases of failures of such structures. Instances of corrosion do exist; however; it appears that the mode of attack for pretensioned PS/C bridges is similar to that of plain reinforcing steel. This results in a slow loss of steel cross section with subsequent spalling and cracking of concrete. Maintenance or replacement can usually be carried out before catastrophic failure occurs.
- Warm, saltwater marine exposures where PS/C elements are subjected to direct spray or tidal action represent one of the most severe environments for prestressed concrete structures. In addition to high-quality concrete and proper construction practices, additional protective measures may be necessary. These may include use of very low permeability concretes, corrosion inhibitors, non-corroding duct materials, and corrosion-resistant coatings on prestressing and reinforcing steel.
- At inland sites, almost all instances of corrosion are confined to beam ends where deicing salts flow through leaking joints or at other locations where salts from the deck can penetrate through drains or bridge railings. Exposure of beam ends to deicing salts should be minimized by the use of more durable joint materials or by minimizing the number of joints in the deck. Use of rigid overlays or membrane systems may also help restrict the amount of salt passing through the deck, especially in the case of box-beam structures, where longitudinal joints are a primary pathway for salt penetration.

CHAPTER 3. SPECIMEN PREPARATION AND TREATMENT

INTRODUCTION

Guidance Available From Technology Review and Field Surveys

Results of the technology review and field surveys summarized in Chapter 2 helped to form the basis for designing further laboratory studies aimed at evaluating the performance of conventional techniques for rehabilitating pre- and post-tensioned bridge elements subject to corrosive environments. In areas where deicing salts are applied to decks, the most prevalent mechanism for corrosion appears to be leakage of deicing solutions through open or failed joints onto ends of beams that sit on top of pier caps located immediately below leaking joints. Box-beam structures appear to be especially susceptible to corrosion and subsequent deterioration. Often, asphaltic or portland cement concrete overlays are placed onto these beams to serve as wearing surfaces. Movement of the beams causes reflective longitudinal cracks between the beams and through the overlays, causing deicing salts to leak through onto the faces of the webs and underside of the beams. Field survey results indicate the greatest frequency of distress of prestressed elements occurs in these types of box-beam structures. In marine areas, exposure is more general, with the entirety of bridge substructure elements subject to exposure of varying degrees. The most aggressive exposures are in direct tidal zones, such as on pretensioned pilings, and where marine spray is blown onto support elements by wind or wave action.

In contrast to problems encountered with pretensioned bridge elements, post-tensioned structures appear to be much more resistant to corrosive environments. The added protection afforded to the tendons or bar by grout and duct encasement makes it more difficult for aggressive substances to penetrate to the level of the prestressing steel. As with pretensioned systems, however, end anchorages, when situated under leaking joints, present a potential avenue of ingress for aggressive solutions. Field observations on marine post-tensioned beams indicate that over the long term, chloride ions may cause complete corrosion of the metallic ducts, penetrate to the level of the steel, and initiate corrosion of the post-tensioning wire or bar.

Selection of Structural Elements for Testing

In order to simulate as closely as possible the conditions existing in actual prestressed concrete structures, nearly full-scale members were used in evaluation of various repair materials for corrosion-damaged structures. The following types of elements were selected as being

representative of many of the structural elements on which deterioration had been observed in the field surveys:

- Pre-tensioned AASHTO Type II girders.
- Pre-tensioned slabs representative of bridge deck panels and exposed webs of box girders.
- Pre-tensioned pilings for marine piers and foundations.
- Post-tensioned beams having multiple-strand anchorage systems with low-relaxation strands in grouted ducts.
- Post-tensioned beams having a single Grade 150 post-tensioning bar in grouted ducts.

Environmental Exposures

The field surveys indicated marine and deicing environments to be the most severe in terms of susceptibility of prestressed concrete elements to corrosion-induced deterioration. In order to study these effects in a controlled laboratory environment, there existed a need to simulate the field exposures. The following approaches were initially chosen as a means of reproducing (as closely as possible) these exposures in a laboratory situation:

- Exposure of the ends of pre- and post-tensioned beams to salt solution runoff to simulate leaking joints over beam ends and anchorage areas.
- Exposure of the soffits of beams and slabs to spray of salt solution to simulate exposure to marine spray.
- Exposure of pilings to periodic immersion in a salt solution to simulate tidal exposure in a marine environment.

As noted later in this report, some of these exposures were subsequently modified due to problems in maintaining the salt spray systems and the need to further accelerate the ingress of chloride ions into the members. Details of test specimens and exposures are given in the following sections.

DESIGN AND PREPARATION OF TEST SPECIMENS

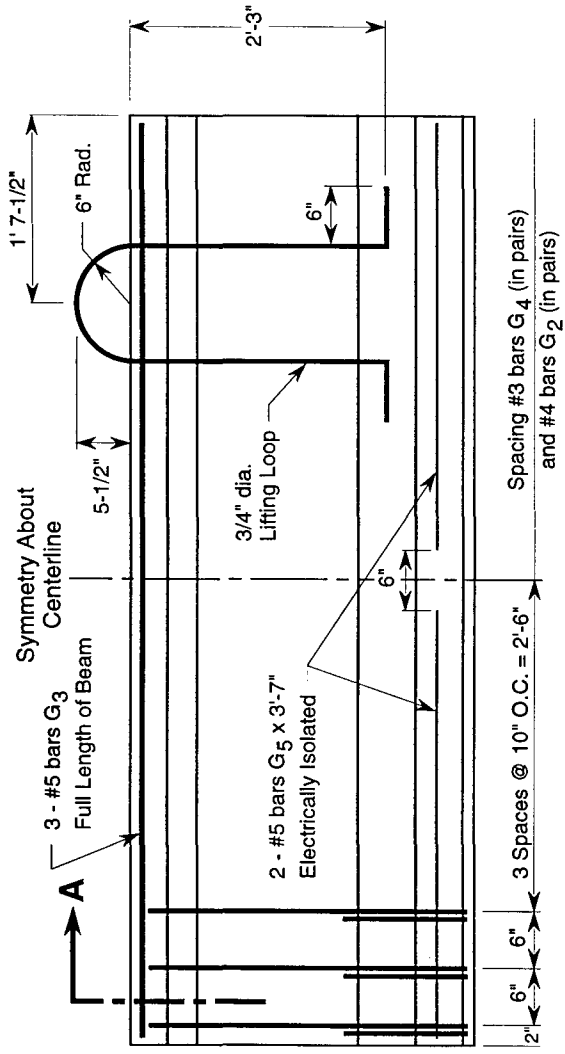
In order to approach as closely as possible the real conditions experienced by bridge members, the test specimens were designed to be nearly full scale in terms of at least their cross section and the minimum length needed to achieve the desired prestress levels over the middle region of each specimen. This also allowed realistic assessment of application techniques for protective systems, such as spray-applied sealers and patching repair materials. A total of 24 such specimens were included in the test program. Five types of test specimens were included to represent both pre-tensioned and post-tensioned bridge superstructures and foundation elements. Configurations and details are given for each type of specimen in subsequent sections.

Pre-Tensioned Concrete Beams

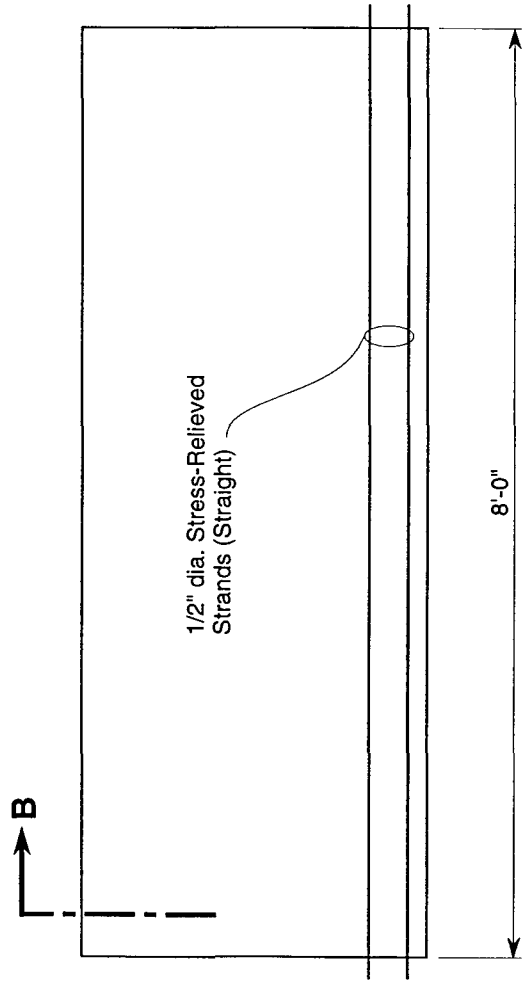
Pre-tensioned concrete beam specimens consisted of 2.4-m- (8-ft-) long AASHTO Type II sections as shown in Figure 1. The girders contained ten 12-mm (0.5-in), grade 270 low-relaxation seven-wire prestressing strands. The magnitude of force in each strand prior to prestress transfer was 75% of the guaranteed ultimate tensile strength (GUTS) or approximately 137,800 N (30,980 lbf). All strands were straight (not draped) and were subsequently cut flush with the ends of the beams. The beams also contained stirrup and longitudinal plain reinforcing bars as shown in Figure 1. Two longitudinal bars were deliberately left electrically isolated from the main cage for the purpose of making macrocell measurements (i.e., measurements of electrical current developed between bars in chloride-contaminated and chloride-free concrete). A total of 10 such beam specimens were constructed.

Pre-Tensioned Concrete Slabs

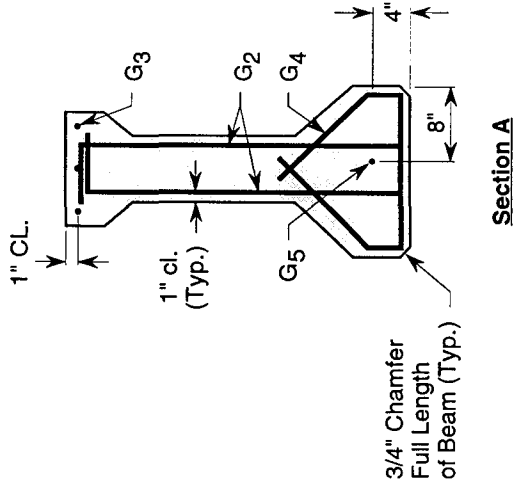
Pre-tensioned concrete slab specimens consisted of 2.4-m- (8-ft-) long by 0.6-m- (2-ft-) wide by 100-mm- (4-in-) thick elements as shown in Figure 2. The slabs contained four 12-mm (0.5-in), grade 270 low-relaxation seven-wire prestressing strands. The magnitude of force in each strand prior to prestress transfer was 75% of the GUTS or approximately 137,800 N (30,980 lbf). All strands were straight and were subsequently cut flush with the ends of the slabs. The slabs also contained transverse and longitudinal plain reinforcing bars as shown in Figure 2. Four longitudinal bars were deliberately left electrically isolated from the main cage for the purpose of making macrocell measurements. A total of five such slab specimens were constructed.



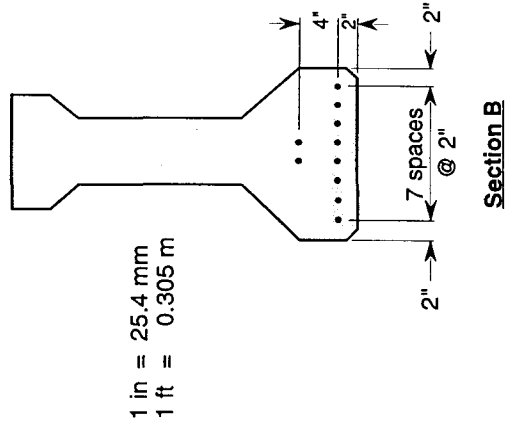
Elevation of Beam
(Showing Steel Reinforcement)



Elevation of Beam
(Showing Prestress Steel)



Section A



Section B

Figure 1. Design details for pretensioned concrete beam specimens.

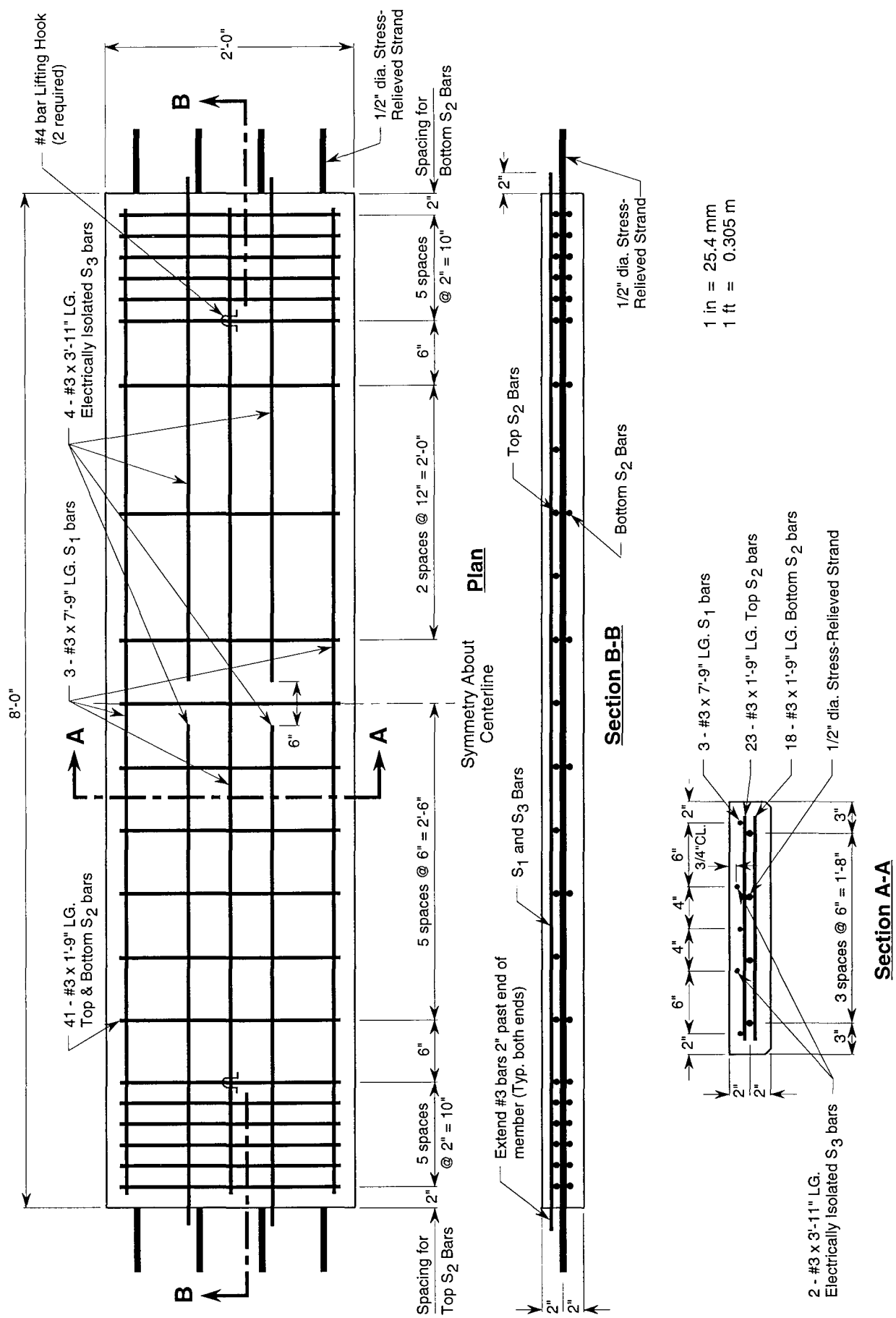


Figure 2. Design details for pretensioned concrete slab specimens.

Pre-Tensioned Concrete Piles

Pre-tensioned concrete pile specimens were 2.4 m (8 ft) long and 355 by 355 mm (14 by 14 in) in cross section as shown in Figure 3. The piles contained six 12-mm (0.5-in), grade 270 low-relaxation seven-wire prestressing strands. The magnitude of force in each strand prior to prestress transfer was 75% of the GUTS or approximately 137,800 N (30,980 lbf). All strands were straight and were subsequently cut flush with the bottom end and protruded approximately 200 mm (8 in) from the top of the piles. The piles also contained spiral reinforcement along the length of the pile and additional plain steel reinforcement at both ends as shown in Figure 3. A single electrically isolated plain steel bar was placed along the central axis of the piles; however, this was not used, as no macrocell measurements were conducted on the piles. A total of five such piles were constructed.

Multi-Strand Post-Tensioned Elements

Post-tensioned concrete beam elements were 3.6 m (12 ft) long and 355 by 355 mm (14 by 14 in) in cross section as shown in Figure 4. The beams contained five 15-mm (0.6-in), grade 270 low-relaxation wire strands. After fabrication of the concrete beams, they were transported to the test laboratories where the strands were tensioned to a total of 1,040,840 N (234,000 lbf). All five strands were anchored with three-piece wedges inside an anchor plate at each end. Ducts consisted of corrugated metal tubes 50 mm (2 in) in diameter. A cement paste grout having a w/c of 0.42 and containing a proprietary grout intrusion aid was used to fill the duct and end pocket. The multi-strand specimens also contained tie reinforcement along the length of the beam and plain longitudinal steel reinforcement as shown in Figure 4. A total of two such beams were constructed.

Threadbar Post-Tensioned Elements

Post-tensioned concrete beam elements were 3.6 m (12 ft) long and 355 by 355 mm (14 by 14 in) in cross section as shown in Figure 5. The beams contained a single 35-mm (1.375-in), grade 150 bar that was threaded at both ends, allowing for anchorage to end plates. After fabrication of the concrete beams, they were transported to the test laboratories where the strands were tensioned to a total of 667,200 N (150,000 lbf). Ducts consisted of corrugated metal tubes 50 mm (2 in) in diameter. A cement paste grout having a w/c of 0.42 and containing a proprietary grout intrusion aid was used to fill the duct and end pocket.

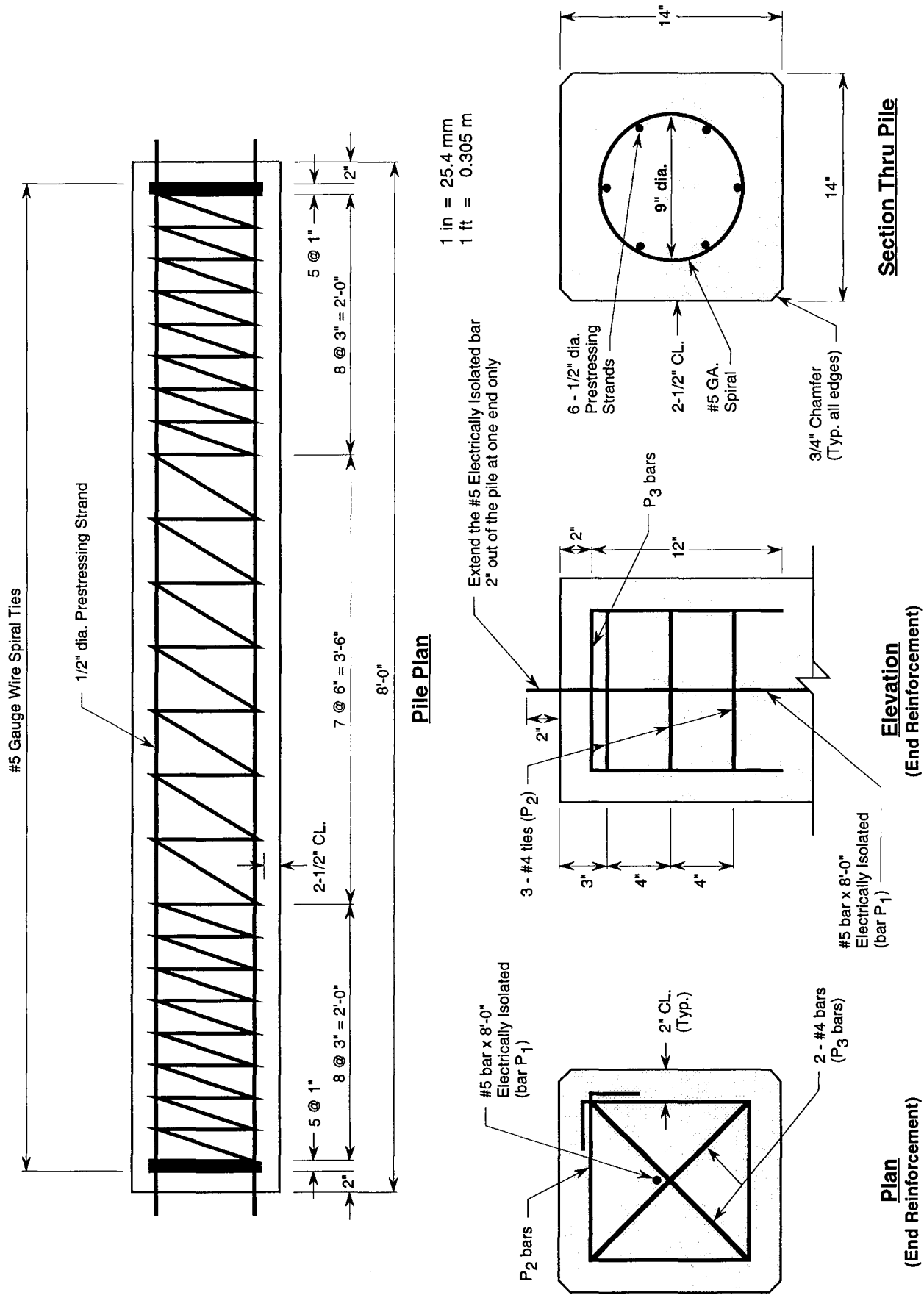


Figure 3. Design details for pretensioned concrete piles.

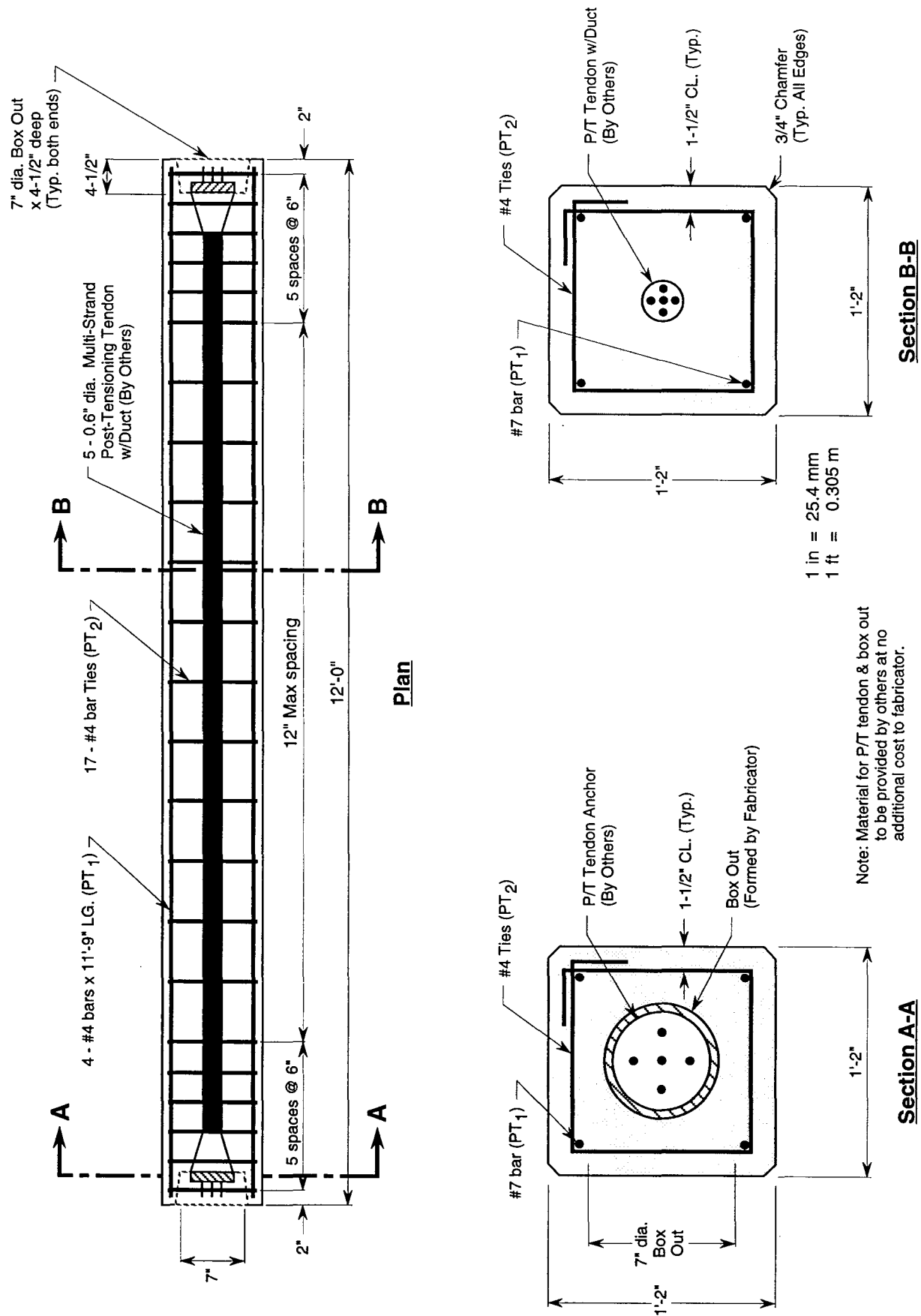


Figure 4. Design details for multi-strand post-tensioned concrete beam specimens.

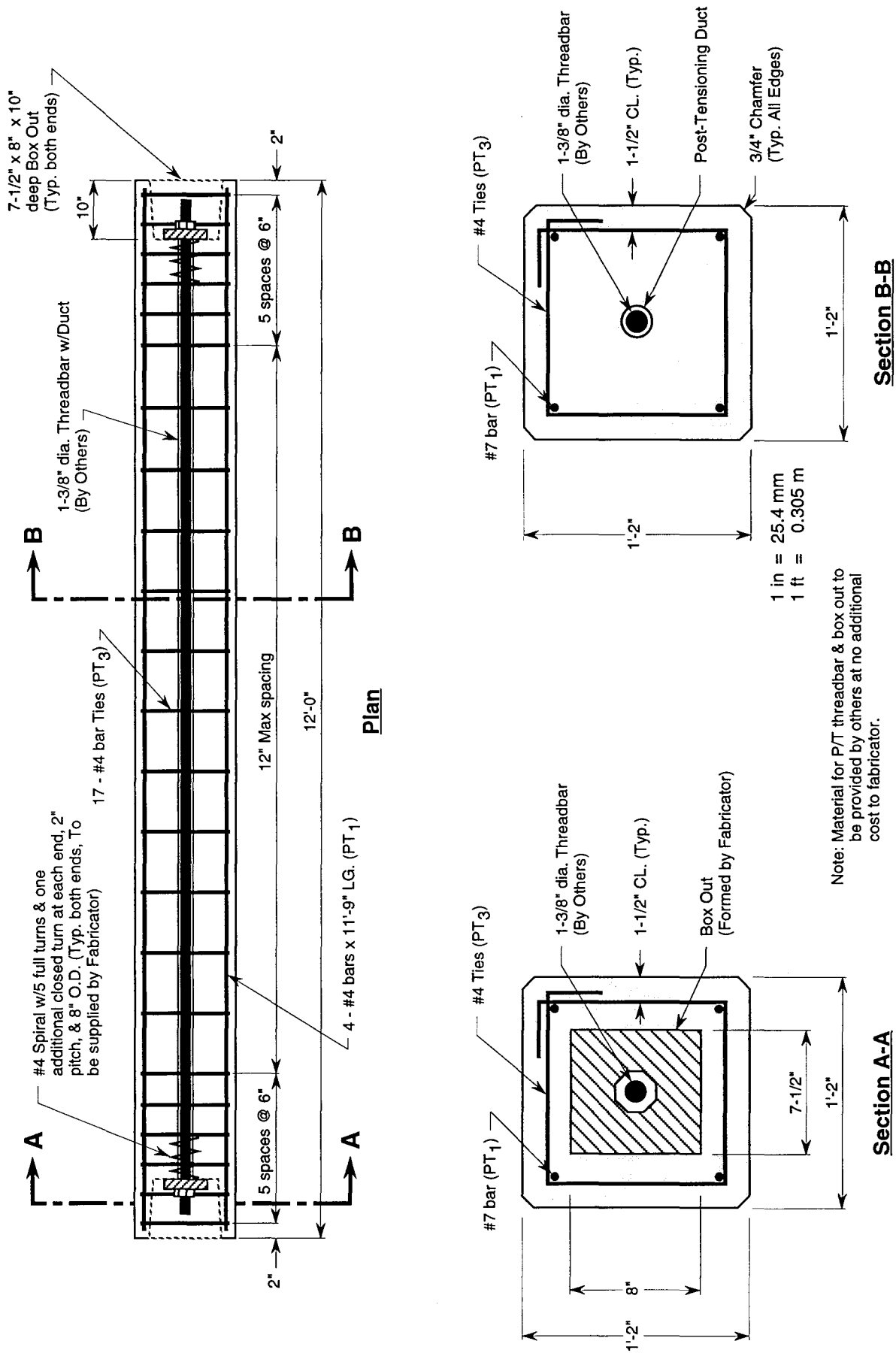


Figure 5. Design details for threadbar post-tensioned concrete beam specimens.

The threadbar specimens also contained tie reinforcement along the length of the beam and plain longitudinal steel reinforcement as shown in Figure 5. A total of two such beams were constructed.

Specimen Preparation

All specimens were cast at a local precasting facility. The post-tensioning was done at the test laboratories, while pretensioning was done at the precast facility. Steel placement was set by the fabricator and verified by the investigators. Electrical connections were made to the reinforcing steel, and electrical continuity of the reinforcing bars to the pretensioning strands was verified. Permanent electrical connections were made to the continuous reinforcement and to the isolated macrocell bars, and lead wires were run through the forms to the outside. All slabs and beams were cast on a single day using a total of nine batches of concrete. Pilings were cast approximately 3 weeks later using a total of five batches of concrete.

Materials used for the concrete mixes consisted of: (1) Type III portland cement, (2) a natural sand (Illinois FA-2), and (3) a crushed limestone having a maximum topsize of 12 mm (1/2 in). Admixtures included: (1) a Type F high-range water reducer and (2) a Vinsol[®] resin-based air-entraining admixture. The concrete mix design is shown in Table 1. Slumps ranged from 64 to 114 mm (2.5 to 4.5 in). Air content ranged from 5.0 to 7.5 percent. Required compressive strengths were 27.5 MPa (4000 lbf/in²) for release of tendons, and 34.4 MPa (5000 lbf/in²) after 28 days of moisture curing. Strengths achieved for each casting are given in Table 2.

Table 1. Mix proportions used for precast concretes (yd³ basis).

Material	Amount
Cement - lb	660
Coarse Aggregate - lb	1820
Fine Aggregate - lb	1260
Water - lb	258
HRWR - fl oz	80
AE Admixture - fl oz	6

1 lb = 0.454 kg, 1 fl oz = 29.57 mL, 1 yd³ = 0.765 m³

Table 2. Strength of precast concretes.

Specimen Casting	Release Strength - lbf/in ²	28 Day Strength - lbf/in ²
Beams	5480	6720
Slabs	4200	6540
Piles	5660	6720

$$1 \text{ lbf/in}^2 = 0.0069 \text{ MPa}$$

INITIATION OF CORROSION

Specimen Exposures

After curing, specimens were transported to the laboratory where indoor exposures were scheduled. While the large lab space was heated in the winter months to prevent freezing, no climate control as such was available in this area. Therefore, over the 4 years of exposure, temperature extremes ranged from near 16°C (60°F) during the late Fall to near 32°C (90°F) on a few hot summer days. Post-tensioning hardware was installed, and post-tensioning procedures were carried out in this laboratory. Setup of the specimens within the allocated space is shown in Figure 6. At this point, salt spray and immersion systems were fabricated to allow exposure of the specimens to different configurations of chloride exposure. Spray bars, tanks, and other hardware were tested using tapwater; however, no exposure to saltwater was carried out prior to the electrical acceleration of chloride ingress described in the next section of this report. The concepts for each exposure are shown in Figures 7, 8, and 9 for slab and American Association of State Highway and Transportation Officials (AASHTO) beam soffits, AASHTO and post-tensioned beam ends, and piles, respectively. The soffit exposures (Figure 7) represent marine conditions where salt spray primarily contacts the undersides of beams and decks. Here the entire underside was sprayed with a 15% sodium chloride solution, except for approx. 200 mm (8 in) on either end where the beams were supported on a stack of masonry block units. The beam end exposures (Figure 8) represent deicing applications where salt solutions leak through joints and run down the beam ends at the anchorages. Here, the spray was confined to areas 200 mm (8 in) from each end of the beam. Finally, 380-L (100-gal) high-density polyethylene tanks were used to hold the prestressed piles. The tidal cycle was programmed to allow for two cycles per 24-hour period, the

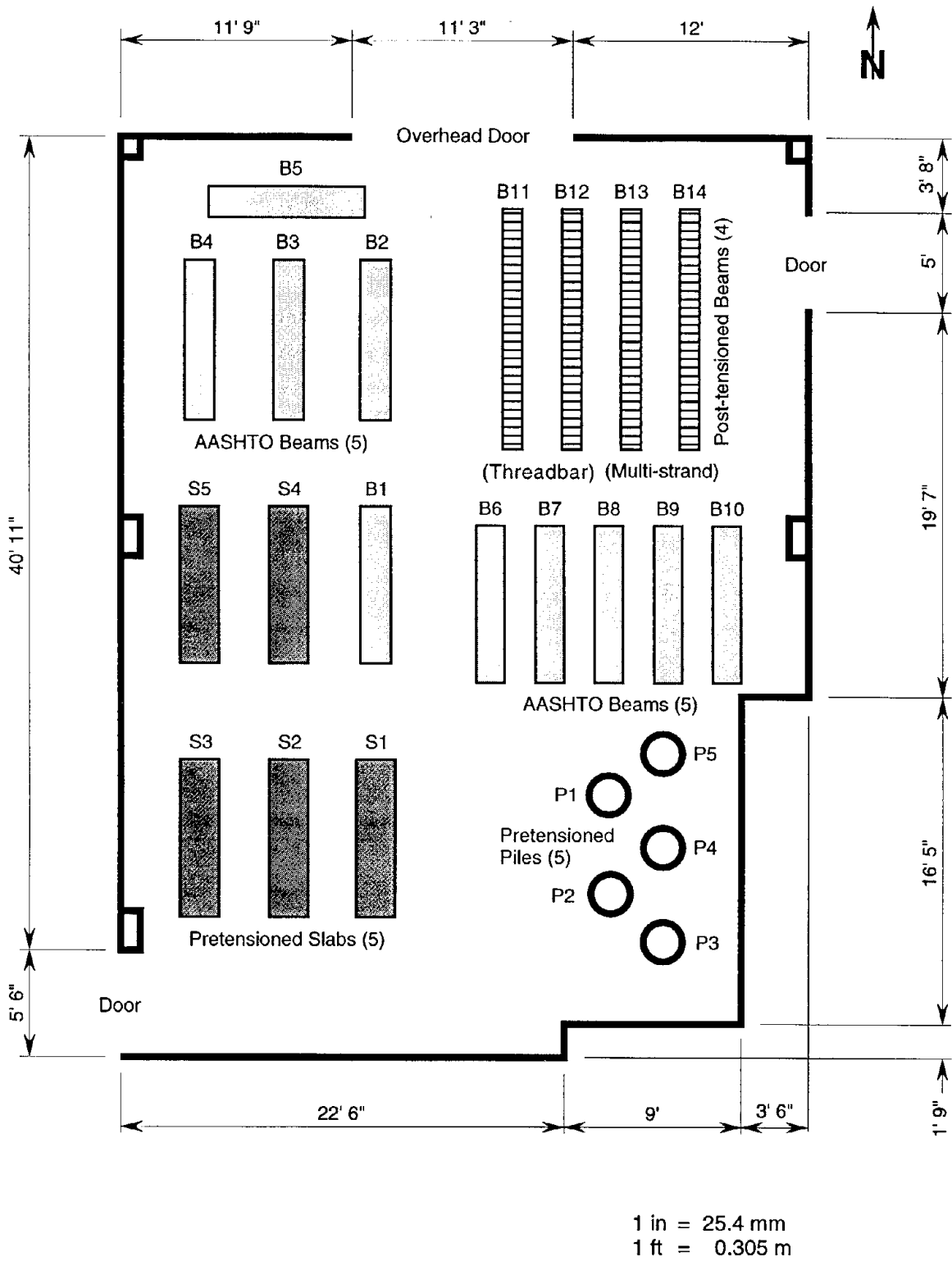


Figure 6. Arrangement of test specimens in laboratory.

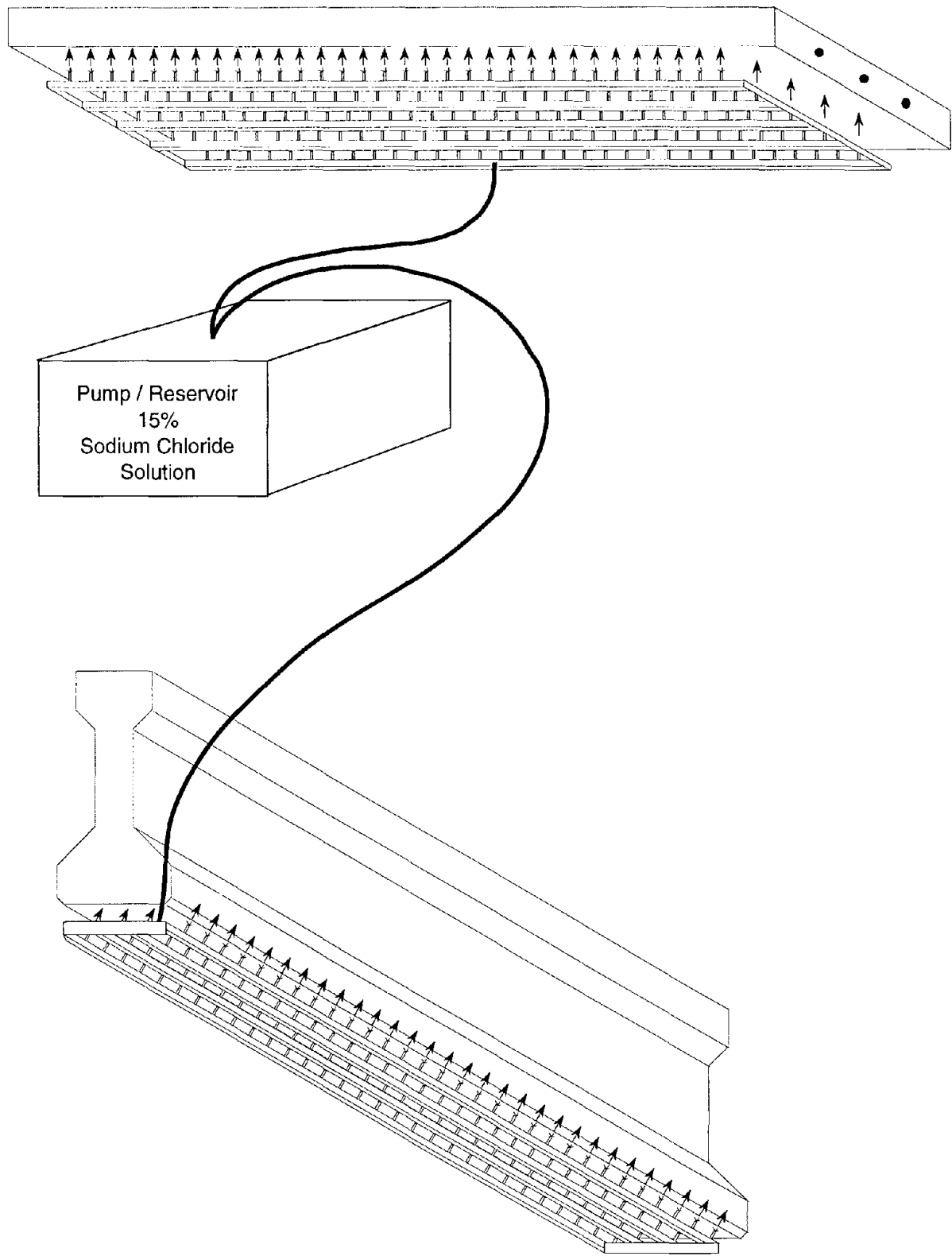


Figure 7. Splash system for exposure of soffits of AASHTO beams and pretensioned slabs.

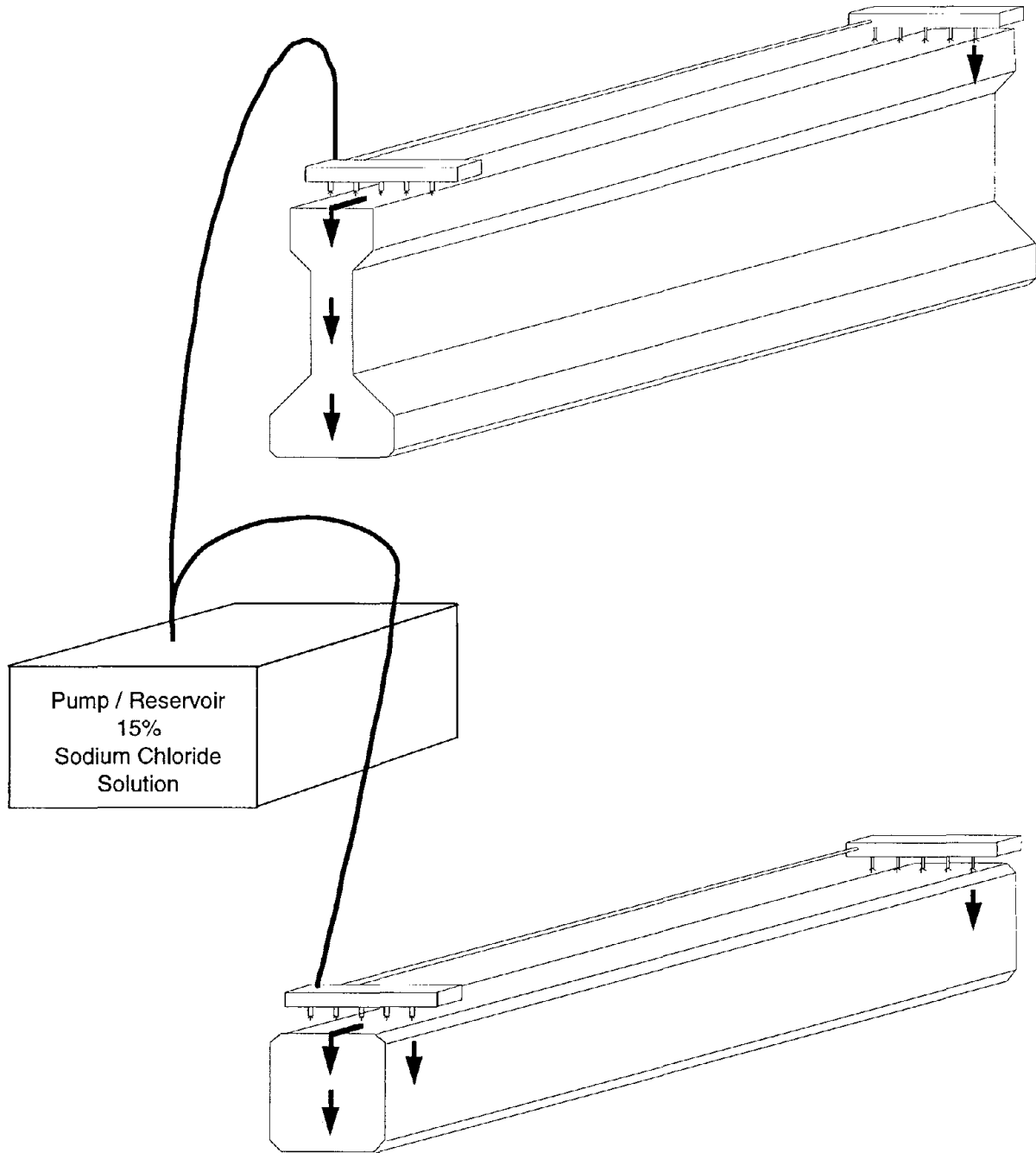


Figure 8. Spray applications of sodium chloride solutions at beam ends.

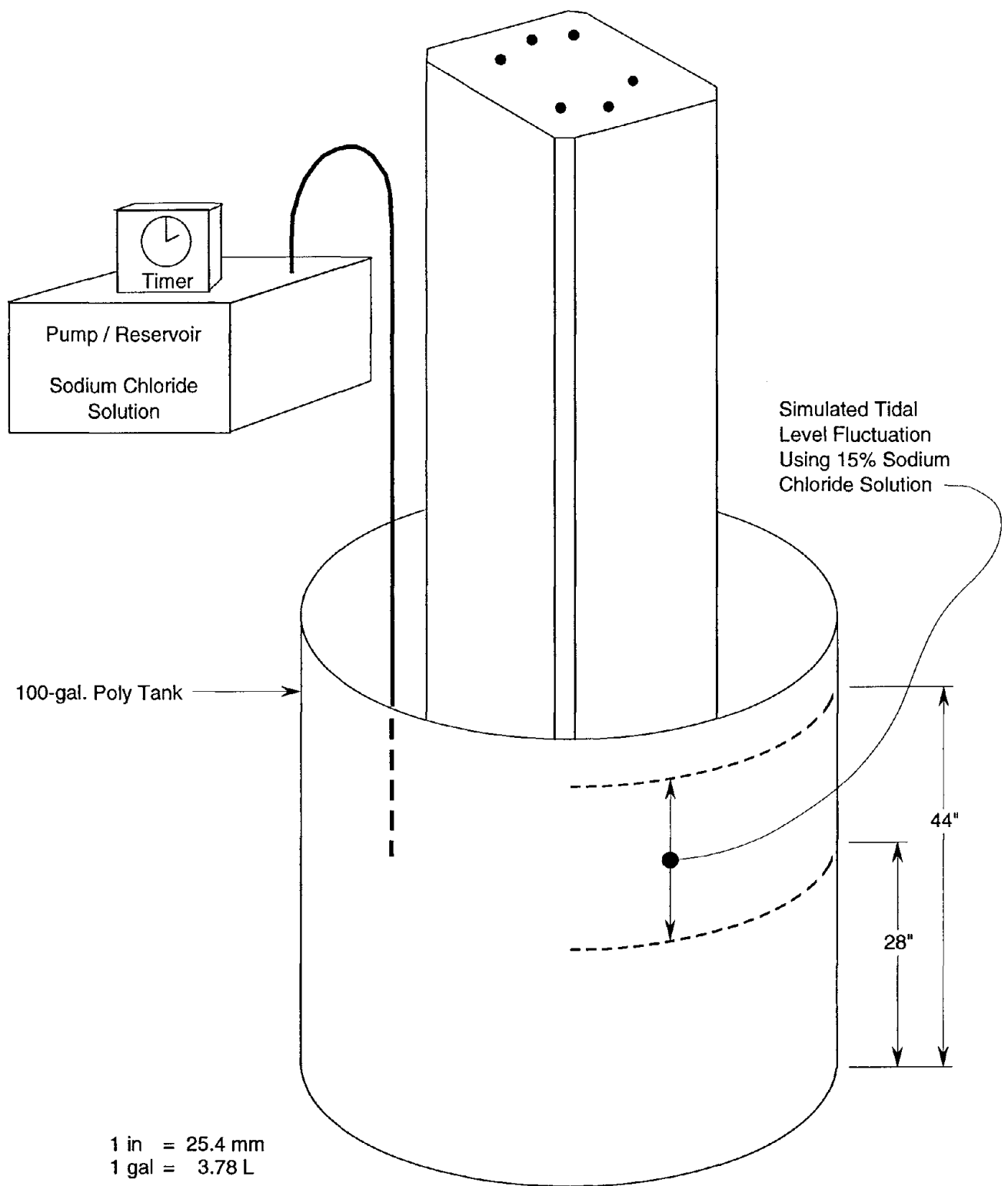


Figure 9. Tanks for simulation of marine tidal exposure for pretensioned piles.

tidal zone extending from 710 to 1110 mm (28 to 44 in) from the bottom of each pile, as shown in Figure 9. Those portions of the pile below this zone were continuously immersed in saline solution; those portions above this zone were atmospherically exposed.

Acceleration of Corrosion

As the overall objective of the project was to study the effects of conventional repairs on protecting prestressed elements from corrosion, it was necessary to rapidly induce corrosion in the model elements. Repairs could then be made and resubjected to corrosive conditions so performance could then be monitored within the time period allocated to the research program. It was felt that accelerated ingress of a 15% sodium chloride solution would be needed to establish corrosive conditions at the level of the tendons, which was at least 37 mm (1.5 in) below the exposed surface for slabs and beams and 64 mm (2.5 in) for the prestressed piles.

It was known from a previous FHWA study⁽⁴⁾ that chloride could be forced to migrate into concrete under the influence of an applied electrical field. However, as the objective of these early studies was to develop a rapid test procedure for chloride permeability, very high current densities of 5000 to 10,000 mA/m² (500 to 1000 mA/ft²) were used. It was felt that such high levels of current, when applied to the full-scale specimens, might generate large amounts of heat and cause unwanted damage to the specimens. More recent work in the area of electrochemical chloride removal^(5,6) has demonstrated that significant amounts of chloride may be removed from concrete under current densities between 1000 and 5000 mA/m² (100 to 500 mA/ft²) provided that sufficient time is allowed for the removal to occur. In principle, the same parameters should apply to chloride ingress, since it is necessary only to reverse the polarity to accomplish the desired effect.

In order to evaluate the time and current densities needed to accelerate chloride migration to the level of the steel, three additional 0.3- by 0.6-m (1- by 2-ft) reinforced concrete slabs containing unstressed 12-mm- (0.5-in-) dia. seven-wire strands were prepared. Tendon size and concrete cover were kept the same as for the actual specimens. A concrete mix using a Type III cement content of 392 kg/m³ (660 lb/yd³), similar to the one used in full-scale specimens, was employed. In order to monitor the strength gain of slabs and define the time to start the test, test cylinders were cast from the same concrete and cured under moist conditions. When the concrete reached a strength of 34 MPa (5000 lbf/in²), slabs were demolded and moved to the testing area. Sides of the slabs were coated with epoxy to prevent drying in the lateral direction. Two small brass plates were affixed to the surface of each slab with gel epoxy to serve as primary cathodes. The slabs

were then ponded with a 15% solution of sodium chloride, and current densities of 700, 1400, and 2500 mA/m² (70, 140, and 250 mA/ft²) were applied. After 3 weeks, cracks had developed in the surface of the slab subjected to the highest current, and corrosion products could be seen exuding from the surface. Corrosion products also were seen to be exuding from the locations at which tendons passed through the sides of the slabs. This slab was taken out of service and samples were taken for analysis of chloride profiles. Chloride contents ranged from 0.2 to 0.3% by weight of concrete, well within corrosive levels.⁽⁷⁾ The slab was broken open, and significant amounts of corrosion were observed on the embedded tendons. After 6 weeks, the slab subjected to 1400 mA/m² (140 mA/ft²) was exuding corrosion products, and cracks had propagated to the slab surface. Chloride analyses detected a level of 0.5 to 1% chloride at the strand. After 10 weeks, the current applied to the remaining slab was discontinued, and the specimen was examined. As with the previous runs at higher current levels, large amounts of chloride were found to have migrated to the steel. In this case, chloride levels at the strands ranged from 0.7 to 1.2%. Total charge passed through the slab surface over the 10-week period was approximately 235 Amp-h. Based on the results of these tests, a current density of 700 mA/m² (70 mA/ft²) was selected for acceleration of chloride into the actual test specimens, as the desired results could be achieved at this lower level of current.

Plans were made for acceleration of chlorides into the piles, slab soffits, and beam soffits that had been scheduled for salt-spray application. For those specimens where salt spray was to be applied to beam ends only, no electrical acceleration of chloride ingress was carried out, as it was felt that the flow of current might drive chloride into other areas of the specimens where it was not intended to penetrate. This included five of the AASHTO pretensioned beams and the four post-tensioned specimens. These were exposed to the 15% NaCl spray only. For the remaining specimens, expanded wire mesh was affixed to the soffits of the beam and slabs and the exterior surface of the piles that lie at and below the upper limit of the tidal zone. Surfaces were then sprayed (immersed in the case of the piles) with 15% NaCl and the voltage was adjusted to achieve the desired current density of 700 mA/m² (70 mA/ft²). Voltages required to achieve this current were close to 6 V dc. It should be noted that the application of current was staggered for the three specimen types. The slabs were treated first, followed by the AASHTO beams, and finally the piles in the tidal exposure. Beams and piles were undergoing non-accelerated exposure to 15% NaCl at the same time that current was being impressed on the slabs.

There was a distinction made between two categories of specimens that were exposed to electrical acceleration of chloride ingress. Those specimens placed in "Category A" were scheduled for evaluation of patch-type repairs, normally carried out when concrete has suffered a significant

degree of distress in the form of cracking, spalling, etc. Specimens numbered 1, 2, and 3 (beams 1, 2, and 3 and slabs 1, 2, and 3) were assigned to Category A. Those specimens placed in "Category B" of each set were scheduled for application of sealers and coatings, which often are applied to existing field structures that have been exposed to corrosive environments for a period of time, but have not yet exhibited distress. Specimens numbered 4 and 5 (beams 4 and 5 as well as slabs 4 and 5) were placed in Category B. Accordingly, the objective of acceleration of chloride ingress in Category B specimens was simply to migrate a significant amount of chloride into the concrete, while the objective for the Category A specimens was to both induce corrosion on the embedded metals and to allow for cracking and spalling of the concrete.

Chloride drill samples were taken at various times during the application of current as an aid in determining the exact length of the acceleration process. Final chloride profiles, immediately after application of electrical current was discontinued, are shown in Figure 10. Results are shown as the average of samples taken at two positions on two specimens from each set of slabs, beams, and piles. The periods of application of electrical current, in weeks, are shown on the figure. All chloride contents are at, or above, corrosion threshold at the level of the tendons. It should be noted that actual average clear covers over tendons are shown, which deviated somewhat from the design cover shown in the plans (Figures 1 through 3). Application of anodic electrical current to slabs and beams was discontinued after 2 and 3 weeks, respectively. Half-cell readings taken a few days after cessation of applied voltage were in the range of -400 to -500 mV vs. CSE (Copper/Copper Sulfate reference electrode) for slabs and beams and -500 to -700 mV vs. CSE for pilings. The more electronegative values for pilings were likely due to the submerged condition restricting oxygen flow to the cathodes of the corrosion cells. At this time, considerable amounts of corrosion products could be seen exuding from holes drilled for plastic inserts used to affix the cathode mesh to the slab and beam surfaces. These half-cell data, the chloride contents, and the presence of corrosion products exuding from the ends of the tendons all indicated that the steel was indeed in a corrosive condition.

It was felt that further application of current would simply convert steel into these liquid corrosion products, and would fail to generate crack and spall-inducing stresses in the specimen. The mesh was removed and specimens 1, 2, and 3 of each set were re-subjected to the "natural" spray application of salt solution. Specimens 4 and 5 were allowed to dry and were prepared for application of coatings and sealers. After 5 months of additional salt spray, slab and beam specimens 1, 2, and 3 were re-examined. Other than a few small tight cracks, no signs of distress to the concrete due to corrosion of tendons were noted. In addition, sounding of the concrete indicated it to be in good condition, with no evidence of hollow areas or delaminations. Reasons

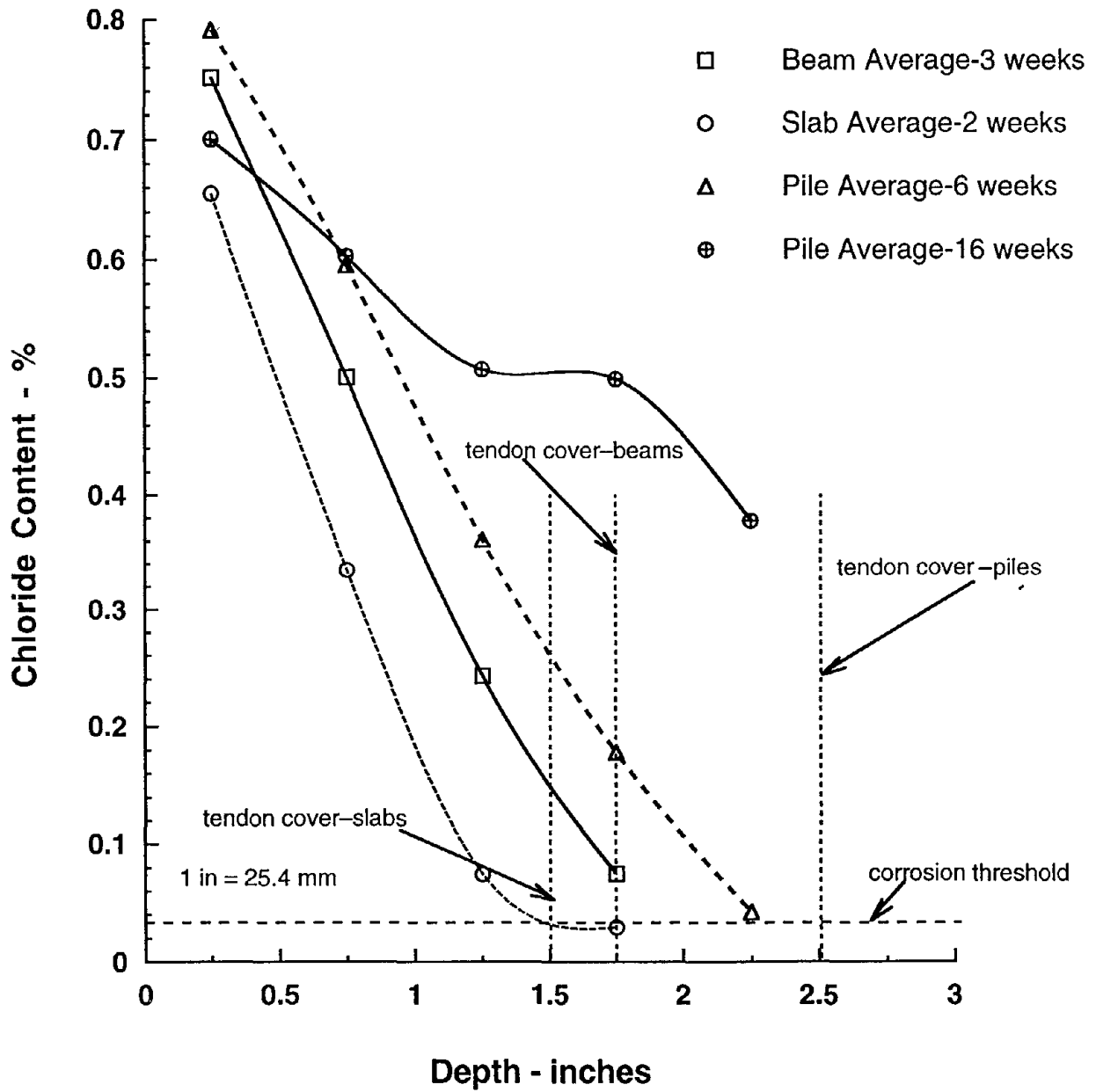
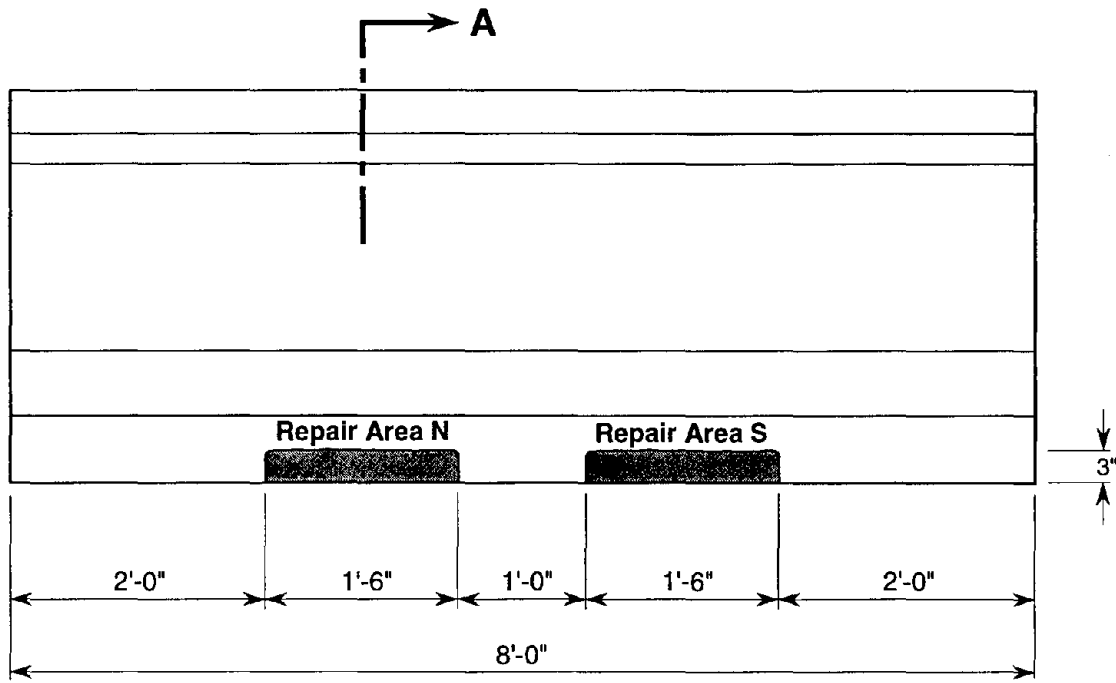


Figure 10. Average chloride contents measured on specimens after electrical acceleration.

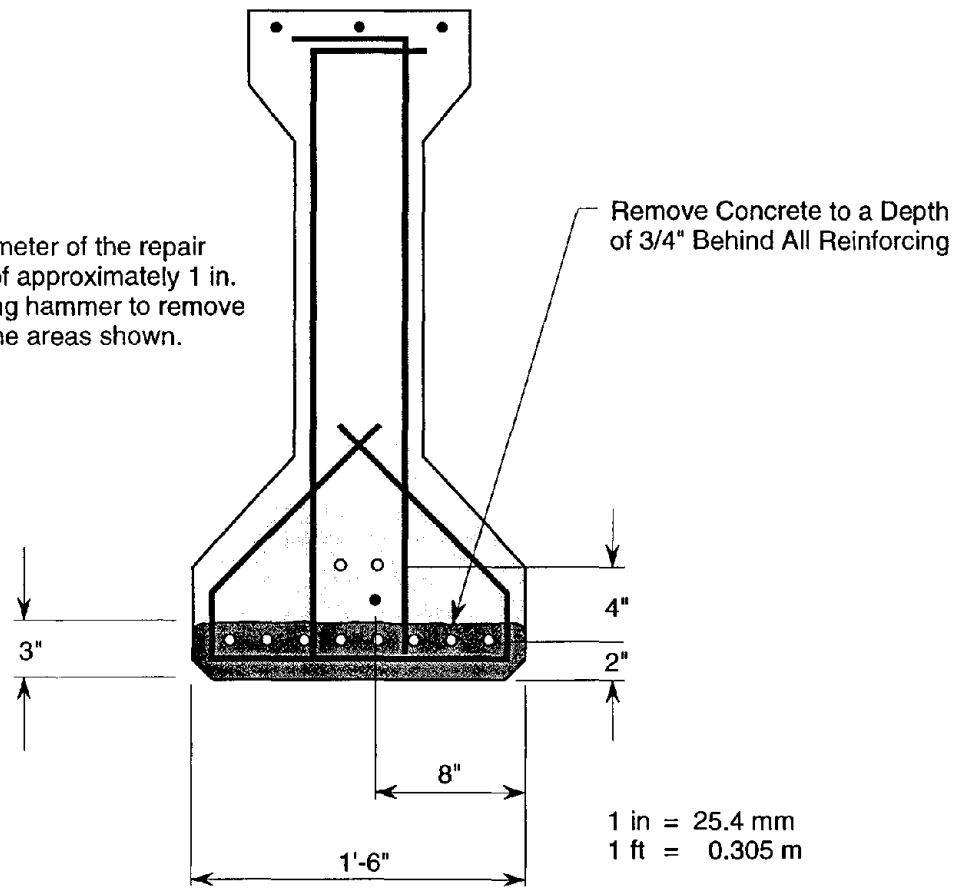
for the failure to induce any distress in the concrete included the following possibilities: (1) prestress force had prevented the corrosion reaction from exerting sufficient tensile stress on the concrete to create spalls and cracks, (2) the anodic chloride acceleration technique created corrosion products with different physical characteristics than corrosion products formed by chloride ions naturally diffusing through concrete, and (3) holes for plastic inserts drilled into the specimens in order to anchor the mesh used to apply current may have served as pathways for relief of pressure generated by corrosion products (during the anodic application, "stalactites" of corrosion products were observed growing down from some of these anchors).

While application of anodic current had induced corrosion of embedded prestressed and plain reinforcement as planned, the amount of concrete distress necessary to allow for repairs to be made had not occurred. It was necessary, therefore, to artificially create spalls in the concrete that could then accept the repair materials. The spalls were made by cutting around the desired repair area with a concrete saw to a depth of 12 to 25 mm (1/2 to 1 in), then chipping out the concrete to a level of 19 mm (3/4 in) behind the tendons. Two repair areas were created on each specimen. These were denoted by their location on the specimens relative to the position of the specimens in the test room, either north (Area N) or south (Area S). Drawings showing location, size, and detailing of each repair are included as Figures 11 through 14.

No repair areas were created on nine beam end specimens (four post-tensioned and five pretensioned AASHTO beams) at this point since, as noted earlier, anodic current could not be confined adequately on these specimens and no acceleration of chloride ingress was carried out in this case. These non-repaired specimens were exposed to the salt spray for a period of approximately 8 additional months after repairs had been carried out on the soffits of slabs and beams and the piles. Penetration of chloride was very slow under the non-accelerated conditions, and chloride contents did not exceed corrosion threshold amounts at the level of the tendons. In addition, maintenance problems continued with salt-spray systems applied to the ends of these specimens. Clogging of spray lines and filters prevented uniform application of spray to all specimens. Pump failures and other disruptions of operations led to discontinuance of the salt spray exposure on these specimens. For these reasons, these nine specimens were moved to outdoor long-term storage after 64 weeks of indoor salt-spray exposure. However, distress was slow to develop under these conditions, and time did not permit application and monitoring of repairs to these nine specimens within the time limit of the research program.



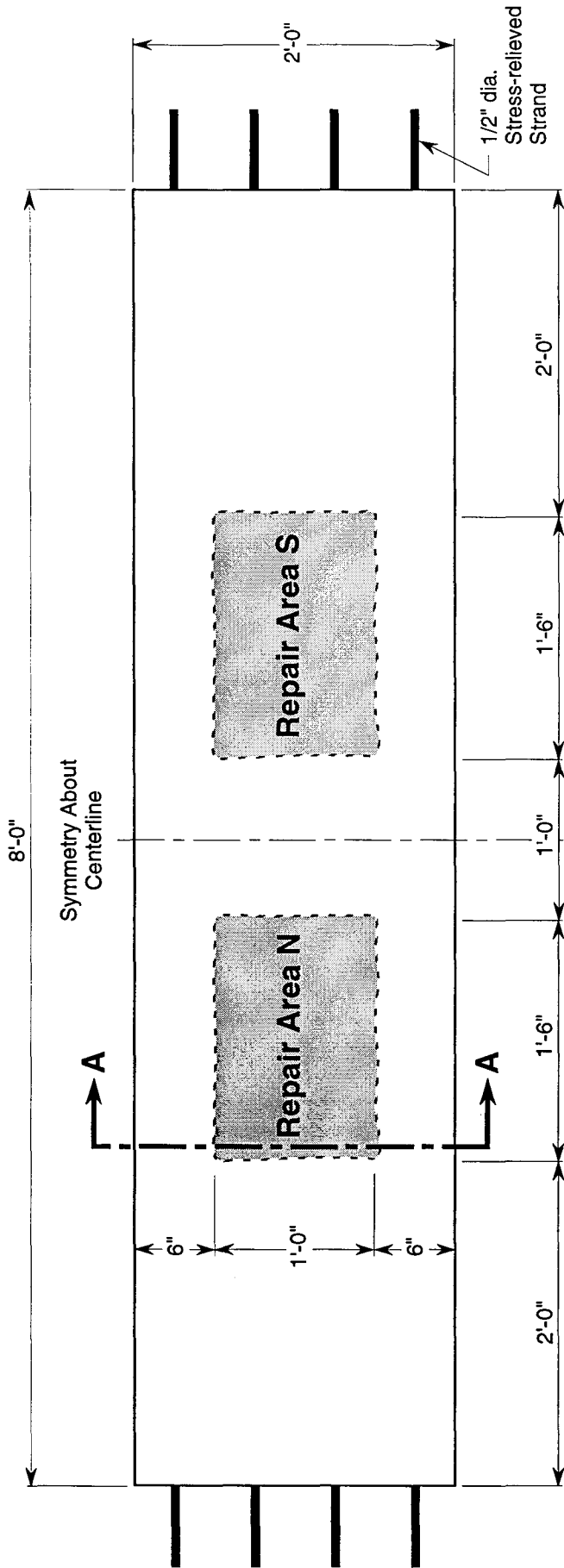
Note: Saw cut the perimeter of the repair area to a depth of approximately 1 in. Then use chipping hammer to remove the concrete in the areas shown.



1 in = 25.4 mm
1 ft = 0.305 m

Section A

Figure 11. Repair area details for pretensioned beam specimens.



Plan

Remove Concrete to a Depth of 3/4" Behind All Reinforcing

Note: Saw cut the perimeter of the repair area to a depth of approximately 1 in. Then use chipping hammer to remove the concrete in the areas shown.

1 in = 25.4 mm
1 ft = 0.305 m

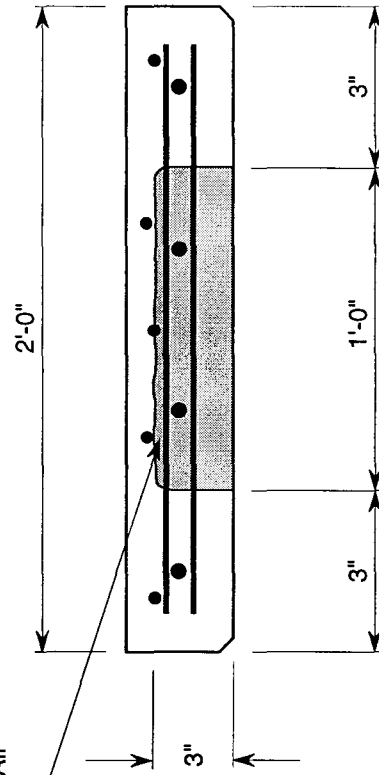


Figure 12. Repair area details for pretensioned slab specimens.

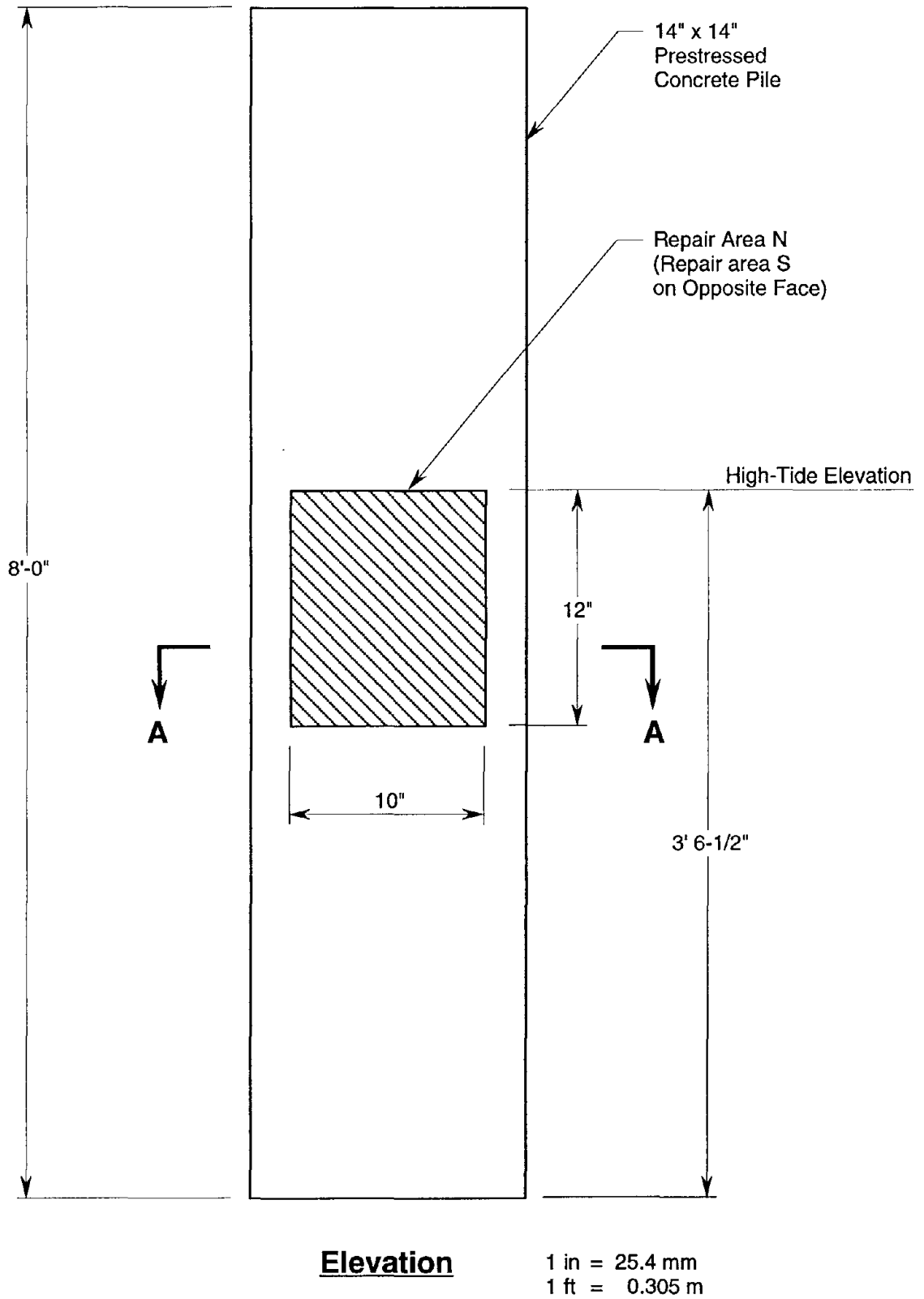
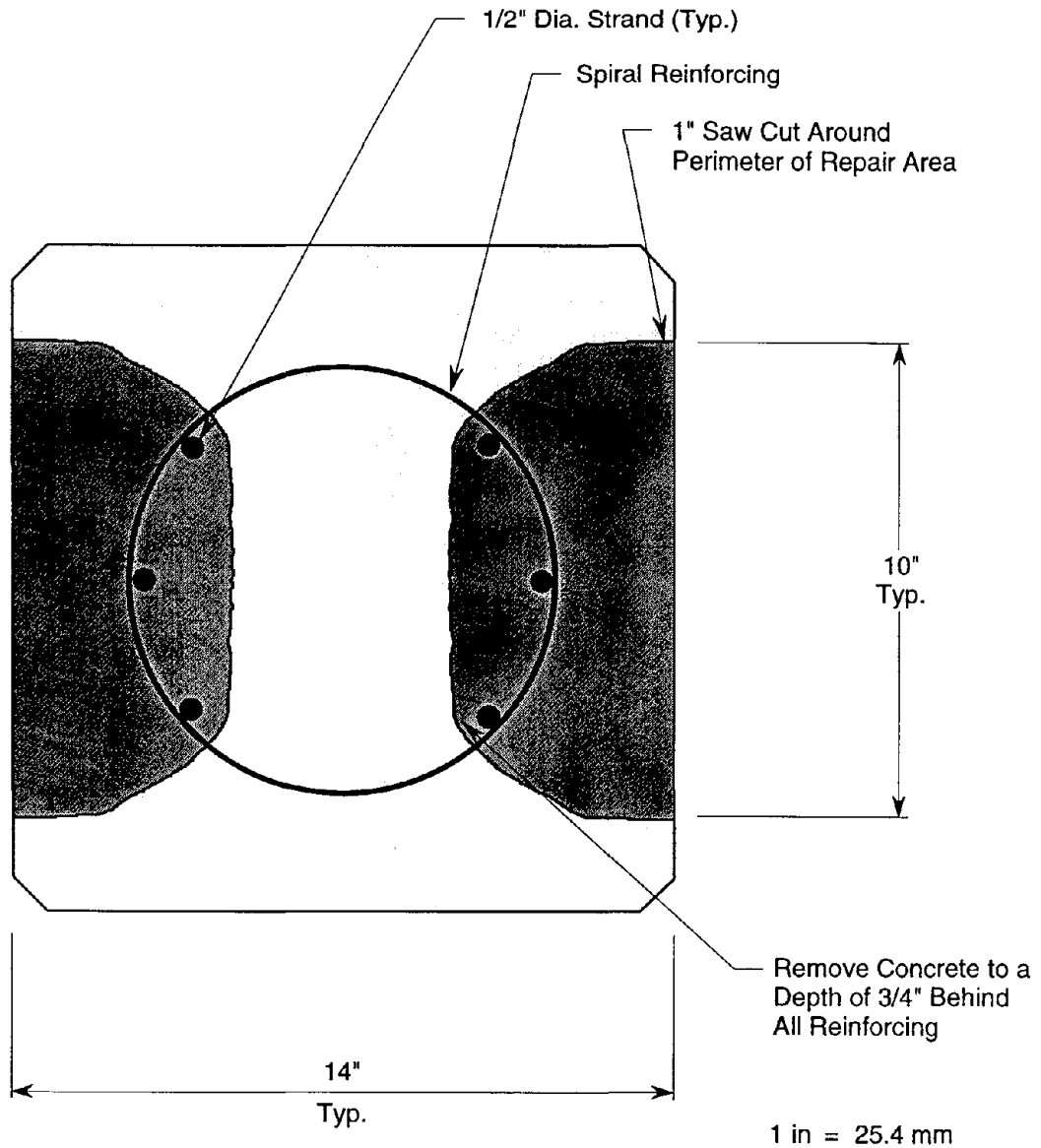


Figure 13. Elevation view of repair area details for pretensioned pile specimens.



Section A-A

Note: Saw cut the perimeter of the repair area to a depth of approximately 3/4". Then use a chipping hammer to remove the concrete in the area shown.

Figure 14. Plan view of repair area details for pretensioned pile specimens.

REPAIR PROCEDURES

Test Plan and Materials

Two categories of rehabilitation for prestressed concrete structural members were evaluated under this program. These were categorized as:

- Category A - Those repairs where portions of the concrete section are removed and replaced with some type of patching material. This category would be used when significant amounts of concrete had cracked or spalled and repairs were necessary for safety considerations or continuity of operations. Category A remedial actions normally consist of the following sequence:
 - Removal of deteriorated, chloride-contaminated concrete back to sound concrete and around embedded reinforcement and prestressing steel.
 - Sandblasting of concrete surfaces and exposed steel in the repair area. Normally, steel is sandblasted at the same time as concrete and corrosion products are removed.
 - Coating of prestressing steel and plain reinforcement.
 - Installation of repair material.
- Category B - Those repairs where no concrete removal is performed. This category would be used, for instance, on structures in aggressive environments, either as an initial treatment or where the structure had been exposed for some period of time, but no significant distress had occurred. Typically, category B treatments would consist of sealing or coating of the concrete after sandblasting of the surface.

For Category A, three types of patching materials were included. These were: (1) a conventional repair concrete (no special admixtures) mix containing a "pea-gravel" coarse aggregate with a 9-mm (0.375-in) topsiize that could be applied either by hand placement or shotcreting, (2) a proprietary fiber-reinforced, acrylic latex-modified mortar extended with 40% pea gravel aggregate, and (3) silica fume concrete containing a corrosion inhibitor. Two types of corrosion inhibitors, an organic amine-based product and a calcium nitrite inhibitor, were tested. Two types of coatings for embedded steel were also used. These were: (1) a two-part room-temperature cure, field-applied liquid epoxy coating; and (2) a single-component liquid epoxy zinc-rich primer. Both materials are commonly used for coating of exposed reinforcing steel during

rich primer. Both materials are commonly used for coating of exposed reinforcing steel during concrete repairs. For the purposes of this report, they will be referred to as "epoxy" and "zinc" coatings. However, it should be noted that these materials are not the same as fusion-bonded epoxy or hot-dipped galvanized zinc coatings applied to new reinforcing steel under factory conditions. Assignment of repair materials to particular specimens is given in Table 3. Patches are denoted N (north) or S (south), reflecting the orientation in the test area.

Table 3. Assignment of repair materials to test specimens.

Steel Coating	Repair Concrete			
	Conventional	Polymer Modified	Inorganic Inhibitor	Silica Fume Organic Inhibitor
2-Part Epoxy	S1N, B1N, P3N	S2N, B2N, P2N	B3N, P1N	S3N
Zinc-Rich Primer	S1S, B1S, P3S	S2S, B2S, P2S	B3S, P1S	S3S

N – north patch on specimen

S – south patch on specimen

Four materials were selected for the category B surface applications. These were: (1) a two-component marine-grade epoxy coating utilizing an epichlorohydrin/bisphenol A base resin and polyaliphatic amine curing agent; (2) a 40% solution of an alkyltrialkoxo silane (ATS) in isopropanol; (3) a 20% solution of an oligomeric alkyl-alkoxy siloxane (AAS) in a blend of naphtha and diacetone; and (4) a two-component clear penetrating sealer consisting of a primer containing a 20% solution of an oligomeric alkoxy siloxane/silane in mineral spirits and a topcoat consisting of a solution of methyl methacrylate in xylene (AS/MM). Assignments of materials to specific specimens are given in Table 4.

Table 4. Assignment of coatings/sealers to test specimens.

Coating/Sealer	Specimen Type		
	Piles	Slabs	Beams
2-Part Epoxy		S4	
40% ATS	P4		B5
20% AAS	P5	S5	
2-component AS/MM			B4

Repair Applications

Category A (Patch Repairs). Category A specimens were oriented so that all repairs could be carried out on horizontal surfaces. Repair area dimensions were marked on each specimen as previously shown in Figures 11 through 14. A masonry saw was used to cut around each area to a depth of about 12 to 25 mm (1/2 to 1 in). The saw was also used to make a series of cuts inside each area to allow for easier removal of the concrete by chipping. A small 2-kg (5-lb) air-powered chipping hammer was then used to chip out each area and to leave a clearance of about 19 mm (3/4 in) behind all tendons running through the area. While all tendons were adequately exposed, some plain reinforcement was partially uncovered at the back of some of the patches. This steel was not fully chipped out because exposure of this steel would have resulted in an unusually deep patch and might have damaged the members. Tendons did show evidence of corrosion rust staining and fractures in a few of the wires. The plain reinforcement appeared to be more heavily corroded than the pretensioned steel. After all chipping had been completed, all exposed concrete and steel surfaces were sandblasted to remove corrosion products and to prepare the surfaces for patch materials. While steel was blasted to clean metal, no particular profiling was done, such as is used when preparing metal surfaces for installation of protective coatings.

Exposed steel in the repair areas at the north end of the specimens (Area N) was coated with the two-part liquid epoxy repair material. Exposed steel in the repair areas at the south end of the specimens (Area S) was coated with the zinc-rich liquid epoxy coating. After the coatings had cured, placement of repair materials was initiated. Mixture designs and properties for the conventional and silica fume concretes are given in Tables 5, 6, and 7. The proprietary acrylic latex-modified concrete was prepared using a 22.7-kg (50-lb) bag of dry product, 3.8 L (1 gal) of liquid acrylic polymer, and 9.1 kg (20 lb) of dry 9-mm (0.375-in) coarse aggregate. All materials were mixed in a countercurrent laboratory pan mixer. A bond coat was scrubbed onto the concrete in each area just prior to placement of the repair mix. This consisted of a plain cement grout for the conventional repair concrete, a latex cement grout for the latex concrete, and a cement/silica fume grout containing corrosion inhibitor for the silica fume concretes. Placement was done by tamping of the concretes into the repair areas. Areas were struck off with a wood float and finished with a magnesium float. All conventional and silica fume repair areas were moist cured under wet burlap covered by polyethylene sheeting for 3 days. Latex-modified concrete repair areas were moist cured for 1 day, then exposed to laboratory air, as is common practice for latex-based materials. After all repairs had cured, specimens were returned to their previous

Table 5. Properties and proportions for conventional concrete mixture used for category A repairs.

FRESH CONCRETE PROPERTIES			
Contract Number	50329	Slump	2.75 in
Mix Number	Conventional	Air Content	5.75%
Date Cast	11.24.93	Measured Unit Weight	144 pcf
Maximum Aggregate Size	3/8 in		

Lab Weights and Equivalent Cubic Yard Weights					
Material	Lot Number	Specific Gravity	SSD Lab Quantity	Lab Volume Cu. Ft.	Batch Quantity per Cu. Yd.
Cement	Type I	3.15	33.9 lb	0.1725	698 lb
Fine Aggregate	Sand	2.64	83.5 lb	0.5069	1720 lb
Coarse Aggregate No. 1	Coarse	2.67	56.3 lb	0.3379	1160 lb
Liquid Admixture No. 1	WR	1.20	25 mL	0.0003	2.49 fl. oz./cwt. cement
Liquid Admixture No. 2	AE	1.01	3 mL	.00001	0.30 fl. oz./cwt. cement
Net Mix Water	Lab	1.00	13.6 lb	0.2179	280 lb

Totals 187.3 1.236 3858 Yield = 26.79

Liquid Admixture Data				
	Brand Name	Type	% Solids	added water-pcy
Liquid Admixture No. 1	WRDA-82	WR	45	0.718
Liquid Admixture No. 2	Darex AEA	air-entrainer	5.75	0.124

Batch Data		
Water-to-Cement Ratio	0.401	(including water in admix.)
Water-to-Cementitious Ratio	0.401	(including water in admix.)
% Fine to Total Aggregate	60.0	%
Air-to-Paste Ratio	0.193	(including mineral admix.)
Paste-to-Aggregate Ratio	0.463	(including mineral admix.)
Percent Paste	35.6	(including mineral admix.)
Calculated Unit Weight	142.9	pcf
Theoretical Air Free Unit Weight	151.6	pcf
Calculated Air Content	5.0	%

- 1 in = 25.4 mm
- 1 lb = 0.454 kg
- 1 °C = (°F - 32)/1.8
- 1 pcf = 0.028 m³
- 1 fl.oz = 29.57 mL
- 1 cu.yd. = 0.7645 m³

Table 6. Properties and proportions for silica fume concrete mixture with inorganic corrosion inhibitor used for category A repairs.

FRESH CONCRETE PROPERTIES			
Contract Number	50329	Slump	3.5 in
Mix Number	Silica fume - inorganic inhibitor	Air Content	5.5%
Date Cast	11.24.93	Measured Unit Weight	145.9 pcf
Maximum Aggregate Size	3/8 in		

Lab Weights and Equivalent Cubic Yard Weights					
Material	Lot Number	Specific Gravity	SSD Lab Quantity	Lab Volume Cu. Ft.	Batch Quantity per Cu. Yd.
Cement	Type I	3.15	31.7 lb	0.1613	661 lb
Mineral Admixture No. 1	Silica Fume	2.20	3.17 lb	0.0231	66 lb
Fine Aggregate	Sand	2.64	67 lb	0.4067	1397 lb
Coarse Aggregate No. 1	Coarse	2.67	72 lb	0.4322	1502 lb
Liquid Admixture No. 1	HRWR	1.20	131 mL	.00130	13.97 fl. oz./cwt. cement
Liquid Admixture No. 2	DCI	1.30	728 mL	.00333	77.66 fl. oz./cwt. cement
Liquid Admixture No. 3	Darex	1.01	75 mL	.00013	8.00 fl. oz./cwt. cement
Net Mix Water	Lab	1.00	12.2 lb	0.1955	254 lb
Totals			186.9	1.223	3814 Yield = 26.14

Liquid Admixture Data				
	Brand Name	Type	% Solids	added water-pcy
Liquid Admixture No. 1	WRDA-19	HRWR	40	4.157
Liquid Admixture No. 2	DCI	Corrosion Inhibitor	33.00	27.95
Liquid Admixture No. 3	Darex AEA	air-entrainer	5.75	3.147

Batch Data	
Water-to-Cement Ratio	0.385 (including water in admix.)
Water-to-Cementitious Ratio	0.350 (including water in admix.)
% Fine to Total Aggregate	48.5 %
Air-to-Paste Ratio	0.185 (including mineral admix.)
Paste-to-Aggregate Ratio	0.459 (including mineral admix.)
Percent Paste	35.2 (including mineral admix.)
Calculated Unit Weight	144.4 pcf
Theoretical Air Free Unit Weight	152.8 pcf
Calculated Air Content	4.5 %

- 1 in = 25.4 mm
- 1 lb = 0.454 kg
- 1 °C = (°F - 32)/1.8
- 1 pcf = 0.028 m³
- 1 fl.oz = 29.57 mL
- 1 cu.yd. = 0.7645 m³

Table 7. Properties and proportions for silica fume concrete mixture with organic corrosion inhibitor used for category A repairs.

FRESH CONCRETE PROPERTIES			
Contract Number	50329	Slump	4 in
Mix Number	Silica fume - organic inhibitor	Air Content	2.5%
Date Cast	11.23.93	Measured Unit Weight	150.8 pcf
Maximum Aggregate Size	3/8 in		

Lab Weights and Equivalent Cubic Yard Weights					
Material	Lot Number	Specific Gravity	SSD Lab Quantity	Lab Volume Cu. Ft.	Batch Quantity per Cu. Yd.
Cement	Type I	3.15	31.7 lb	0.1613	683 lb
Mineral Admixture No. 1	Silica Fume	2.20	3.17 lb	0.0231	68 lb
Fine Aggregate	Sand	2.64	67 lb	0.4067	1443 lb
Coarse Aggregate No. 1	Coarse	2.67	72 lb	0.4322	1551 lb
Liquid Admixture No. 1	HRWR	1.19	180 mL	.00182	19.20 fl. oz./cwt. cement
Liquid Admixture No. 2	Corr. Inhib.	0.97	182 mL	.00163	19.41 fl. oz./cwt. cement
Liquid Admixture No. 3	AE	1.01	20 mL	.00003	2.13 fl. oz./cwt. cement
Net Mix Water	Lab	1.00	12.2 lb	0.1955	263 lb
Totals			186.4	1.222	3939 Yield = 26.12

Liquid Admixture Data				
	Brand Name	Type	% Solids	added water-pcy
Liquid Admixture No. 1	Rheobuild 1000	HRWR	40	5.85
Liquid Admixture No. 2	Rheocrete 222	Corrosion Inhibitor	23.00	6.188
Liquid Admixture No. 3	Darex AEA	air-entrainer	5.75	0.867

Batch Data		
Water-to-Cement Ratio	0.385	(including water in admix.)
Water-to-Cementitious Ratio	0.350	(including water in admix.)
% Fine to Total Aggregate	48.5	%
Air-to-Paste Ratio	0.082	(including mineral admix.)
Paste-to-Aggregate Ratio	0.457	(including mineral admix.)
Percent Paste	33.1	(including mineral admix.)
Calculated Unit Weight	148.7	pcf
Theoretical Air Free Unit Weight	152.5	pcf
Calculated Air Content	1.1	%

- 1 in = 25.4 mm
- 1 lb = 0.454 kg
- 1 °C = (°F - 32)/1.8
- 1 pcf = 0.028 m³
- 1 fl.oz = 29.57 mL
- 1 cu.yd. = 0.7645 m³

orientations and salt-spray exposure was re-initiated. Results of the monitoring program are presented in Chapter 4 of this report.

Category B (Coatings and Sealers). After treatment in the accelerated corrosive environment, Category B specimens were the first to be removed and prepared for applications of protective treatments. Specimens were allowed to dry and then were sandblasted to remove surface laitance and residual salt from the exposure, and to open the surface for better penetration of sealers and coatings. Application was carried out using manufacturers' instructions for each material. All penetrating sealers were spray applied. The two-part epoxy coating was applied by hand brush. Application rates and notes on technique are given in Table 8.

Table 8. Application rates of coatings/sealers to test specimens.

Coating/Sealer	Application Rate (ft ² /gal)	Notes
2-part epoxy	145 each coat (2 coats)	Apply 2 successive coats
40% ATS	125	Mist with water after application
20% AAS	125	Single application
2-component AS/MM	100 (primer)/200(topcoat)	Topcoat 2 h after primer

$$1 \text{ ft}^2/\text{gal} = 0.0245 \text{ m}^2/\text{L}$$

Specimens were returned to the test area after a period of a few days and salt-spray exposures were re-initiated. Results of the monitoring program are presented in Chapter 4 of this report.

CHAPTER 4. RESULTS

CATEGORY A - CONCRETE REMOVAL/REPLACEMENT

After installation of repairs, specimens were again sprayed with a salt solution. Shortly after restarting the spray system, significant problems were encountered in maintaining the spray equipment. The fine-spray nozzles exhibited almost continual clogging, in spite of efforts to flush frequently with fresh water, periodic cleaning of filter screens (a time-consuming process), and attempts to reduce ambient dust in the area caused by other operations that had not been as frequent during the initial period of the study. Various modifications to the spray system were attempted, but without success. The method of exposure to salt solution was then altered so that the soffits of the slabs and beams were exposed to a pond of saltwater for 1 week, then allowed to dry for 1 week. This was accomplished by turning the specimens upside down and forming a dike on the top (formerly bottom) surface so that approximately 12 mm (0.5 in) of saltwater could be placed into the dike. The diked area included the entire top surface of the specimens. The pond was then covered with polyethylene sheeting to prevent evaporation. At the end of each 1-week pond period, the saltwater was vacuumed off, the surface was flushed quickly with tapwater, and was allowed to dry for 1 week. The 1-week pond/1-week dry cycle was adopted for all slab and beam specimens.

Slab Repairs

Half-Cell Measurements. Half-cell measurements using a copper/copper sulfate electrode (CSE) were carried out on the concrete surface along each tendon in the slabs. Readings were obtained every 0.3 m (1 ft) along the tendons. The measurements were made after flushing the surface with fresh water at a frequency of approximately once every calendar quarter.

An initial set of half-cell measurements was made at the end of the first four wet/dry cycles. Results are shown in Tables 9, 10, and 11 for slabs 1, 2, and 3, respectively. All potentials are within the values generally considered to be representative of a corrosive condition. Potentials are somewhat less electro-negative on slab 1 than on slabs 2 and 3. Within each slab, however, there is little apparent difference between the average level of potential on repair and original concrete areas. Since it is highly unlikely that the chloride ions from the ponding solutions had penetrated through the repair materials at this early stage, the potentials most likely reflected the fact that the steel in all repair areas was coated, and the half-cell was measuring contributions from the uncoated steel at the periphery of the repair areas.

Table 9. Half-cell potentials measured on slab 1 after four wet/dry cycles.

Distance - ft	Tendon A	Tendon B	Tendon C	Tendon D
		Potential (mV vs. CSE)		
1.0	473	442	407	423
		REPAIR AREA N		
2.0	401	378	385	403
2.5	437	385	424	467
3.0	411	416	410	439
4.0	423	408	420	413
		REPAIR AREA S		
5.0	386	378	409	385
5.5	366	375	389	454
6.0	384	445	418	426
7.0	355	397	416	433

1 ft = 0.305 m

Table 10. Half-cell potentials measured on slab 2 after four wet/dry cycles.

Distance - ft	Tendon A	Tendon B	Tendon C	Tendon D
		Potential (mV vs. CSE)		
1.0	552	585	577	558
		REPAIR AREA N		
2.0	492	582	549	449
2.5	576	584	571	510
3.0	581	585	594	523
4.0	523	526	534	515
		REPAIR AREA S		
5.0	560	581	590	570
5.5	564	585	618	585
6.0	516	573	567	558
7.0	572	521	521	563

1 ft = 0.305 m

Table 11. Half-cell potentials measured on slab 3 after four wet/dry cycles.

Distance - ft	Tendon A	Tendon B	Tendon C	Tendon D
		Potential (mV vs. CSE)		
1.0	575	530	460	472
		REPAIR AREA N		
2.0	499	506	399	382
2.5	522	459	381	379
3.0	498	467	394	369
4.0	581	549	555	503
		REPAIR AREA S		
5.0	519	431	398	463
5.5	492	378	382	445
6.0	502	437	438	390
7.0	519	550	521	472

1 ft = 0.305 m

The trend of the potentials within the slab repair areas over the entire 100 cycles of testing is shown in Figure 15. Initially, there was a significant difference in potentials for slab 2 vs. slabs 1 and 3 until about halfway through the exposure program. After about 60 cycles, potentials for all of the slabs began to converge, though the "N" patch on slab 1 did continue to exhibit the lowest potentials in the set throughout the course of monitoring. The generally higher potentials for slab 2 repairs throughout most of the monitoring appear to be reflected in cracking and visual appearance of the repair areas. Figures 16, 17, and 18 show crack maps at 100 cycles for all repair slabs. Cracking is more extensive in slabs 2 and 3 than it is in slab 1. A visual comparison of the surface of repair areas in slabs 1 north vs. slab 2 north is given in Figures 19 and 20. There is more efflorescence and exudation of corrosion products from slab 2 (Figure 20) than from slab 1 (Figure 19).

Chloride Analysis. After completion of 100 cycles, the exposures were terminated and samples were obtained from each slab for chloride analysis. Sample locations were at the center of each repair area. Samples were taken with a rotary drill bit at 12-mm (0.5-in) increments from the surface of the slab to a depth of 50 mm (2 in). Drill powder samples were analyzed for acid-soluble chloride ions according to ASTM C 1152. Results are shown in Figure 21. The highest amounts of chloride penetrated into the conventional concrete repair areas (slab 1). While the surface layer (0 to 12 mm [0 to 0.5 in]) for slab 3 contained more chloride than the corresponding layer of slab 1, the chloride contents for these two slabs were almost identical for the next layer.

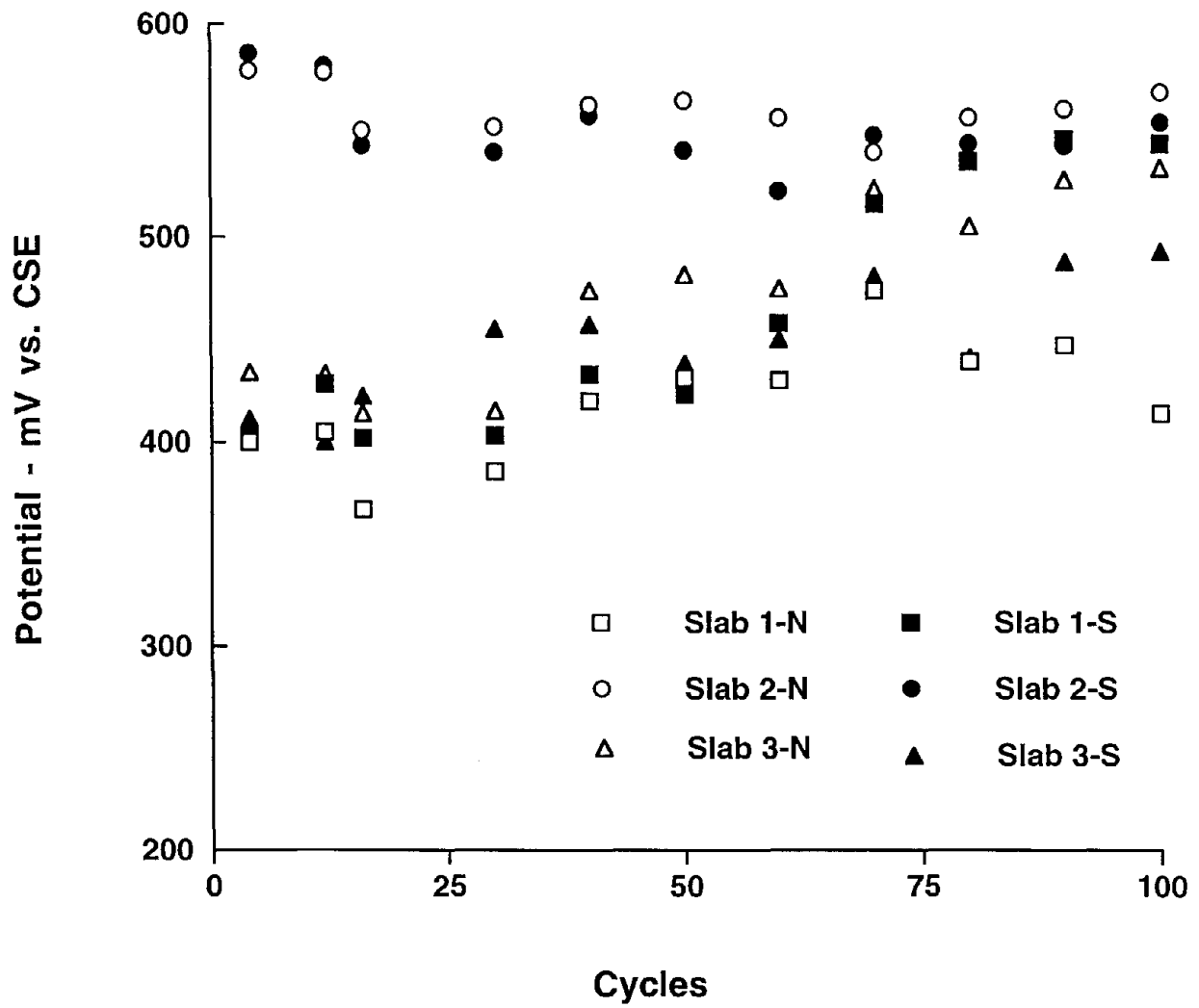


Figure 15. Average half-cell potentials in slab repair areas over 100 cycles of testing.

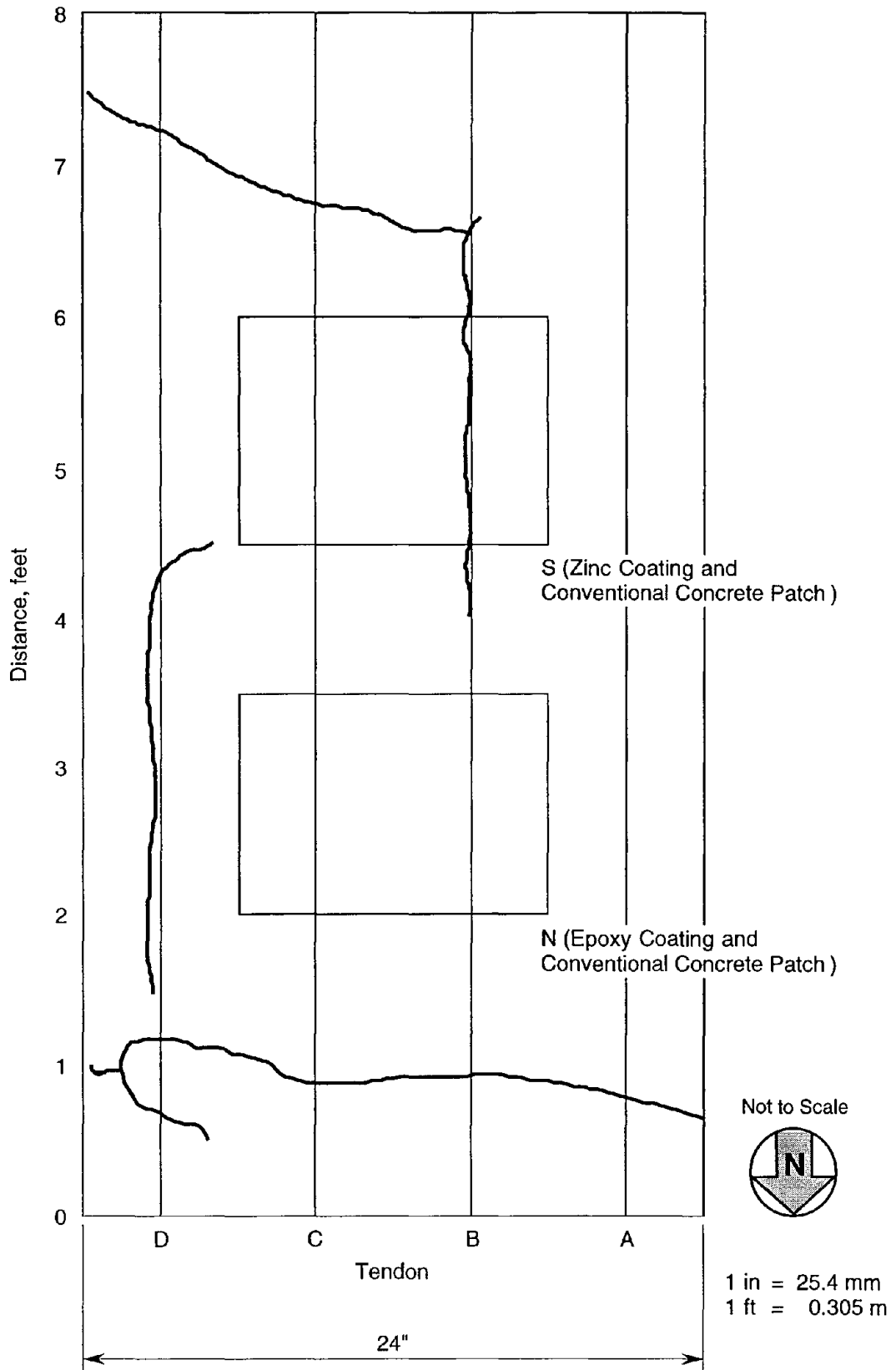


Figure 16. Crack map for slab 1 at 100 cycles of exposure.

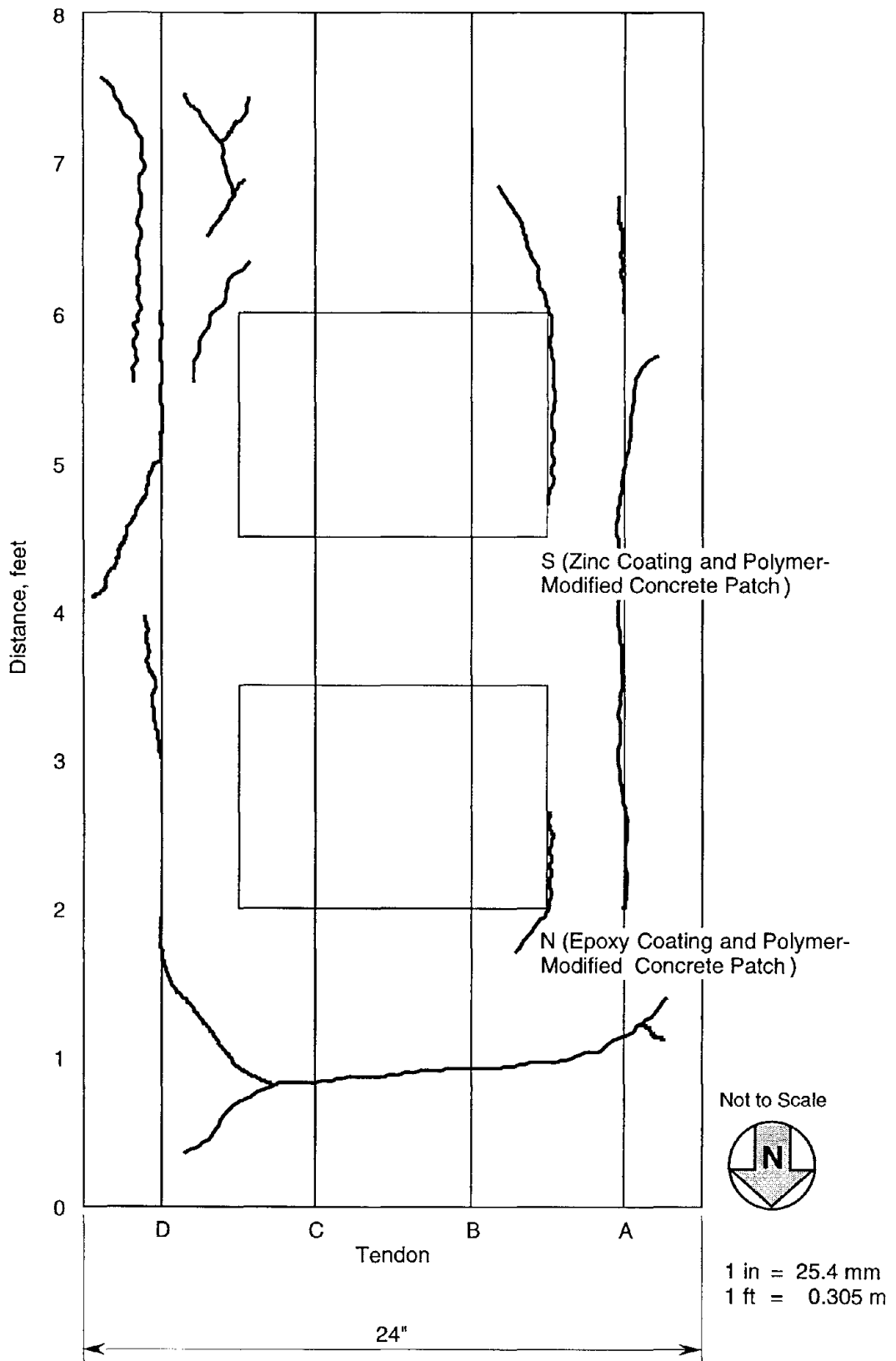


Figure 17. Crack map for slab 2 at 100 cycles of exposure.

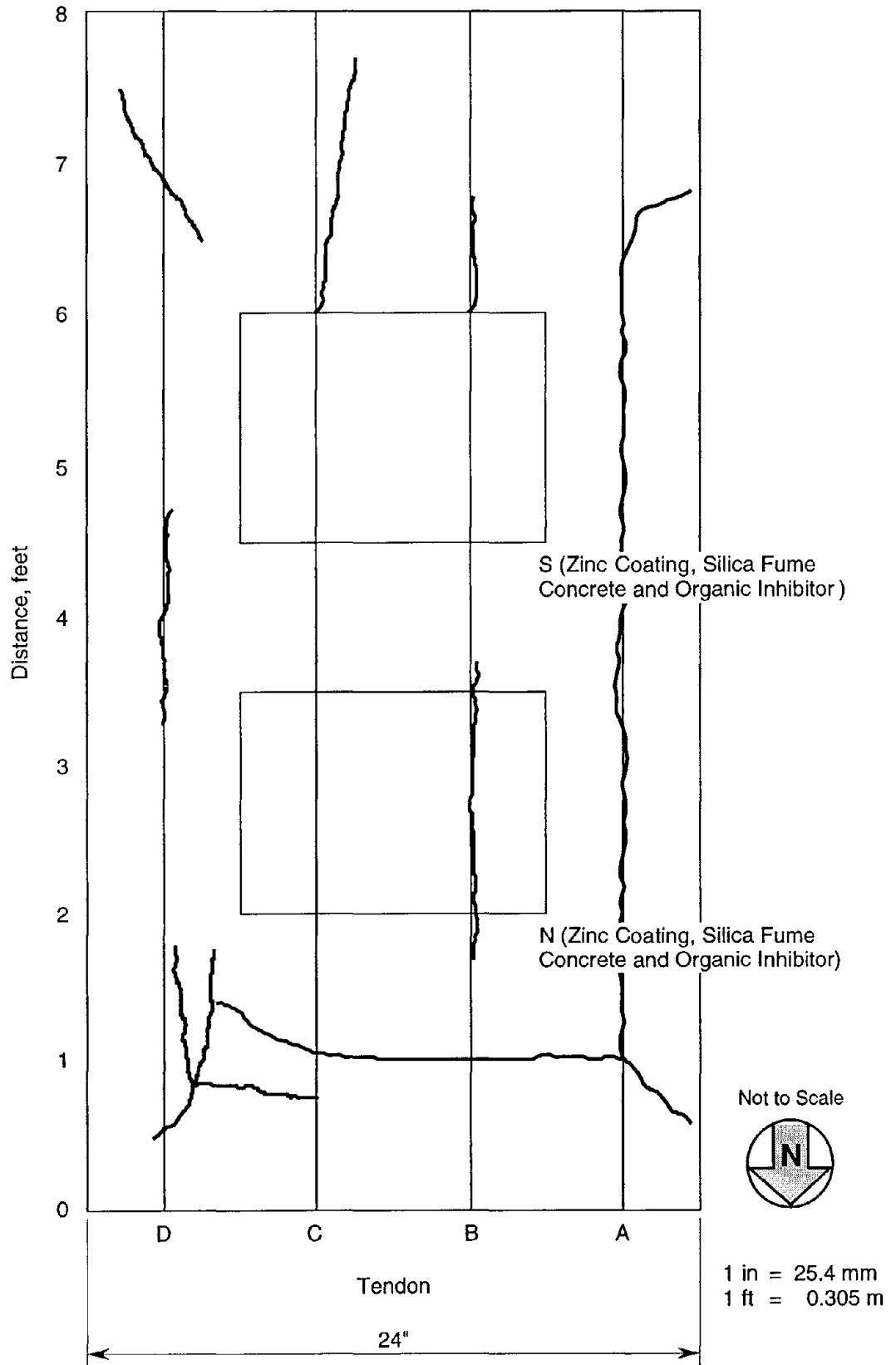


Figure 18. Crack map for slab 3 at 100 cycles of exposure.

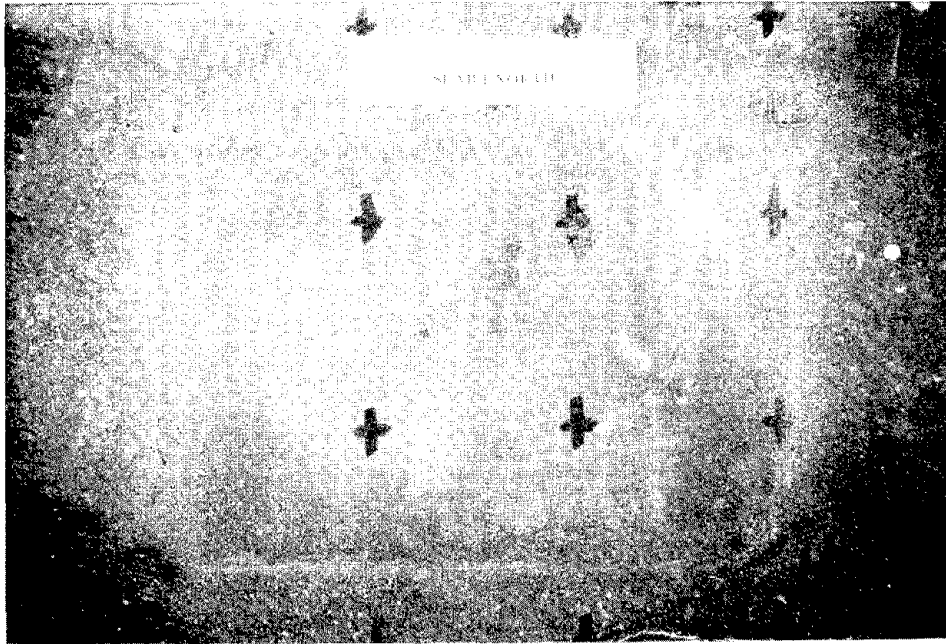


Figure 19. Appearance of north repair area, slab 1, after 100 exposure cycles.

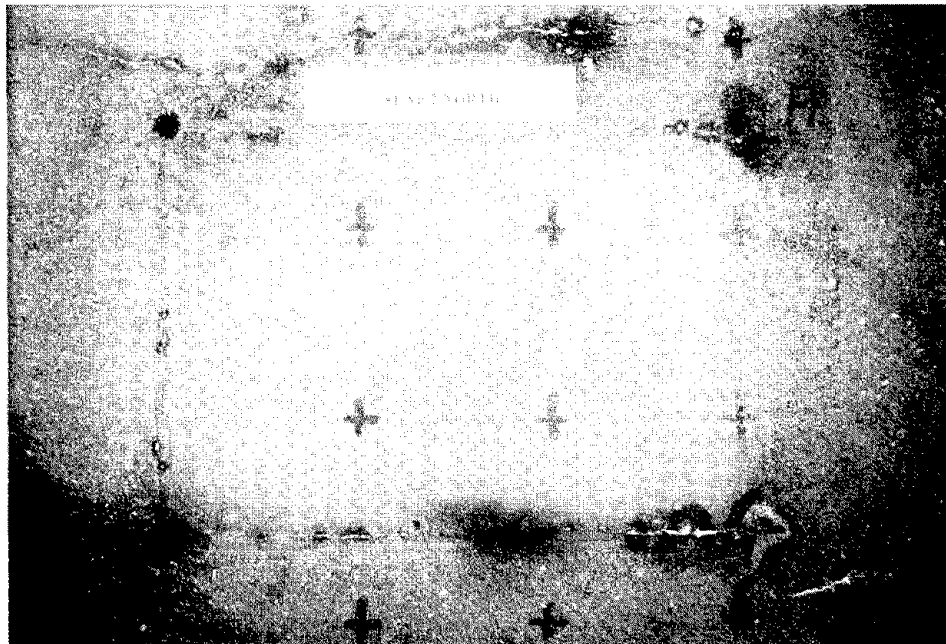


Figure 20. Appearance of north repair area, slab 2, after 100 exposure cycles.

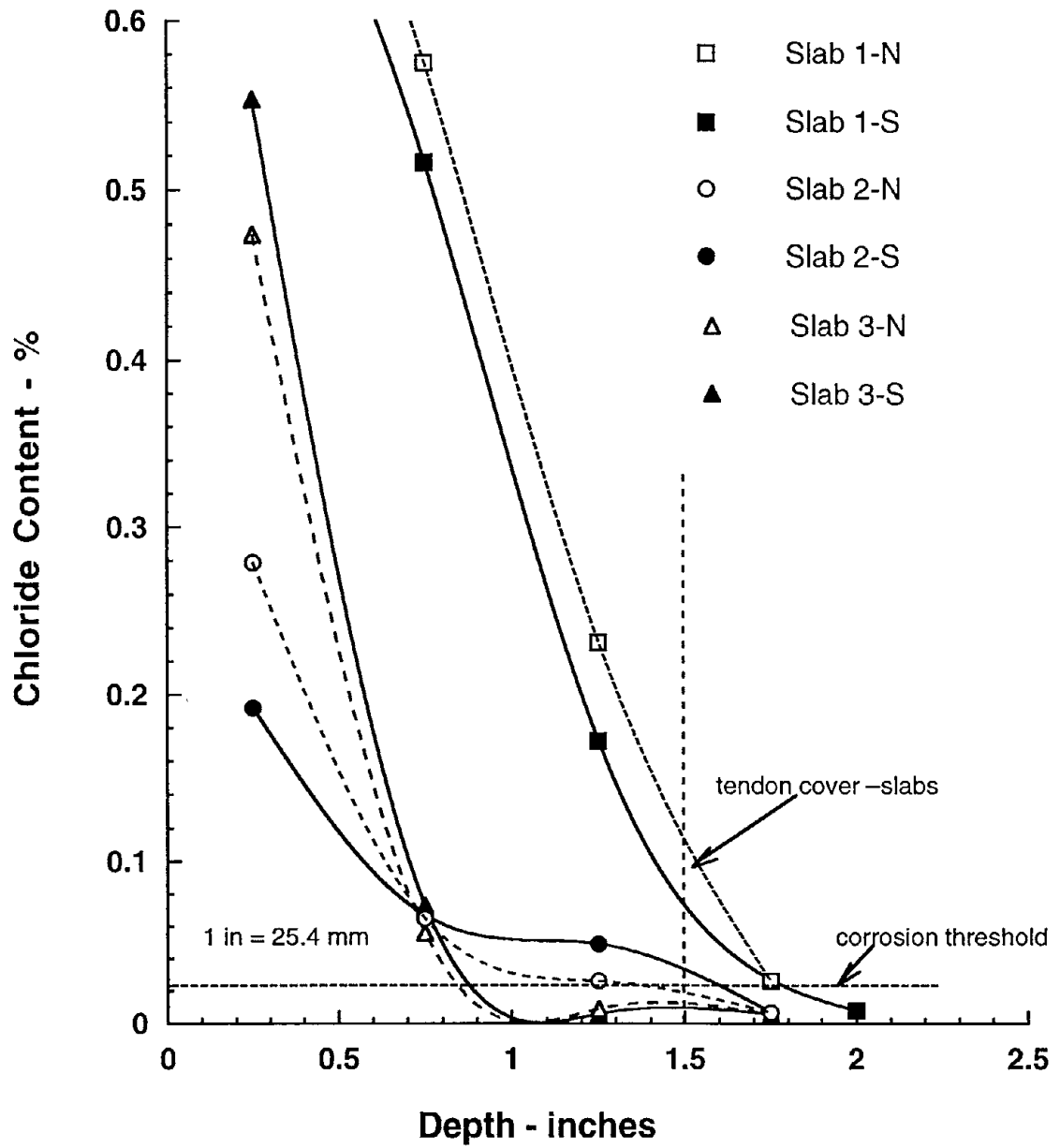


Figure 21. Chloride contents measured on slab repair specimens.

Below 25 mm (1 in), there were detectable amounts of chloride in slab 2, but only baseline amounts in slab 1. The corrosion threshold shown in Figure 21 is based on a value of 0.2% acid-soluble chloride by mass of cement as recommended by ACI Committee 222.⁽⁸⁾ The threshold is significantly exceeded at the average level of strand cover only for slab 1.

A series of additional drill samples were obtained in positions approximately 40 mm (1.5 in) in from the edge of one of the two patches on each slab. Chloride profiles were obtained at each of these locations. Results are shown in Figure 22. For slab 1, there was little difference between the chloride content at the edge of the slab and that in the interior of the patch. For slabs 2 and 3, however, values near the slab edges appear to be greater than those at the center of the patch. As noted earlier, there was more cracking and efflorescence near the edges of slabs 2 and 3 than slab 1. It is possible that chlorides were able to penetrate into these slabs at the edges of the repairs, and then migrate laterally into the slab repair areas. A limited amount of work was done in an attempt to define the extent of lateral penetration of the chloride in slabs 2 and 3. It appears that chloride is able to penetrate approximately 75 mm (3 in) in from the repair edge. Beyond this point, chloride levels are the same as for the interior of the patch.

Dissection. After all drill samples had been obtained and analyzed, the tendons and reinforcing steel in the patch areas were uncovered by air-hammer removal of the concrete cover. Due to the relative thinness of the slabs, this resulted in complete breakout of concrete above and below all steel in the area of the patches. Photographs of steel in slab 1 (conventional concrete patches) in the north (epoxy coating) and south (zinc-rich coating) patches are shown in Figures 23 and 24. There is spotty corrosion and failure of the coating on the tendons in the north patch. There is less coating disruption and corrosion evident on the plain reinforcing steel in this patch. Those bars that do not show a coating were contained within the original concrete at the time the patching was done. In the south patch (Figure 24), the upper tendon shows some corrosion; the lower tendon does not appear to exhibit any external corrosion. After documentation of the external appearance of the tendons, cuts were made in each tendon and the individual strands were pulled back from the bundles. Figure 25 shows some of the interior portions of the strands in the north patch. Strands show rusting on the interior surfaces of the bundle. The same procedure was carried out on the zinc-coated strands. Figure 26 shows strands pulled back from the lower bundle that had not shown any exterior corrosion. Rusting is noticeable on the interior of the strands.

Uncovered tendons and reinforcing steel in patches on slab 2 (latex-modified concrete patches) are shown in Figures 27 (north patch - epoxy) and 28 (south patch - zinc). On the epoxy-coated tendons, the coating disruption and corrosion are more extensive and severe than on the

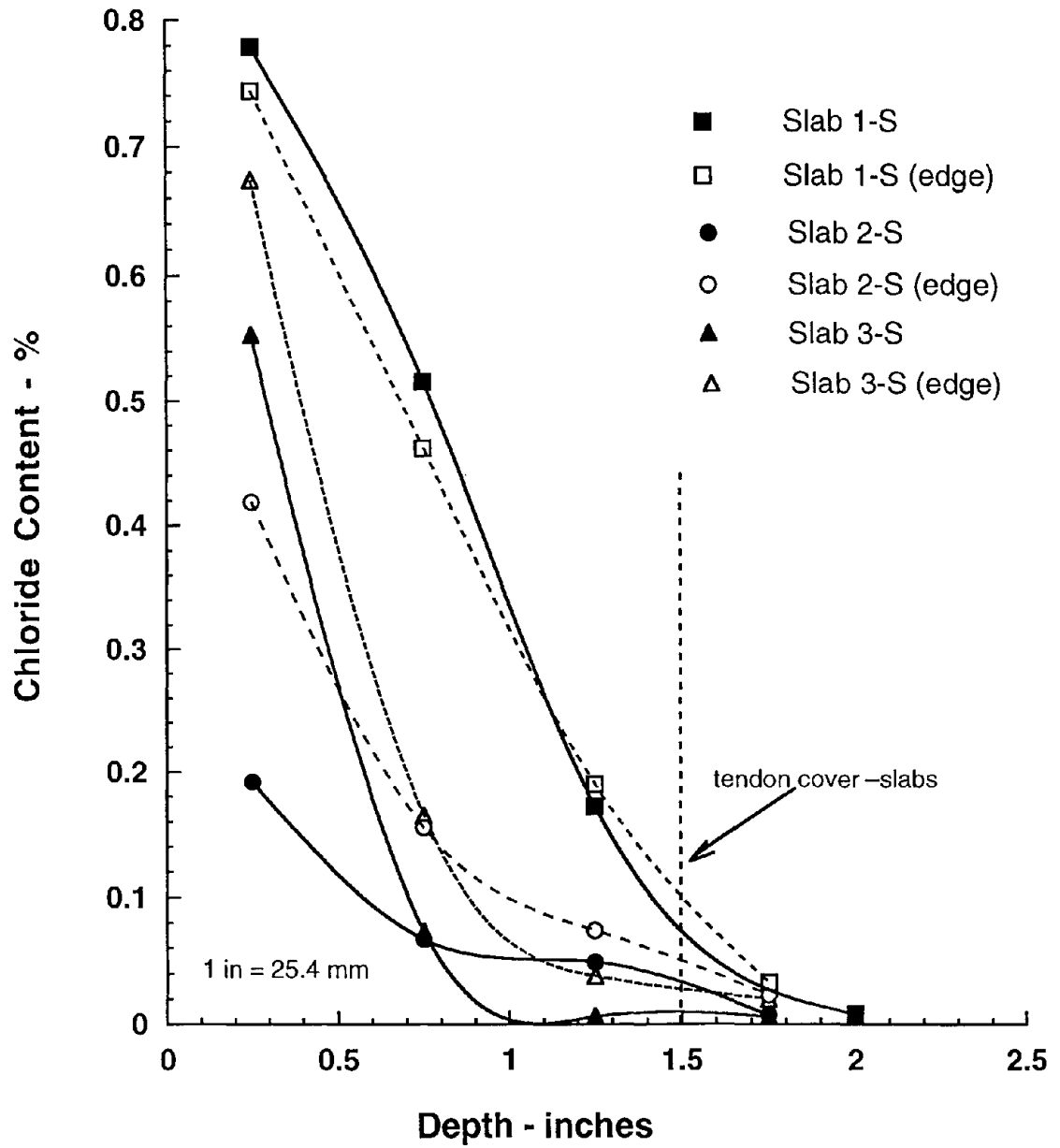


Figure 22. Comparison of chloride contents measured at center and near edges of slab repair patches.



Figure 23. Appearance of uncovered tendons and reinforcing steel in north repair area, slab 1, after 100 exposure cycles.



Figure 24. Appearance of uncovered tendons and reinforcing steel in south repair area, slab 1, after 100 exposure cycles.

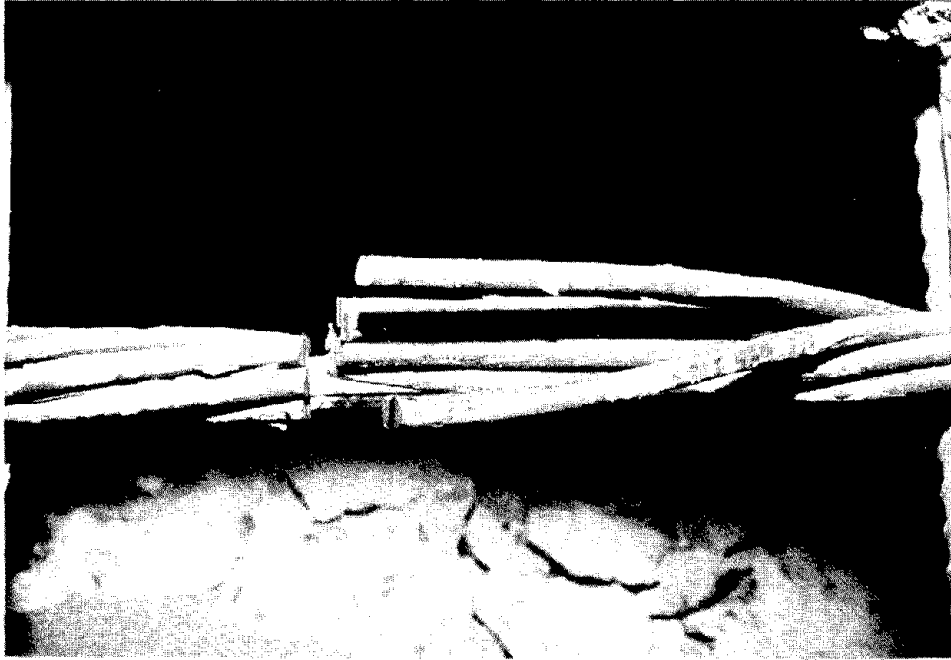


Figure 25. Appearance of interior of tendon bundle in north repair area, slab 1, after 100 exposure cycles.

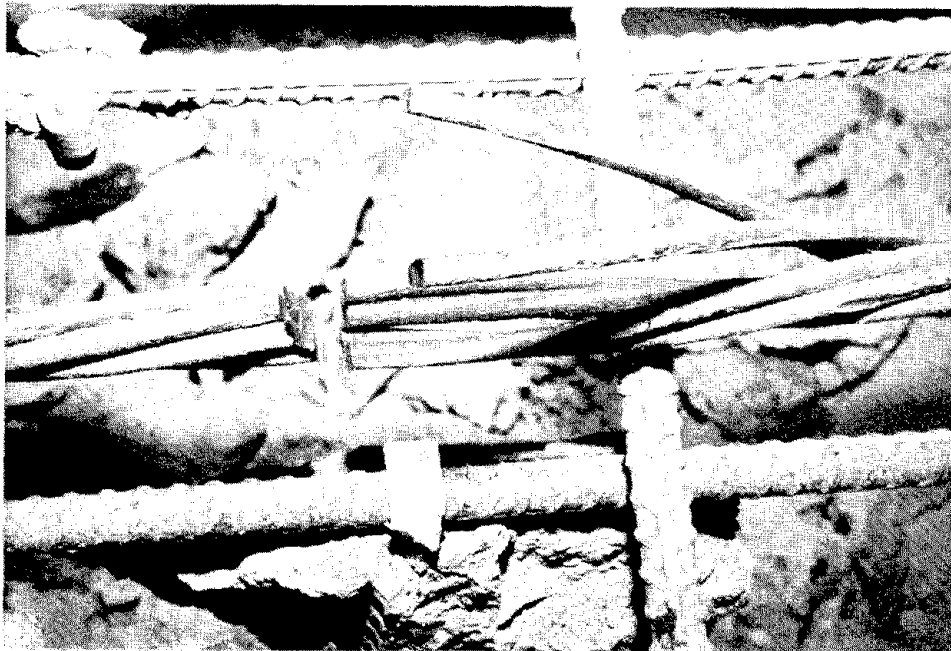


Figure 26. Appearance of interior of tendon bundle in south repair area, slab 1, after 100 exposure cycles.



Figure 27. Appearance of uncovered tendons and reinforcing steel in north repair area, slab 2, after 100 exposure cycles.



Figure 28. Appearance of uncovered tendons and reinforcing steel in south repair area, slab 2, after 100 exposure cycles.

corresponding steel on slab 1. The coating was found to be extensively flaking away from the steel and was easily removed with a knife. In the south patch, there is corrosion on both the upper and lower tendons; however, it is of a lesser magnitude than in the north repair area. On the lower tendon, most of the zinc appeared to have been consumed. Upon cutting and peel-back of the individual strands from the lower tendon in the north repair area, extensive corrosion of the interior of the bundle was observed (Figure 29). When this was done for the zinc-coated tendons in the south repair area, the severity of corrosion was seen to be less (Figure 30).

Uncovered tendons and steel in slab 3 (silica fume concrete with organic corrosion inhibitor) are shown in Figures 31 and 32 for epoxy-coated and zinc-coated steel, respectively. The epoxy coating on the upper tendon in the north patch has been completely destroyed, and extensive corrosion is evident on the strands. There is also exterior corrosion on the lower tendon, and corrosion is seen in spots. The zinc-coated tendons in the south patch (Figure 32) appear to have performed better than the epoxy. Most of the corrosion in this area is confined to the left-most side of the lower tendon. Figures 33 and 34 show the interiors of the tendon bundles in slab 3. Again, there is corrosion evident on the interior surfaces for both epoxy- and zinc-coated strand.

Based on the visual inspection of the slab repair areas, a rough assessment of the performance of the slabs would be: slab 1 > slab 3 > slab 2. That is, slab 1 shows the best performance (least corrosion), slab 2 the worst (most corrosion). This is especially true for the repair areas containing epoxy-coated steel. By reference again to Figure 21, however, it can be seen that the highest chloride contents at the level of the tendons are seen in slab 1, which shows the least corrosion. In fact, the bulk chloride contents of most of the repair areas in slabs 2 and 3 are well below accepted threshold corrosion values. Slab 1 did show the least electro-negative half-cell readings and the least cracking and evidence of corrosion from visual examination of the surface of the repair areas during the 100 cycles of testing. Half-cells for slab 2 were the most electro-negative of all slab specimens throughout the test period. Given the general tendency for all the specimens to exhibit corrosion of varying severity on the interior of the bundles, it may be postulated that coating disruption and subsequent corrosion were induced by chlorides trapped within the tendon bundles, and that these chlorides may have been present before the cyclic exposures were initiated. As the tendons were subjected to high anodic currents in the initial attempt to draw chloride into the slabs and induce damage, these chlorides could have become trapped in the interstices between strands. It is also possible that chlorides migrated laterally through the bundles during the course of the exposure, given the significantly higher chloride contents at the slab edges as shown in Figure 22. We believe that such a mechanism may be operative under actual field conditions, and not simply an anomaly due to the application of anodic current to the test slabs. Chloride can certainly build



Figure 29. Appearance of interior of tendon bundle in north repair area, slab 2, after 100 exposure cycles.



Figure 30. Appearance of interior of tendon bundle in south repair area, slab 2, after 100 exposure cycles.



Figure 31. Appearance of uncovered tendons and reinforcing steel in north repair area, slab 3, after 100 exposure cycles.

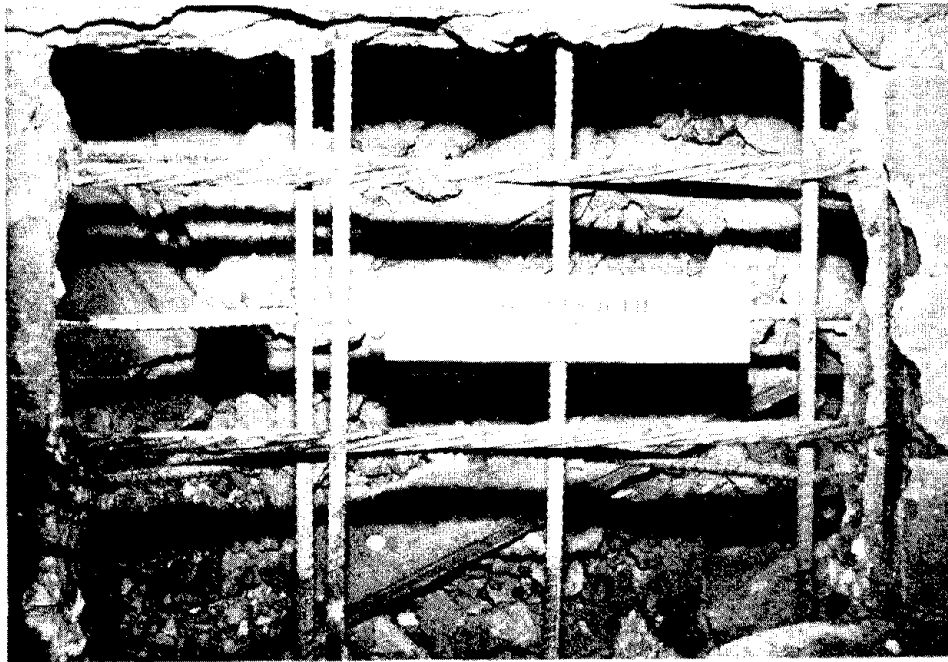


Figure 32. Appearance of uncovered tendons and reinforcing steel in south repair area, slab 3, after 100 exposure cycles.

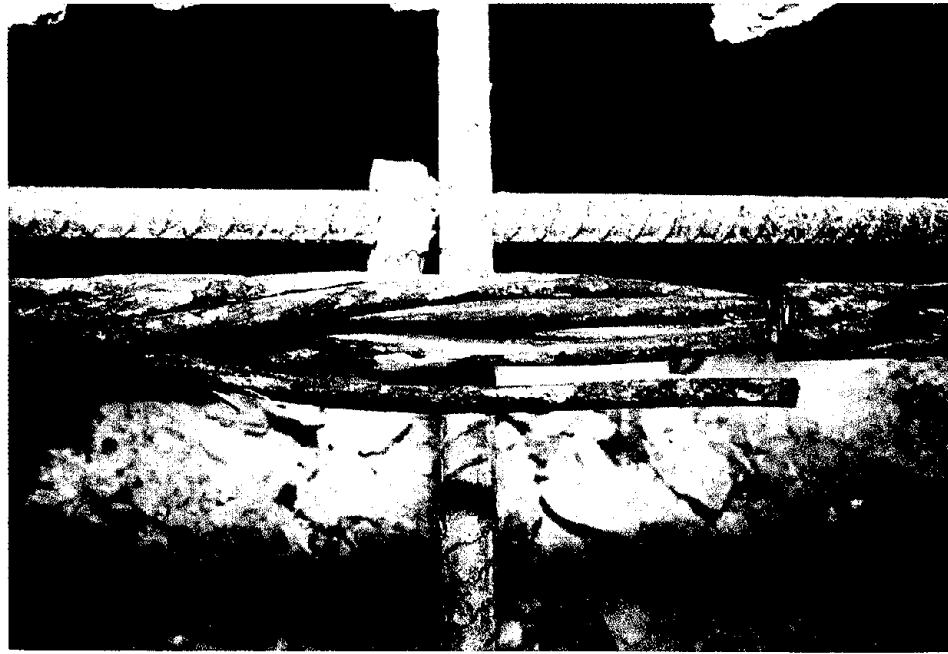


Figure 33. Appearance of interior of tendon bundle in north repair area, slab 3, after 100 exposure cycles.

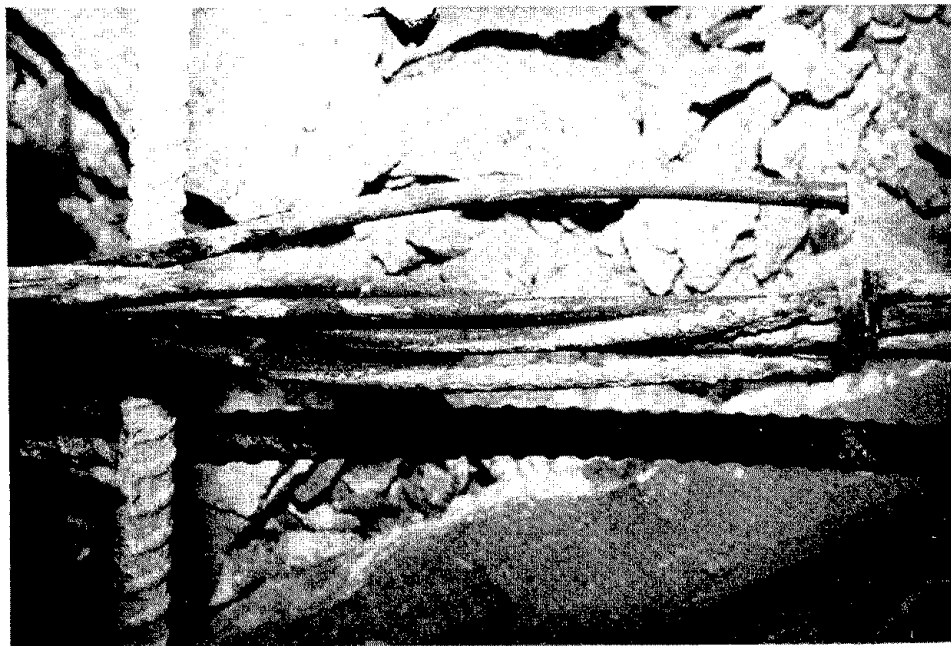


Figure 34. Appearance of interior of tendon bundle in south repair area, slab 3, after 100 exposure cycles.

up to high levels within prestressed concrete elements over many years, as was seen in samples taken from field structures inspected as part of the initial phase of this project. Removal of unsound concrete and sandblasting of steel in areas to be patched would not necessarily remove chloride contamination from interstices between wires in tendon strands. Upon application of the patch, moist conditions are again created that may foster further corrosion, and moisture and chlorides may also migrate laterally from the original (unpatched) concrete at the edges of the repair areas.

Beam Repairs

Half-Cell Measurements. An initial set of half-cell measurements was made at the end of the first four wet/dry cycles. Readings were obtained along alternate tendons every 0.3 m (1 ft) along the tendons. Results are shown in Tables 12, 13, and 14 for beams 1, 2, and 3, respectively. As for the pretensioned slab repair specimens, all potentials are within the values generally considered to be representative of a corrosive condition. Again, as for the slab set, potentials are somewhat less electro-negative on beam 1 than on beams 2 and 3.

Table 12. Half-cell potentials measured on beam 1 after four wet/dry cycles.

Distance - ft	Tendon A	Tendon C	Tendon E	Tendon G
	Potential (mV vs. CSE)			
1.0	373	444	431	388
1.5	457	522	508	466
	REPAIR AREA N			
2.5	394	405	409	406
3.0	400	414	426	424
4.0	421	456	473	492
	REPAIR AREA S			
5.0	405	406	414	414
5.5	396	387	384	381
6.5	435	489	477	470
7.0	463	514	522	481

1 ft = 0.305 m

Trend of potentials within the beam repair areas over the entire 100 cycles of testing is shown in Figure 35. Potentials for beam 2 in both repair areas stay the highest throughout the course of monitoring. While potentials for beams 1 and 3 were comparable to 30 cycles, at the 40-cycle point, a dramatic decrease in potentials for beam 3 was noted. However, there were no dramatic differences in the appearance of the surfaces of the repair areas in these beams. In fact, as can be

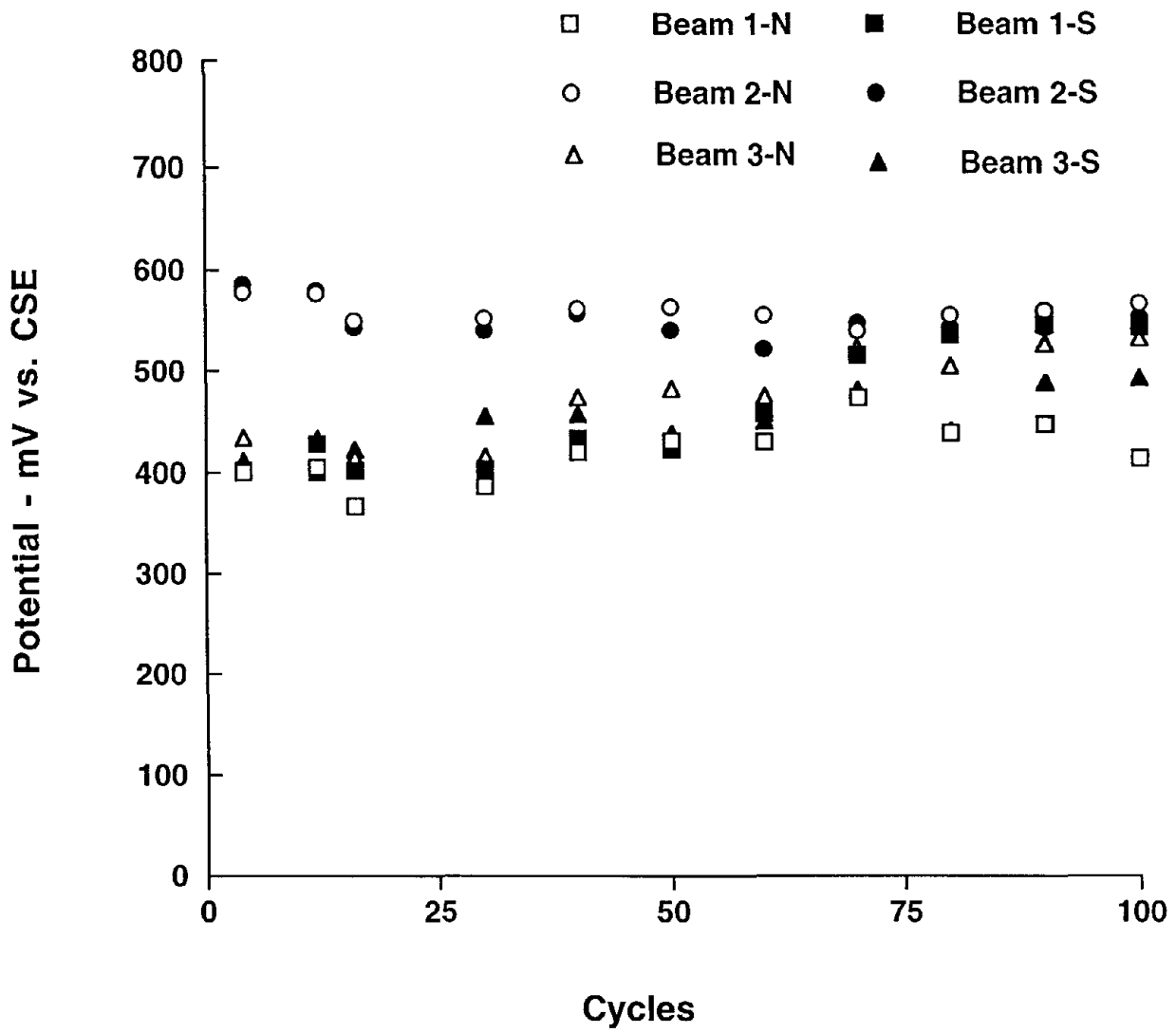


Figure 35. Average half-cell potentials in beam repair areas over 100 cycles of testing.

seen in Figures 36 through 38, cracking and delamination were just as prevalent, if not more so, in beams 1 and 3 than in beam 2.

Table 13. Half-cell potentials measured on beam 2 after four wet/dry cycles.

Distance-ft	Tendon A	Tendon C	Tendon E	Tendon G
	Potential (mV vs. CSE)			
1.0	505	554	563	518
1.5	596	639	640	597
	REPAIR AREA N			
2.5	581	594	597	571
3.0	589	597	613	576
4.0	585	621	619	608
	REPAIR AREA S			
5.0	559	578	563	550
5.5	562	583	584	559
6.5	528	555	534	513
7.0	380	416	415	391

1 ft = 0.305 m

Table 14. Half-cell potentials measured on beam 3 after four wet/dry cycles.

Distance - ft	Tendon A	Tendon C	Tendon E	Tendon G
	Potential (mV vs. CSE)			
1.0	515	590	553	515
1.5	594	599	589	560
	REPAIR AREA N			
2.5	431	426	415	406
3.0	477	501	498	451
4.0	549	572	569	539
	REPAIR AREA S			
5.0	448	422	416	412
5.5	429	449	448	451
6.5	549	583	576	560
7.0	456	496	531	547

1 ft = 0.305 m

Chemical Analysis. After completion of 100 cycles, the exposures were terminated and samples were obtained from each slab for chemical analysis. Sample locations were at the center of each repair area. Samples were taken and analyzed identical to those from the previous slab specimens.

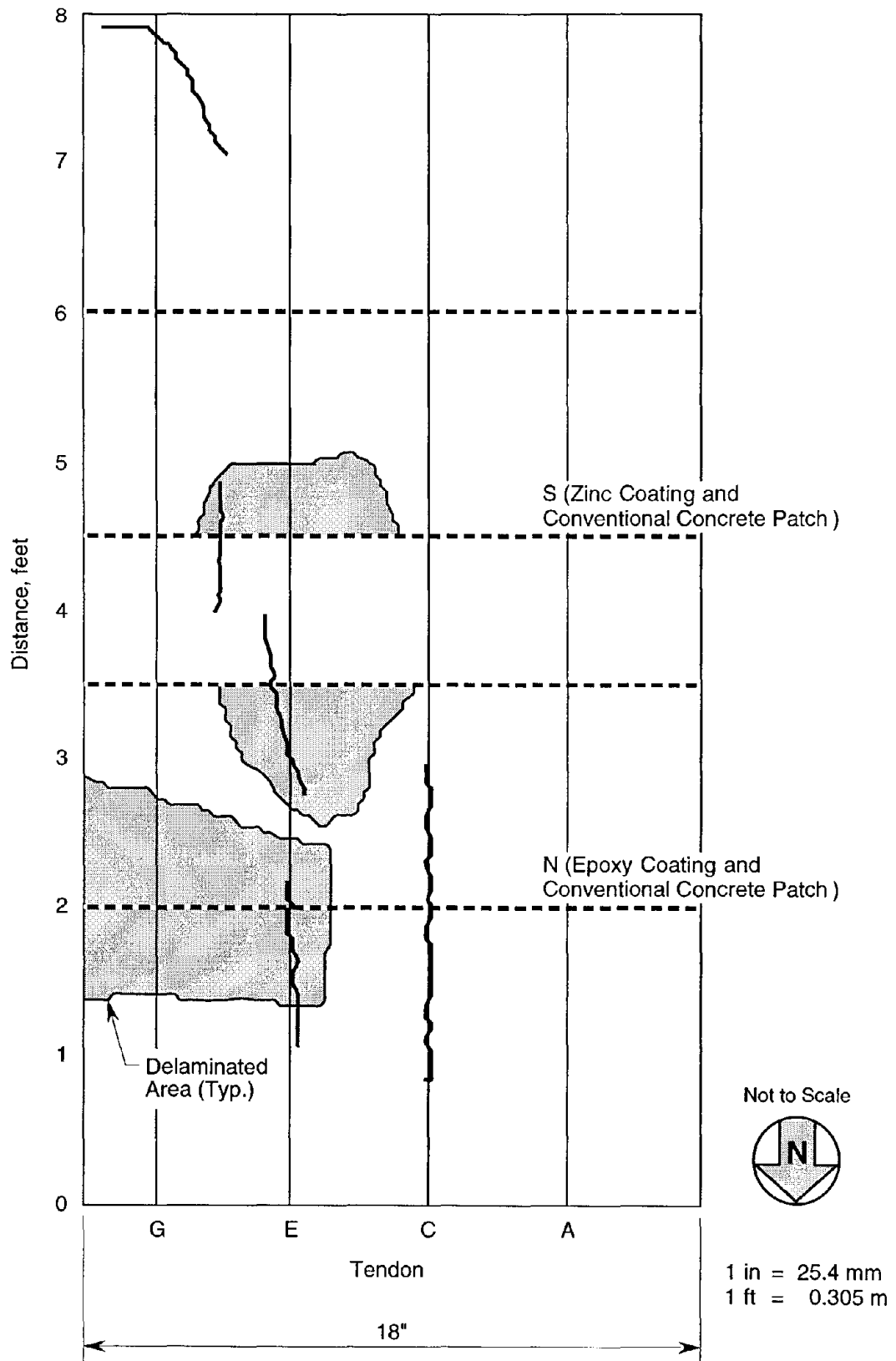


Figure 36. Crack map for beam 1 at 100 cycles of exposure.

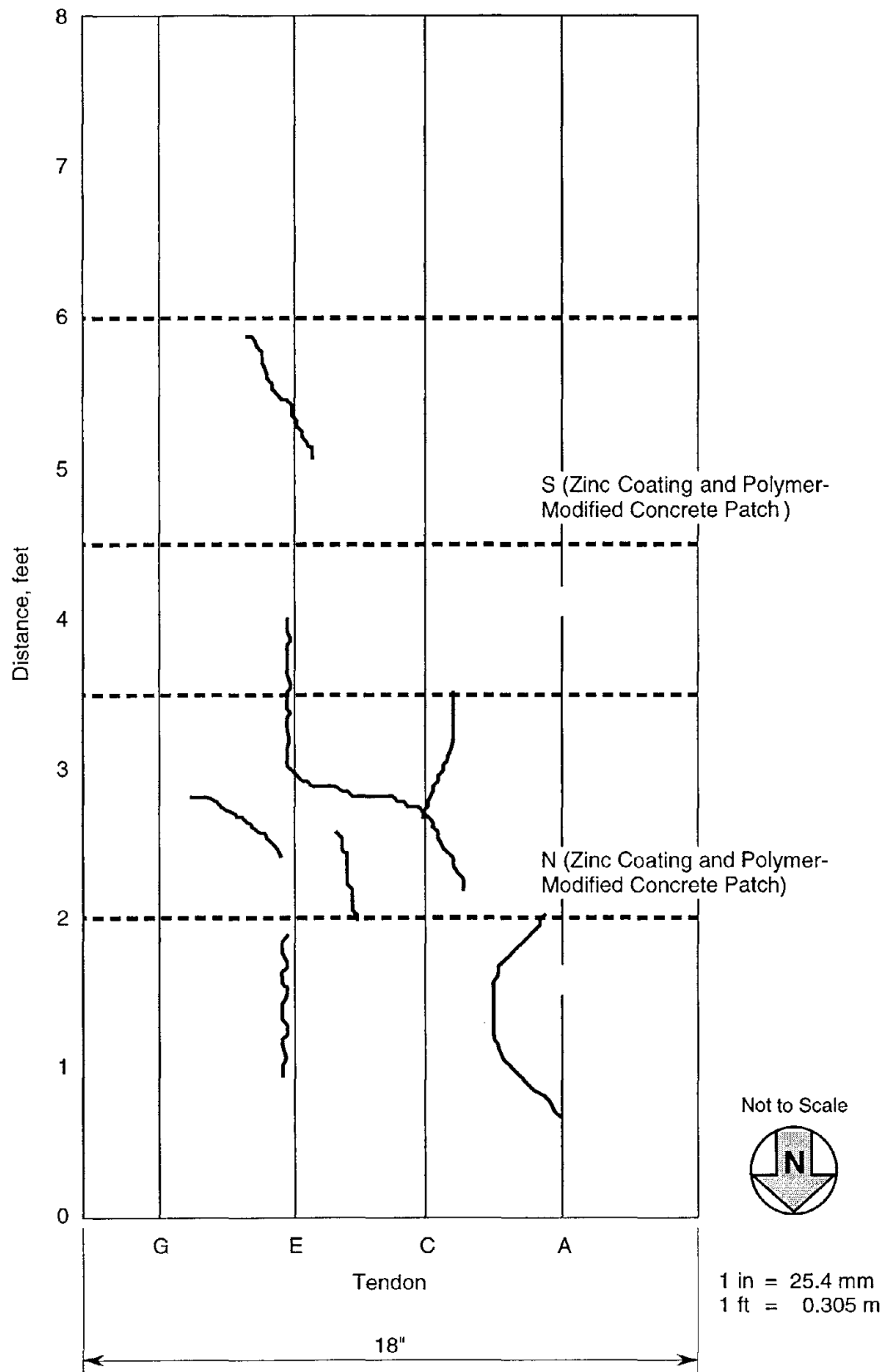


Figure 37. Crack map for beam 2 at 100 cycles of exposure.

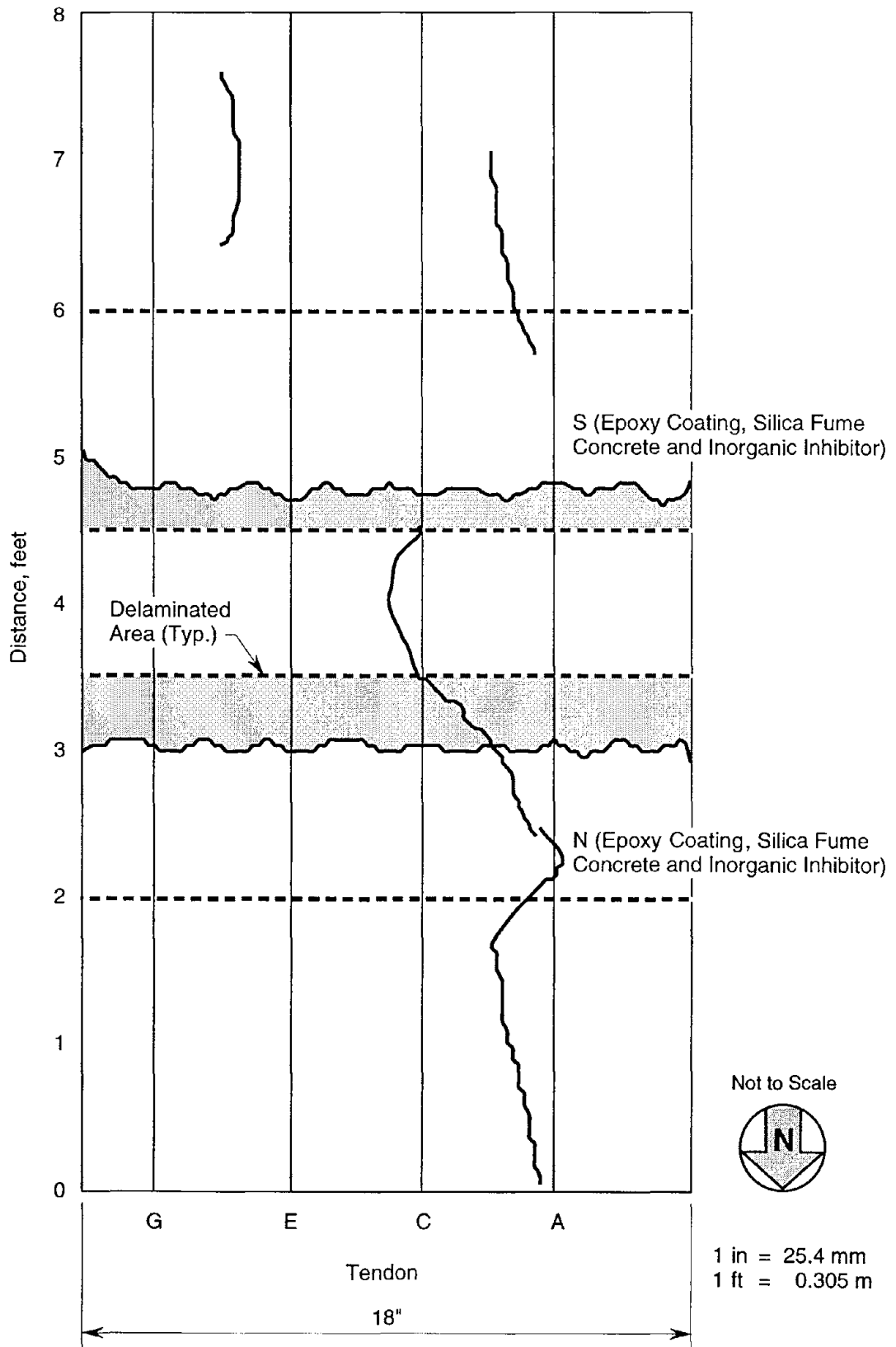


Figure 38. Crack map for beam 3 at 100 cycles of exposure.

Results are shown in Figure 39. In contrast to the slab specimens, the chloride contents vary considerably between the two locations on the same specimen. This may be a function of the greater amount of cracking observed on the beam as opposed to the slab repairs. This tends to be supported by the shape of some of the chloride profiles. Some, such as that for beam 1-N, start at relatively high values of chloride, but fall well below threshold at tendon depth. Other profiles are somewhat "flatter" across the depth, indicative of cracks that may let chloride in to greater depths faster than would penetrate into a crack-free material. Areas 1-S and 2-S show chloride contents that exceed the corrosion threshold at tendon level. All other areas show chloride contents less than threshold at this depth. However, in at least one case (1-N), there is a considerable "reservoir" of chloride that has entered the repair area, and it is likely that the threshold would have soon been exceeded at tendon level for this specimen.

As was done for the slab repairs, a series of additional drill samples were obtained in positions approximately 40 mm (1.5 in) in from the edge of one of the two patches on each slab. Chloride profiles were obtained at each of these locations. Results are shown in Figure 40. Data for slab 2 are not included, as unexpectedly high chloride contents (1 to 2 percent) were obtained. It is likely that this was due to cracking at the patch edge that brought large amounts of chloride into this locality. As can be seen for the remaining two patches, chloride contents at the edge of the slab exceed those at the center for beam 3 at all depths and for beam 1 at the last two sampling increments. As for the slabs, lateral penetration of chloride was found to extend approximately 75 mm (3 in) from the patch edges into the patch.

In beam 3, a nitrite-based corrosion inhibitor had been added to the fresh patching mix at a dosage of 20 L/m³ (4 gal/yd³). Chemical analysis for nitrite ions was carried out on powder samples obtained from the center of each repair area on this beam. Nitrite was extracted from the powder samples in water at room temperature. The nitrite is then diazotized with sulfanilic acid and coupled to an ethylenediamine dye. Nitrite ion concentration is then determined by ultra-violet (UV)-visible spectrophotometry by reference to a calibration curve of absorbance versus concentration. Nitrite ion contents were within a narrow range of 0.17 to 0.22 percent by mass of sample, corresponding to the calculated value of 0.2% by mass based on dosage used. In comparison to the chloride contents shown in Figure 39, the concentration of nitrite ion exceeds all reported chloride contents at the tendon level by a significant amount. It is only at the slab edges where large amounts of chloride were able to penetrate that the situation reversed (i.e., considerably more chloride than nitrite ion).

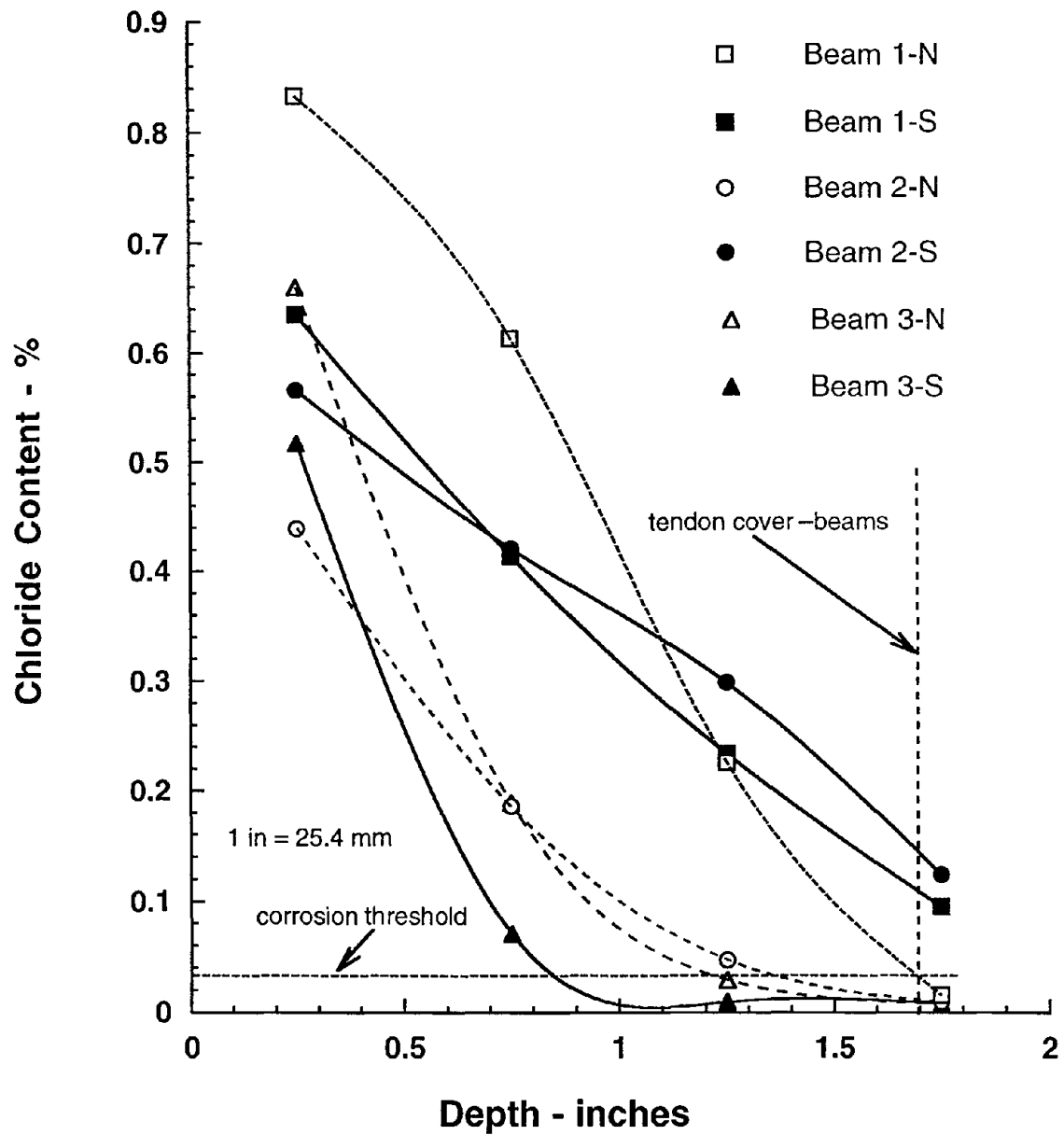


Figure 39. Chloride contents measured on beam repair specimens.

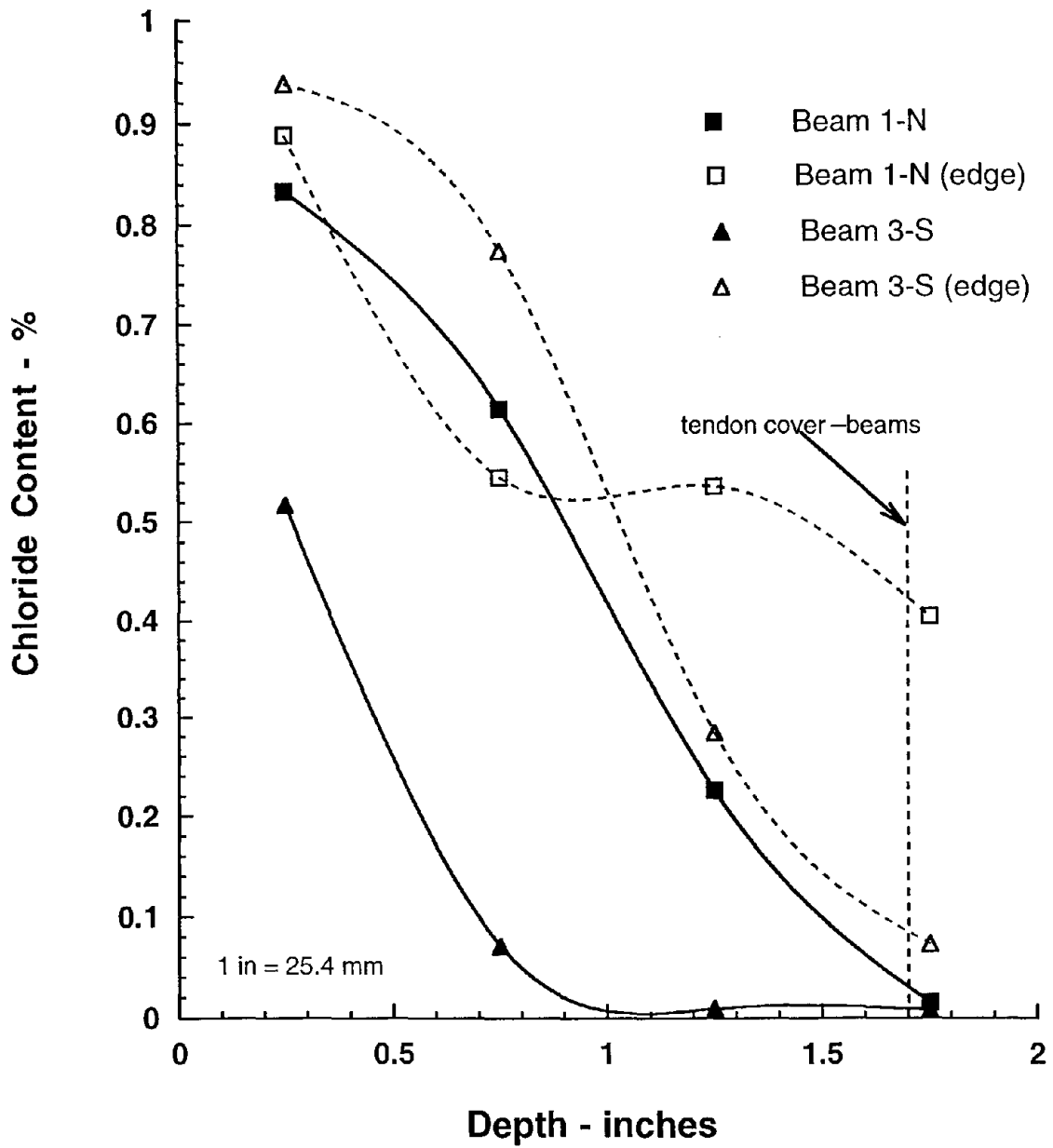


Figure 40. Comparison of chloride contents measured at center and near edges of beam repair patches.

Dissection. After all drill samples had been obtained and analyzed, the tendons and reinforcing steel in the patch areas were uncovered by air-hammer removal of the concrete cover. In comparison with the slabs, it was possible to remove the patch without breakout of the concrete substrate. Photographs of steel in beam 1 (conventional concrete patches) in the north (epoxy coating) and south (zinc-rich coating) patches are shown in Figures 41 and 42. There is significant loss of coating on the tendons in the north patch, and corrosion on the underlying tendon surface, especially near the edge of the patch. The plain reinforcement has also suffered loss of coating and corrosion. In the south patch (Figure 42), coating has also been lost, and there are spots showing corrosion of the tendons. After documentation of the external appearance of the tendons, cuts were made in each tendon and the individual strands pulled back from the bundles. Figure 43 shows some of the interior portions of the strands in the north patch. As in the slab patches, considerable rusting of the tendons in the interior of the bundle is obvious when the strands are pulled back, as can be seen in the middle tendon shown in Figure 43. This can be compared with the exterior surface of the tendon at the bottom of the photo, where, although coating has been lost, no corrosion can be seen on the exterior strand surfaces. The same procedure was carried out on the zinc-coated strands in the south patch. Figure 44 shows strands pulled back from the lower bundle, which had not shown any exterior corrosion. Rusting is noticeable on the interior of the strands.

Uncovered tendons and reinforcing steel in patches on beam 2 (latex-modified concrete patches) are shown in Figures 45 (north-patch epoxy) and 46 (south-patch zinc). On the epoxy-coated tendons, the coating failure is similar to that for the corresponding beam 1 patch; however, there is more corrosion on the tendons, especially at the patch edges. The rebar at the edge of the patch shows significant coating failure and numerous areas of corrosion. In the south (zinc) patch, there is more loss of coating than in the corresponding beam 1 patch and more corrosion at the patch edges. There are areas of corrosion on the reinforcing steel that lies below the level of the tendons. Upon cutting and peel-back of the individual strands from one of the tendons in the north repair area, extensive corrosion of the interior of the bundle was observed (Figure 47). Corrosion of interior strands was also observed in the zinc-coated area (Figure 48).

Uncovered tendons and steel in beam 3 (silica fume concrete with inorganic corrosion inhibitor) are shown in Figures 49 and 50 for epoxy-coated and zinc-coated steel, respectively. Here, in both areas, while there appears to be loss of coating, corrosion is much less prevalent than for the previous two beams. There is no corrosion visible on the reinforcing steel in the epoxy-coated area, and only a couple of minor spots of corrosion on the reinforcing steel in the zinc-coated area.



Figure 41. Appearance of uncovered tendons and reinforcing steel in north repair area, beam 1, after 100 exposure cycles.



Figure 42. Appearance of uncovered tendons and reinforcing steel in south repair area, beam 1, after 100 exposure cycles.



Figure 43. Appearance of interior of tendon bundle in north repair area, beam 1, after 100 exposure cycles.



Figure 44. Appearance of interior of tendon bundle in south repair area, beam 1, after 100 exposure cycles.

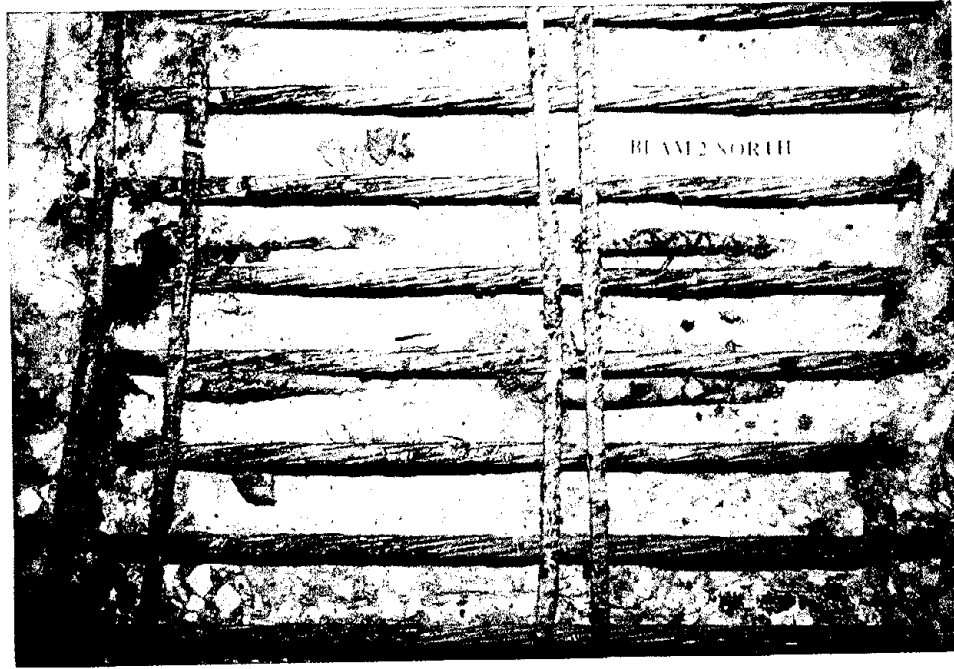


Figure 45. Appearance of uncovered tendons and reinforcing steel in north repair area, beam 2, after 100 exposure cycles.

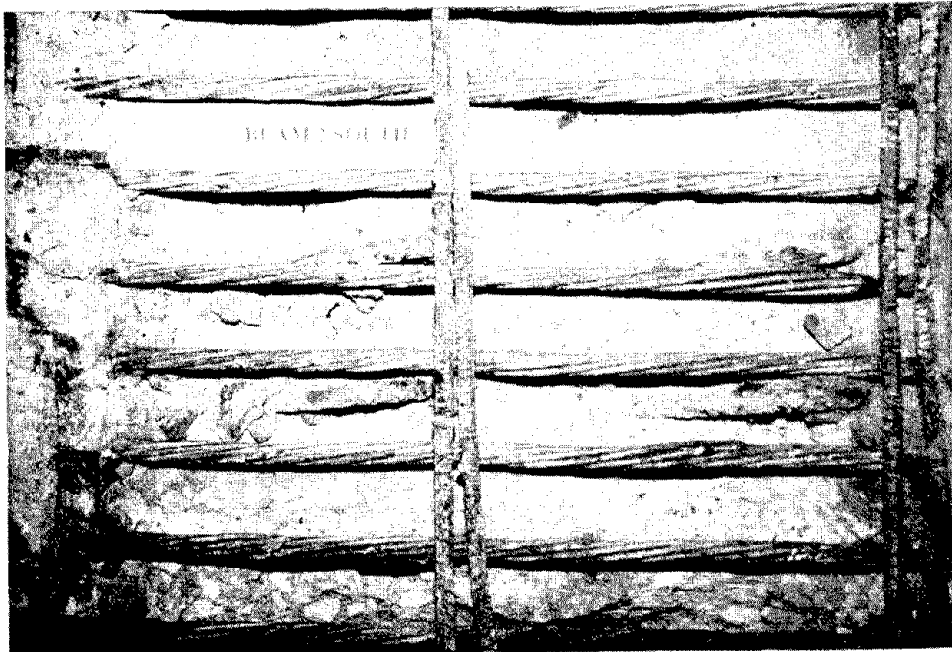


Figure 46. Appearance of uncovered tendons and reinforcing steel in south repair area, beam 2, after 100 exposure cycles.



Figure 47. Appearance of interior of tendon bundle in north repair area, beam 2, after 100 exposure cycles.



Figure 48. Appearance of interior of tendon bundle in south repair area, beam 2, after 100 exposure cycles.



Figure 49. Appearance of uncovered tendons and reinforcing steel in north repair area, beam 3, after 100 exposure cycles.



Figure 50. Appearance of uncovered tendons and reinforcing steel in south repair area, beam 3, after 100 exposure cycles.

While pulling back individual strands does exhibit rusting on the epoxy-coated strands (Figure 51), there is much less on the zinc-coated strands in the inhibited patch (Figure 52).

Based on examination of the tendons and reinforcing steel in the uncovered beam patch areas, a rough assessment of the performance of the beams would be that beam 3 shows the best performance (least corrosion), beam 2 the worst (most corrosion). As was the case for the slabs, this is especially true for the repair areas containing epoxy-coated steel. In contrast to the slabs, however, the surface appearance of the beam patches did not appear to correlate with the underlying performance of the steel. The half-cell potentials (refer to Figure 35) appeared to be quite useful as a non-destructive means of following the behavior of the steel in the beam patches. The most electro-negative potentials were consistently recorded for the beam 2 patches, where the steel was most severely corroded. The most electro-positive potentials were recorded for the beam 3 patches, where the steel was least corroded. Chloride contents (refer to Figure 39), for the most part, did little to explain the ultimate corrosion behavior of the steel in the patches. In fact, at the tendon level for beam 2 (where the worst corrosion occurred) chloride contents were found to be below "threshold" level. Again, as for the slabs, the presence of corrosion within the strand bundles indicates that the cause of the corrosion was not the chloride that penetrated the beam patches from the surface pond over the course of the monitoring, but rather the chloride and moisture trapped within the interstices of the bundle during the initial exposures, or the chloride solution that migrated into the bundle in a lateral direction from the surrounding concrete. The latter scenario would likely be more of a contributing factor at the edges of the patch, where the most severe corrosion was found to occur.

Pile Repairs

Half-Cell Measurements. An initial set of half-cell measurements was made at the end of the first 12 tidal cycles. Readings were made along the center tendon at elevations of 305, 610, 915, 1065, 1220, and 1525 mm (12, 24, 36, 42, 48, and 60 in). Results are shown in Table 15. The readings become progressively more electro-negative as one proceeds from the top to the bottom of the piles. The repair areas effectively define the limits of the tidal zone. At any given level, readings are similar across the piles, with pile 1 being somewhat less electro-negative, especially in the tidal zone. The only visible distress on the patches appeared to be some very fine map cracking, which was limited to the surface of the patches.

The trend of the potentials within the pile repair areas over the entire 215 weeks of testing is shown in Figure 53. In contrast to the beams and slabs, there are no clearly consistent differences



Figure 51. Appearance of interior of tendon bundle in north repair area, beam 3, after 100 exposure cycles.



Figure 52. Appearance of interior of tendon bundle in south repair area, beam 3, after 100 exposure cycles.

Table 15. Half-cell potentials measured on pilings after 12 weeks of tidal cycling.

Height from bottom - inches	Piling No. 1		Piling No. 2		Piling No. 3	
	North Face Potential (mV vs. CSE)	South Face Potential (mV vs. CSE)	North Face Potential (mV vs. CSE)	South Face Potential (mV vs. CSE)	North Face Potential (mV vs. CSE)	South Face Potential (mV vs. CSE)
12	773	782	794	790	784	781
24	694	669	759	775	736	736
36	546	521	587	642	616	647
42	457	487	552	558	542	568
48	405	410	484	488	477	505
60	274	202	216	283	201	274

1 in = 25.4 mm

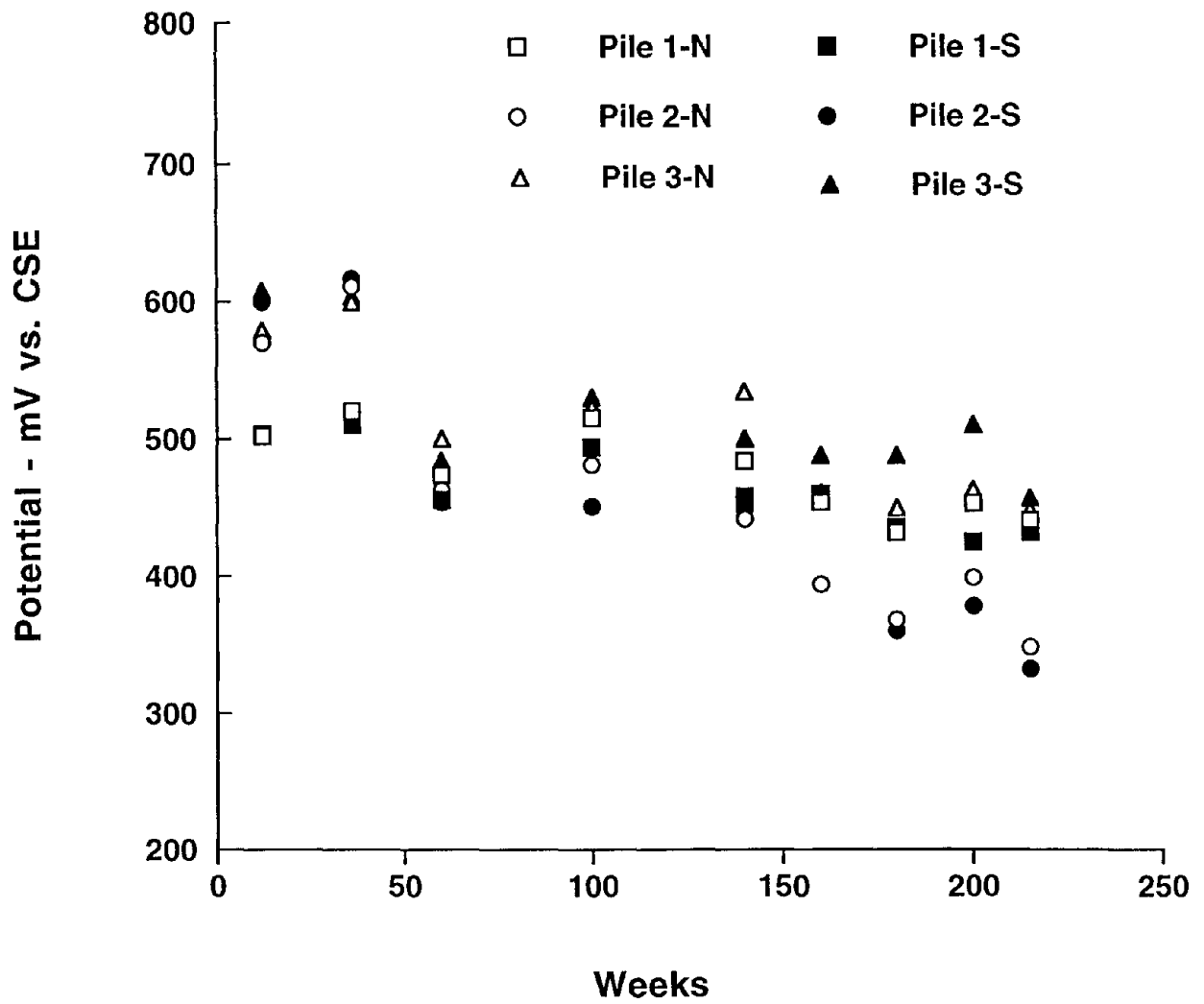


Figure 53. Average half-cell potentials in pile repair areas over 215 weeks of tidal cycling.

between the various repair areas on the pile specimens. Overall, there appears to be a progressive decrease in absolute value of potential over the course of the monitoring. As the repair areas are almost continuously saturated, this may reflect a long-term hydration of the cement, resulting in a denser microstructure, lower permeability, and higher resistivity.

Chemical Analysis. After completion of monitoring, the piles were removed from the tidal tanks and samples were obtained from each specimen for chemical analysis. Sample locations were at the center of each repair area at opposing faces of each pile. Samples were taken at 12-mm (0.5-in) increments down to a level of 64 mm (2.5 in), and analyzed for total chloride ion. Samples taken from pile 1 were also analyzed for nitrite ion content, as the patching material for this pile was silica fume concrete with inorganic corrosion inhibitor. Results are shown in Figure 54. Significant amounts of chloride had penetrated the upper levels of the patches. The silica fume patches (1-N and 1-S) showed the least penetration, along with patch S on pile 2 (latex-modified material). However, there was essentially no chloride ion detected at the level of the prestressing strands in any of these specimens. This is predominantly due to the fact that clear cover for the piles was significantly greater than for the beam or slab specimens. Nitrite ion contents ranged from 0.11% at the first increment (likely reflecting some leaching out into the saltwater) and 0.17% at the remaining levels.

Dissection. After all drill samples had been obtained and analyzed, the tendons and reinforcing steel in the patch areas were uncovered by air-hammer removal of the concrete cover. Photographs of steel in pile 1 (silica fume concrete patches) in the north (epoxy coating) and south (zinc-rich coating) patches are shown in Figures 55 and 56. There was some loss of coating in the epoxy-coated area, but significantly less than in the corresponding patch on the beam or slab specimens. Some rusting was noted in areas where the coating had disbonded from the tendons. In the zinc-coated areas, there was some slight loss of coating, but no noticeable corrosion on the external surfaces of the tendons. After documentation of the external appearance of the tendons, cuts were made in each tendon and the individual strands were pulled back from the bundles. Figure 57 shows some of the interior portions of the strands in the north patch. As in the slab and beam patches, rusting of the tendons in the interior of the bundle is obvious when the strands are pulled back, demonstrating again that corrosion may occur even though the coating overall appears to be sound and chlorides have apparently not penetrated through repaired areas to the steel from the external environment. When the interiors of the other two tendons in this patch were examined, less rusting was observed. The same procedure was carried out on the zinc-coated strands in the south patch. Figure 58 shows strands pulled back from the lower bundle, which had not shown any exterior corrosion. Again, rusting is noticeable on the interior of the strands. The center

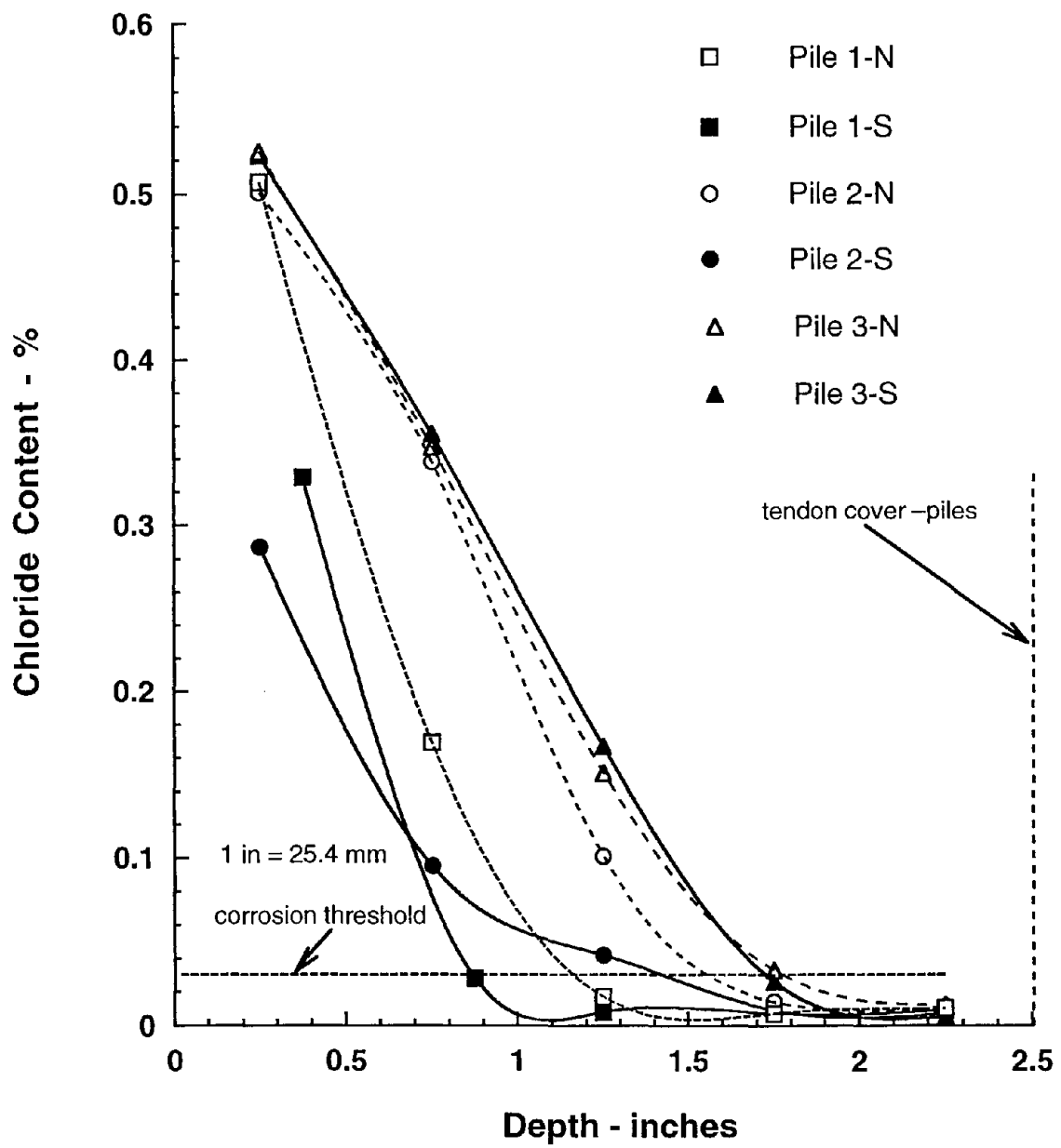


Figure 54. Chloride contents measured on pile repair specimens.



Figure 55. Appearance of uncovered tendons and reinforcing steel in north repair area, pile 1, after 215 weeks of tidal cycling.



Figure 56. Appearance of uncovered tendons and reinforcing steel in south repair area, pile 1, after 215 weeks of tidal cycling.

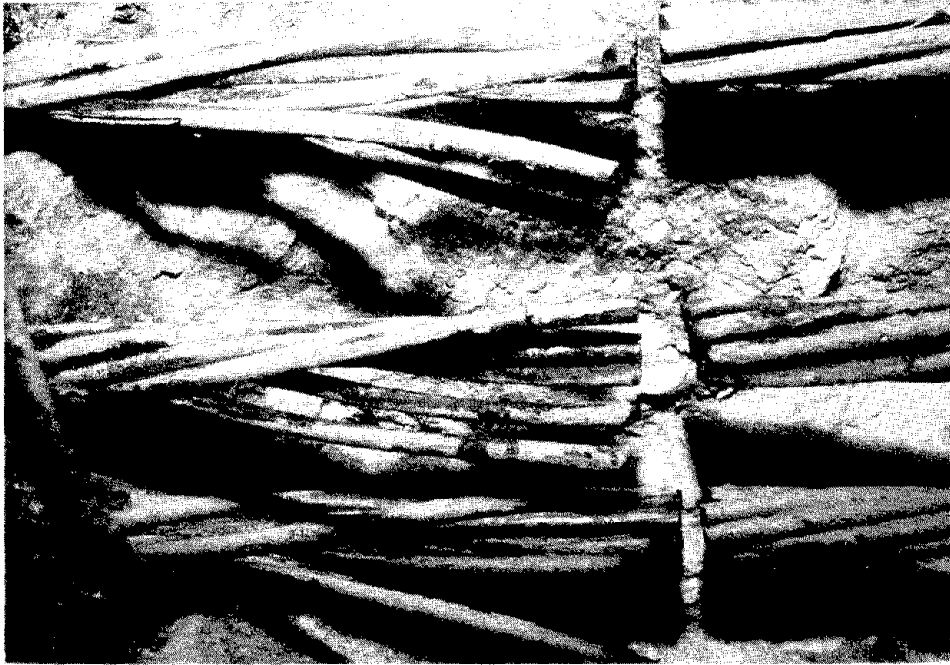


Figure 57. Appearance of interior of tendon bundle in north repair area, pile 1, after 215 weeks of tidal cycling



Figure 58. Appearance of interior of tendon bundle in south repair area, pile 1, after 215 weeks of tidal cycling.

tendon showed the most corrosion on the interior of the strands; less was observed on the two outer tendons.

Uncovered tendons and reinforcing steel in patches on pile 2 (latex-modified concrete patches) are shown in Figures 59 (north-patch epoxy) and 60 (south-patch zinc). On the epoxy-coated tendons, the coating failure is somewhat more extensive than in pile 1. The same is true for the zinc-coated area, where more of the zinc appears to have been lost than in the pile 1 area. Upon cutting and peel-back of the individual strands from the tendons in repair area N (epoxy), widespread corrosion of the interior of the bundles was observed (Figure 61). Corrosion of interior strands was also observed in the zinc-coated area (Figure 62).

Pile No. 3 was patched with a conventional concrete mixture. Photographs of uncovered steel are shown in Figures 63 (epoxy coating) and 64 (zinc coating). There appears to be somewhat more loss of coating and corrosion in the epoxy area for this pile as opposed to the corresponding areas on piles 1 and 2. The zinc section appears comparable to the other two piles. Figure 65 shows the interior surfaces of strands in the epoxy area after cutting and peel-back of the bundles. As for the other piles, the center strands exhibited the most interior corrosion. The corresponding zinc-coated strands are shown in Figure 66. Again, there is corrosion evident on many of the individual strands in the center bundle.

Based on examination of the tendons and reinforcing steel in the uncovered pile patch areas, an approximate assessment of the performance of the piles would be that pile 1 shows the best performance (least corrosion), and the performances of piles 2 and 3 were approximately the same, both showing a moderate amount of coating failure and corrosion. Again, as was the case for the slabs and beams, distress was more prevalent in the areas where epoxy coating was applied to the steel, although the differences between the two coating types were less obvious here than for the slab or beam specimens. As for the beams, the underlying performance of the steel was not reflected in the visual appearance of the patches during the monitoring period. As noted in the discussion of Figure 53, half-cell potentials were not indicative of differences in the behavior of steel in the patches. Again, as for the beams, chloride contents (refer to Figure 54) did little to explain the ultimate corrosion behavior of the steel in the patches, as there was virtually no chloride detected at the level of the tendons. While it is possible that some chlorides may have penetrated laterally as was the case for slabs and beams (no edge samples were taken for the piles), this was not reflected in any increased coating failure or corrosion at the edges of the patch, as was seen for the slab and beam specimens. Quite likely, the improved overall performance of the pile patches can be attributed to: (1) the increased concrete clear cover over the reinforcing steel and

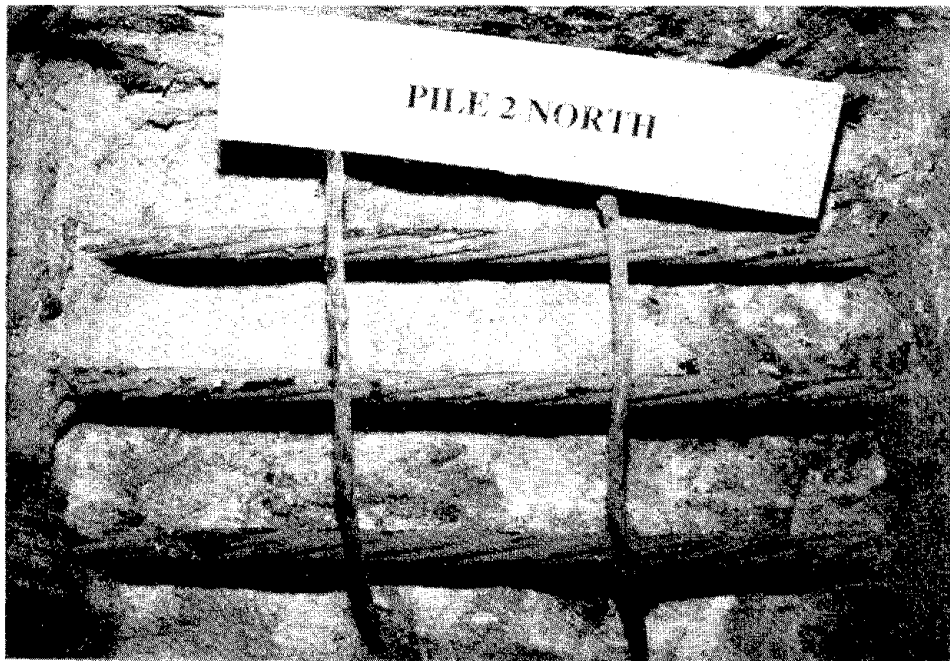


Figure 59. Appearance of uncovered tendons and reinforcing steel in north repair area, pile 2, after 215 weeks of tidal cycling.



Figure 60. Appearance of uncovered tendons and reinforcing steel in south repair area, pile 2, after 215 weeks of tidal cycling.



Figure 61. Appearance of interior of tendon bundle in north repair area, pile 2, after 215 weeks of tidal cycling.

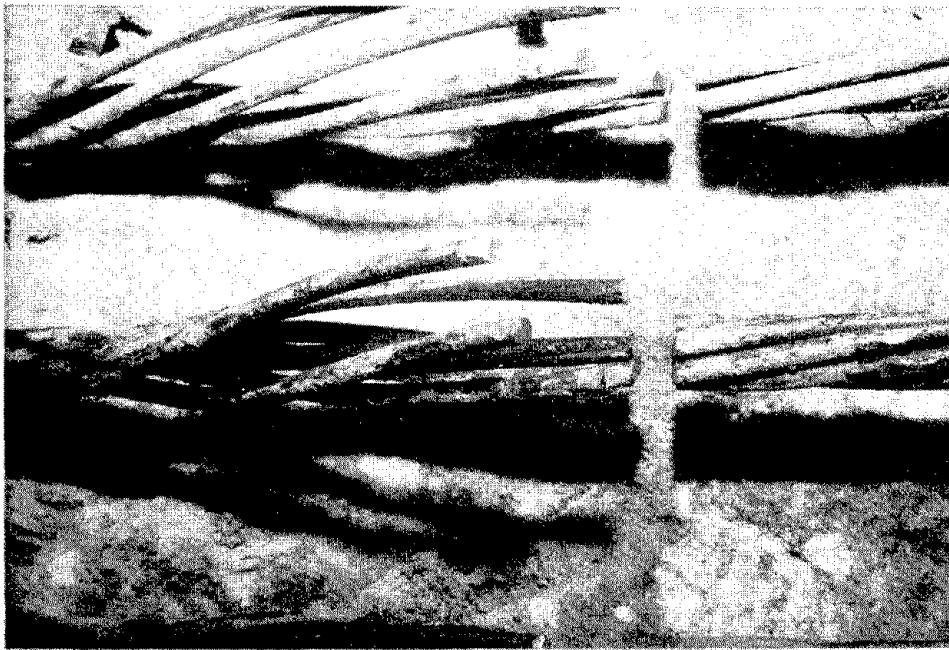


Figure 62. Appearance of interior of tendon bundle in south repair area, pile 2, after 215 weeks of tidal cycling.

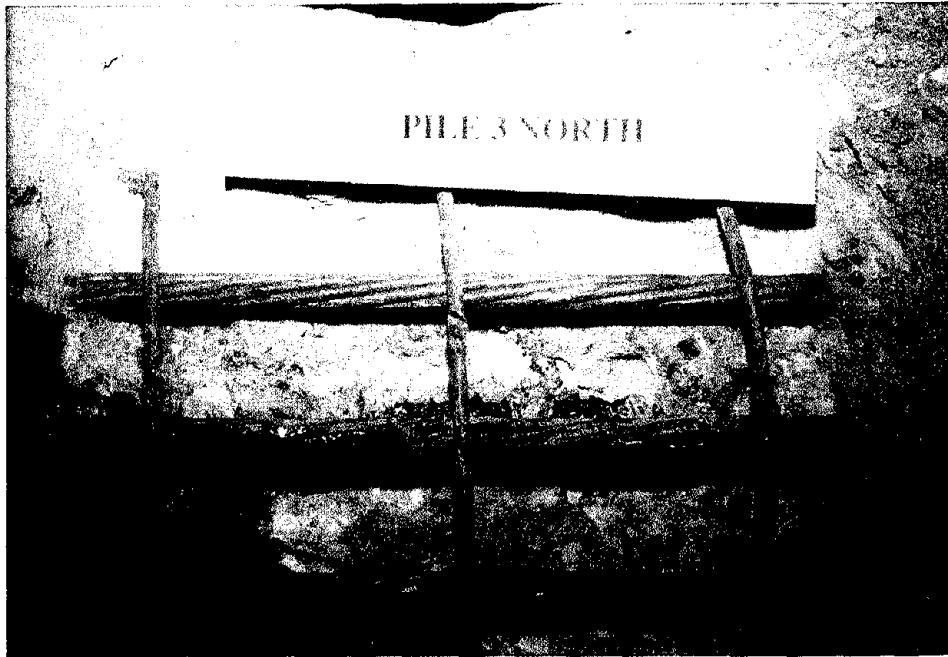


Figure 63. Appearance of uncovered tendons and reinforcing steel in north repair area, pile 3, after 215 weeks of tidal cycling.



Figure 64. Appearance of uncovered tendons and reinforcing steel in south repair area, pile 3, after 215 weeks of tidal cycling.



Figure 65. Appearance of interior of tendon bundle in north repair area, pile 3, after 215 weeks of tidal cycling.



Figure 66. Appearance of interior of tendon bundle in south repair area, pile 3, after 215 weeks of tidal cycling.

tendons, and (2) the fact that the piles were essentially submerged throughout the course of monitoring (the short tidal cycle left little time for drying). Submersion of the piles would have limited oxygen access to the steel, reducing cathodic reactions and corrosion rates.

CATEGORY B - COATINGS AND SEALERS

Pretensioned Slabs

As noted in Chapter 3, after application and curing of sealers and coatings, category B specimens were returned to the environmental exposures. This occurred approximately 6 months prior to installation of repair patches on the category A specimens, so the spray system was initially operational for the category B specimens. A 1-week spray with 15% NaCl followed by a 1-week dry cycle was used. After approximately 7 months of exposure of category B specimens, problems with the saltwater-spray systems, as described previously, were encountered. The specimens underwent a dry period of about 6 weeks while repairs were attempted, and finally the alternative ponding routine was established. Again, this consisted of 1 week of ponding of the coated surface of the specimen with 15% NaCl, followed by 1 week of drying under the ambient laboratory conditions. Slabs underwent a total of 118 such cycles during the course of the monitoring.

Monitoring consisted of: (1) measurement of macrocell currents at 1- to 2-cycle intervals, (2) measurement of half-cell potentials at 2- to 4-cycle intervals, and (3) visual observations. Macrocell currents were measured between the tendons on each slab and four embedded electrically isolated reinforcing bars located 25 mm clear from the top of the slab (saltwater spraying and subsequent ponding were carried out on the bottom of the slabs) as shown in Figure 2. These currents were calculated from the measured voltage drop across a 1-ohm resistor placed in series with the tendons and isolated reinforcing bars. Half-cell potentials were measured along the length of each tendon. Dissection of the specimens after completion of the monitoring was not carried out. This is because these specimens were subjected to the same electrical acceleration of corrosion as the repair series (category A) specimens. However, as no concrete was removed from category B specimens prior to coating, the steel remained in its previously corroded condition. Therefore, no distinction could have been made by visual observation of uncovered steel between corrosion that occurred before or after application of the coatings and sealers.

Macrocell currents measured on sealed and coated slabs over the 118 cycles are shown in Figure 67. Initial currents for all specimens just prior to and after coating are high. The currents

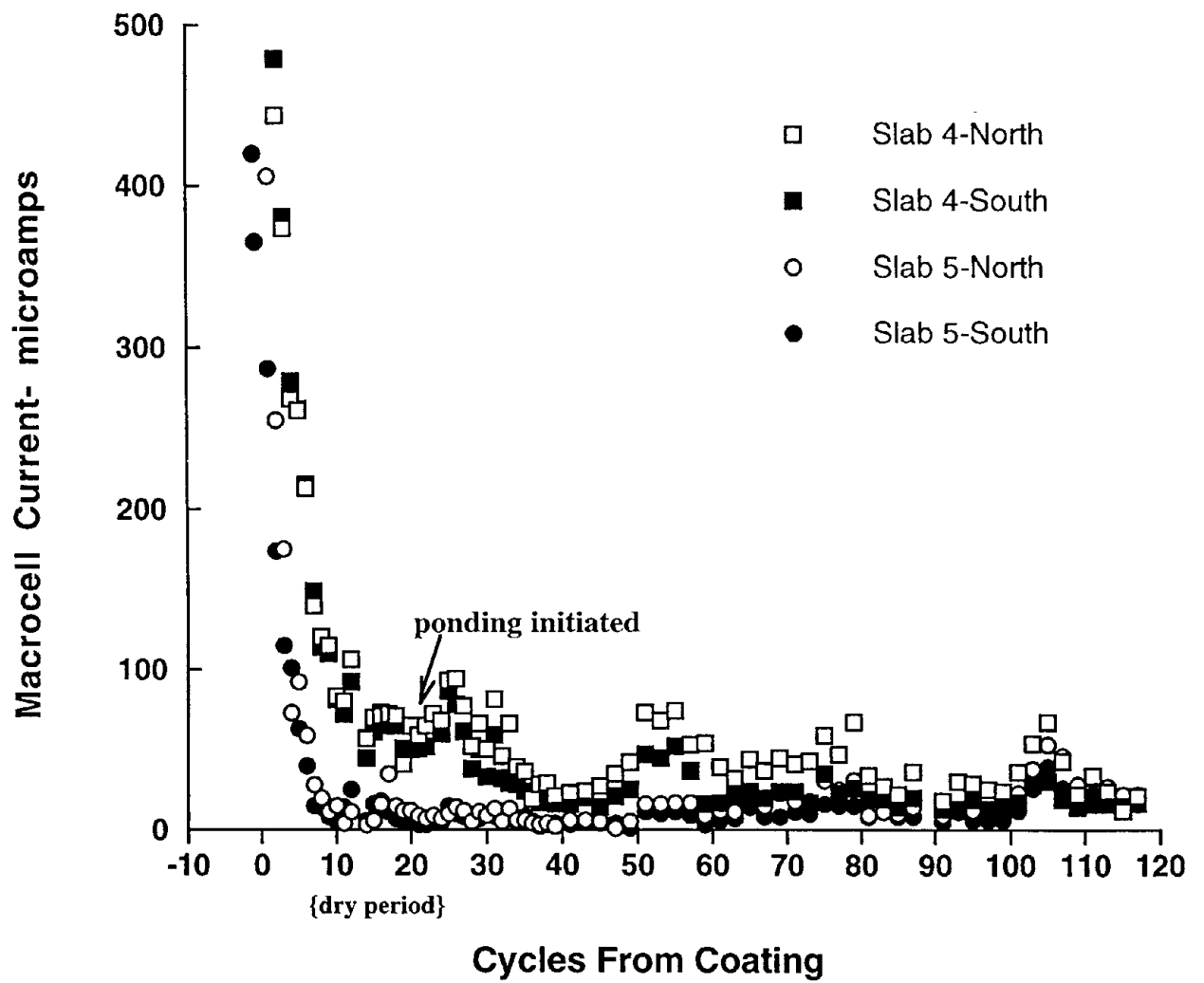


Figure 67. Macrocell currents in coated slab specimens over 118 cycles of testing.

continued to drop in the months after coating, and then appeared to stabilize during the "dry period" when exposure conditions were being altered. At the end of this period, ponding on the weekly cycle was initiated. At this point, slab 5 (alkyl-alkoxy silane sealer) currents were significantly less than those measured on slab 4 (two-part epoxy coating). Currents then began to follow a seasonally cyclic pattern as can be seen in Figure 67. The periods of the highest current, for instance, between cycles 22 to 32, 50 to 60, 75 to 80, and 100 to 110, correspond to the summer months when temperatures were higher and corrosion would be expected to accelerate. It is also of interest to note the time-dependence of the difference between slab 4 and slab 5 currents. Up through about 80 cycles of testing, slab 5 currents were consistently less than slab 4 currents, in both peaks and bases of the seasonal periods. After 80 cycles of testing, however, the measured currents began to be less distinct between the two slabs, and by the last winter of monitoring, the currents essentially overlapped for both slabs. Thus, it appears that slab 4 performance is stable over the period of testing, while slab 5 initially passed less current, but its performance degraded over time.

Half-cell potentials were measured at six positions along two of the tendons in each slab. Because the coatings (especially the two-component epoxy) create a high-resistance layer at the treated (top) surface of the slab, potentials were measured by pre-wetting the bottom surface of the slab and making the measurements from this side. As the strands were placed at the central axis of the slab, cover was essentially equivalent from either the top or bottom surfaces. It should be noted that the "bottom" surface of the slabs in the laboratory monitoring program was actually the top surface of the slabs as cast, since the slabs had been turned upside down when the salt spray was discontinued in order to be able to pond the soffits with saline solution. Results of the half-cell testing are shown in Figure 68. Results are the average of 12 readings on each slab. As for the macrocell current measurements, half-cell readings initially were high (more electro-negative), then fell after application of coatings. They also exhibited the seasonal pattern seen for the macrocell currents. Up through 100 cycles, slab 4 exhibited more electro-negative readings than slab 5. This agrees with the macrocell currents. For the last few readings, as was the case for the macrocell currents, the potentials are similar for the two slabs.

Visual appearance of the slabs after the 118 cycles of exposure is shown in Figures 69 A and B (slab 4, north and south halves) and Figures 70 A and B (slab 5, north and south halves). The two-part epoxy coating (slab 4), though exhibiting some crazing and limited chalking, was still bonded well to the substrate and no extensive failures were noted. There was one small area of rust staining on the north half of the slab, and a larger area where the coating had blistered on the south half of the slab. The only overall defects in the coating were extensive pinholing, which had

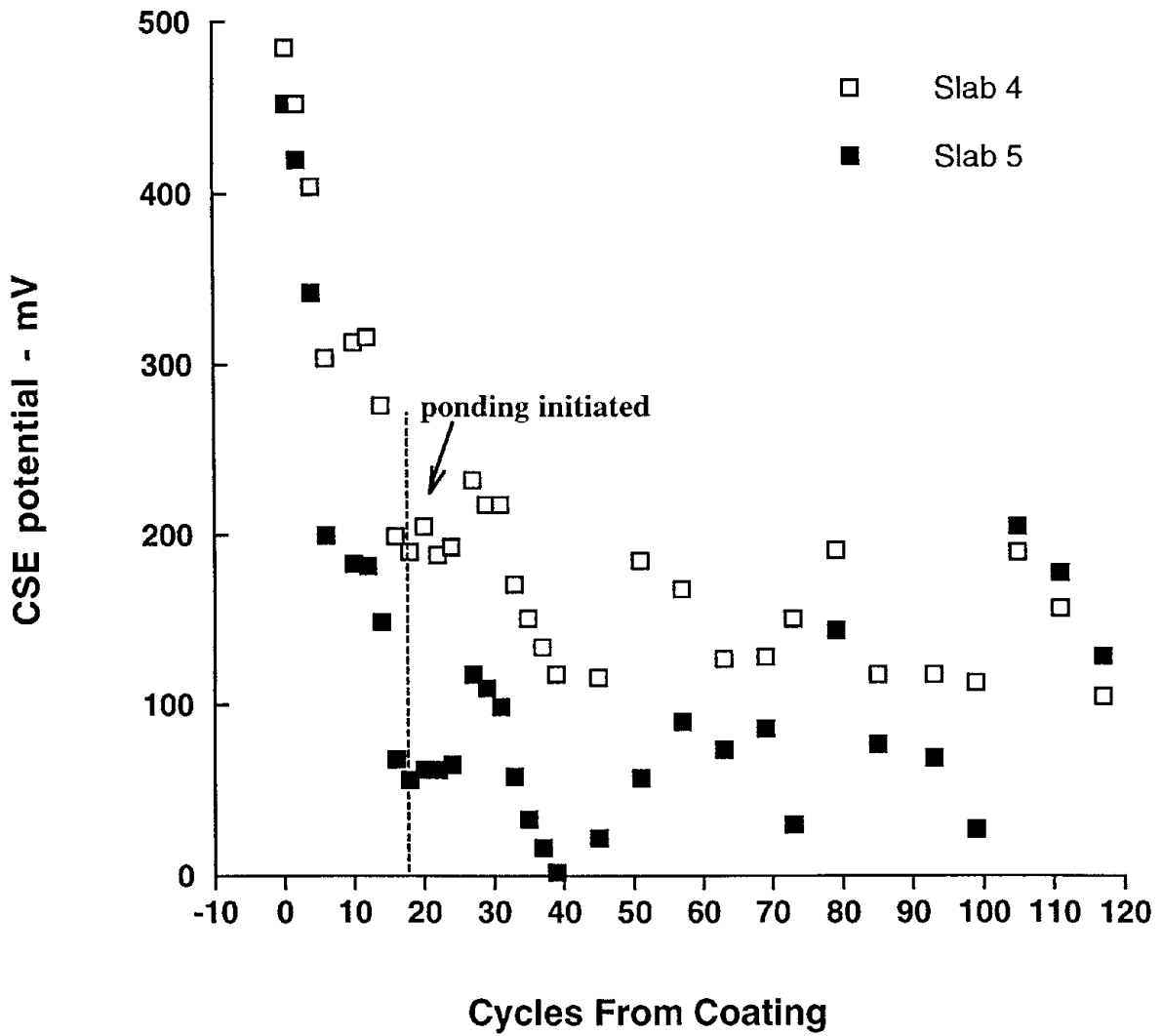


Figure 68. Half-cell potentials in coated slab specimens over 118 cycles of testing.

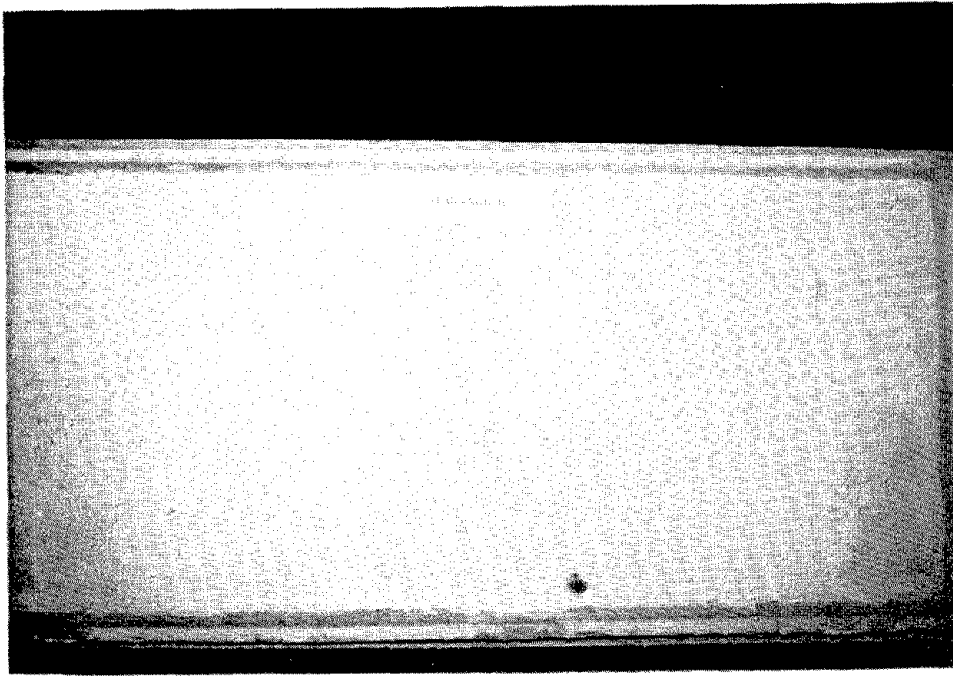


Figure 69 A. Appearance of surface of north half of slab 4 after 118 weekly salt ponding cycles.

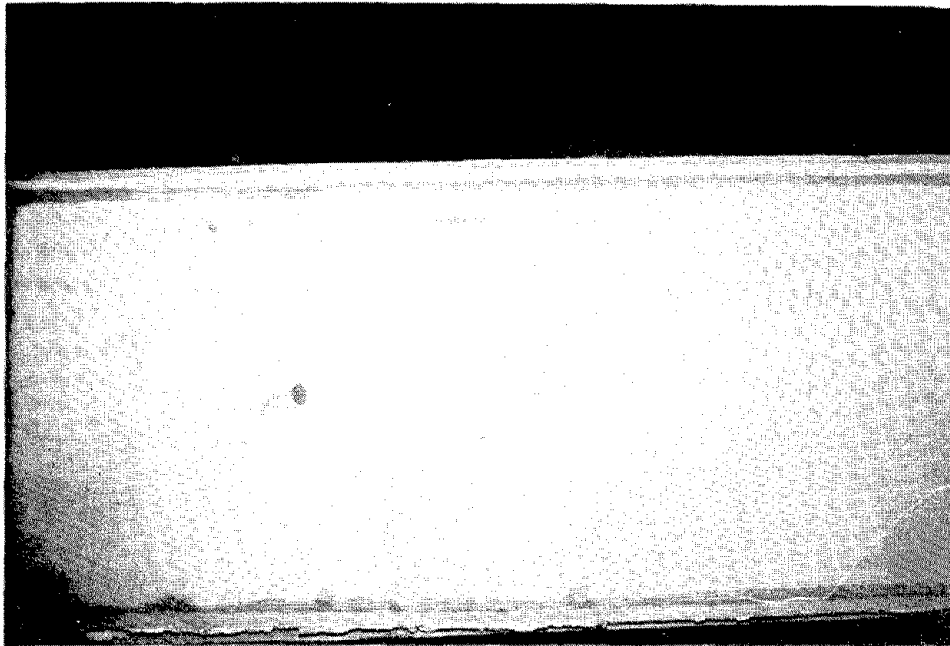


Figure 69 B. Appearance of surface of south half of slab 4 after 118 weekly salt ponding cycles.

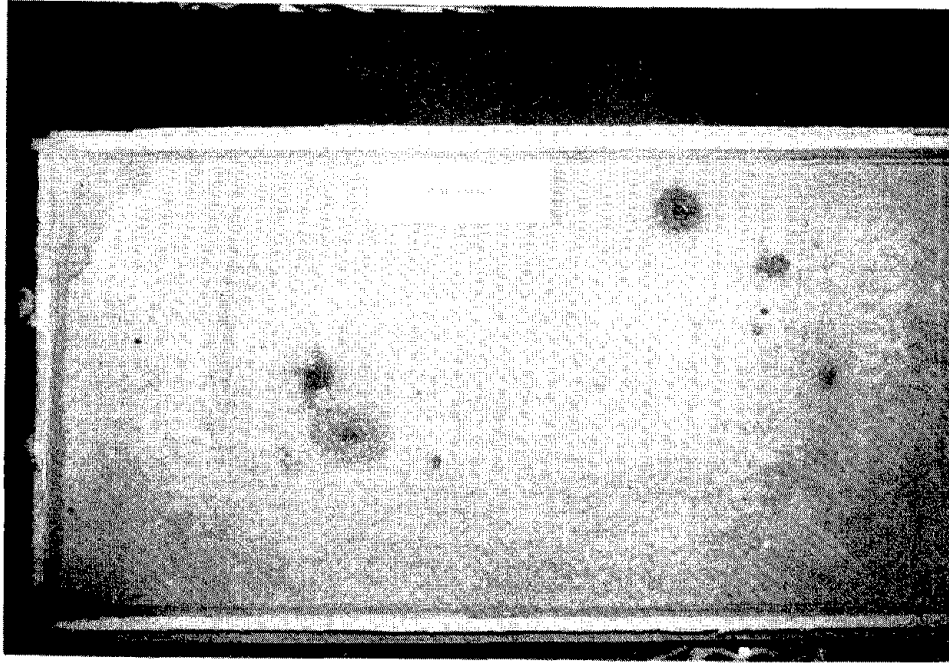


Figure 70 A. Appearance of surface of north half of slab 5 after 118 weekly salt ponding cycles.

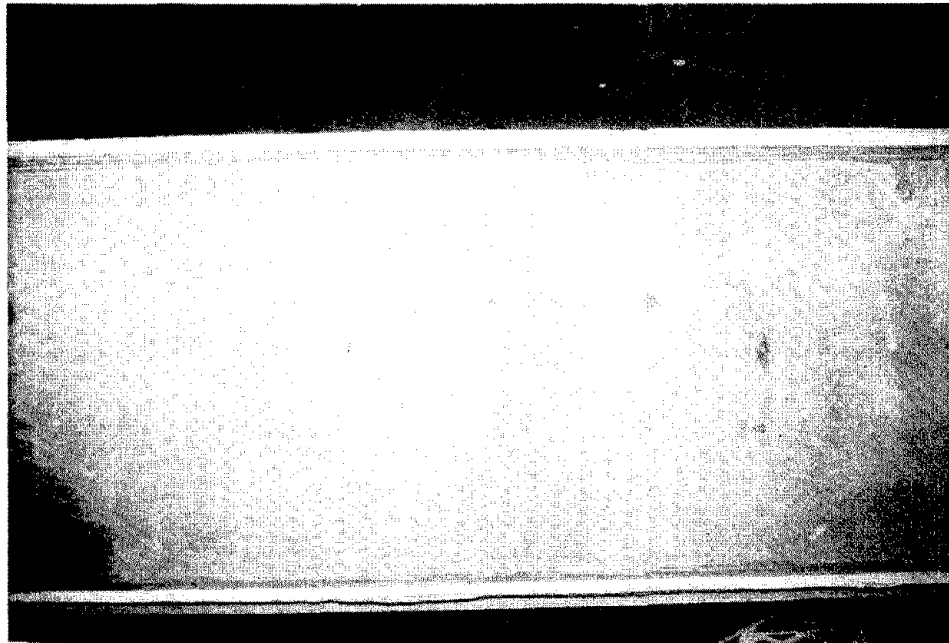


Figure 70 B. Appearance of surface of south half of slab 5 after 118 weekly salt ponding cycles.

been present since initial installation of the coating. The pinholes, however, did not appear to degrade the performance of the coating. Rust staining was somewhat more prevalent on slab 5, which had been treated with the penetrating alkyl-alkoxy silane sealer. As noted in Chapter 3, the rust stains were mostly associated with holes for plastic inserts, which had been drilled into the slabs in order to mount the mesh used in the electrical acceleration of chloride ingress. In the absence of these inserts, it is likely that little or no rust stains would have appeared on these slabs.

Drill samples were obtained from two locations on each slab over a single tendon. Samples were taken at 12-mm (0.5-in) increments and chemically analyzed for total chloride ions. Results are shown in Figure 71 and are compared with chloride profiles for these same slabs taken after acceleration of chloride ingress, but prior to application of coatings. It can be seen that after 118 weekly cycles of ponding, considerably more chloride had penetrated into the slabs. Therefore, it is apparent that these coatings do not fully prevent additional chloride ions from entering the concrete. This is not surprising, as previous studies ^(9,10) have shown that "chloride screening" efficiencies of concrete sealers and coatings may vary widely.

Pretensioned Beams

Category B pretensioned beams received the same treatment, exposure, and monitoring as the corresponding pretensioned slabs. For the beams, macrocell currents were measured between the tendons in each beam and two electrically isolated reinforcing bars located in the lower flange of the beam as was shown in Figure 1. The trend of macrocell currents in the beam specimens is shown in Figure 72. While beam 5 (alkyltrialkoxo silane) currents initially were high, beam 4 (alkoxy siloxane/silane with topcoat of methyl methacrylate) values were significantly less at the start of exposure. Currents for both beams were similar up to about 50 cycles, at which time, beam 5 began to exhibit consistently higher currents. During peak periods, currents for beam 5 approached initial (uncoated) values. Between about 50 to 80 cycles, the data for beam 5-East have been deleted due to malfunction of the shunt resistor in this circuit during this period. The beam macrocell currents exhibit the same seasonal pattern as do the slab currents.

Half-cell potentials were measured at eight positions along both sides of the lower flange of each beam. Again, as the beams had been turned upside down to effect the ponding, this became the upper-most vertical position of the beams. In effect, potential was measured on the two outer-most tendons in the eight-tendon layer at the bottom of the beam (see Figure 1, section B, for details). Clear cover from these outer tendons to the sides of the beam was 50 mm (2 in). Results of the half-cell testing are shown in Figure 73. Results are the average of 16 readings on each beam. As

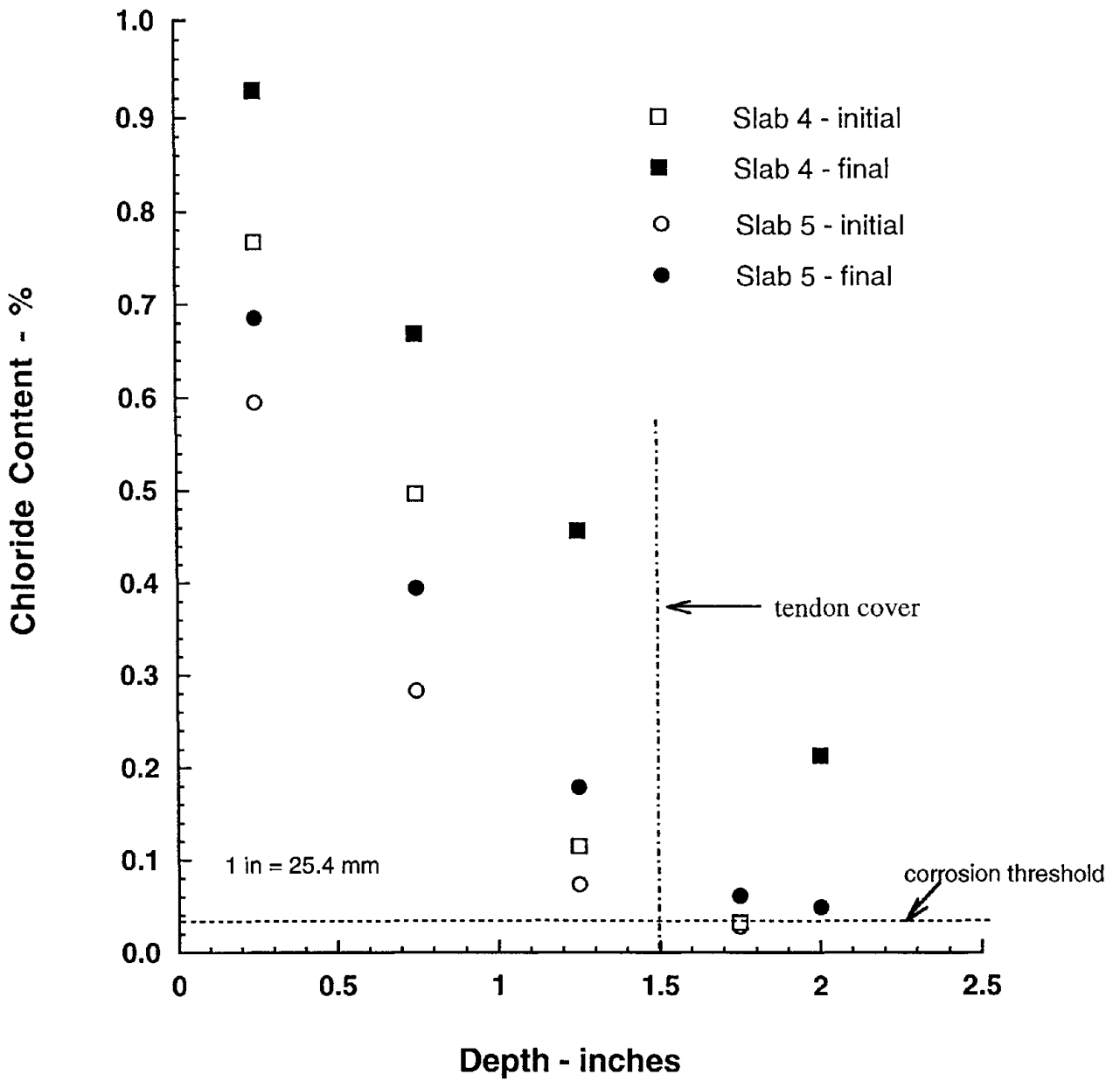


Figure 71. Chloride contents measured on slab specimens prior to and after 118 weeks of exposure.

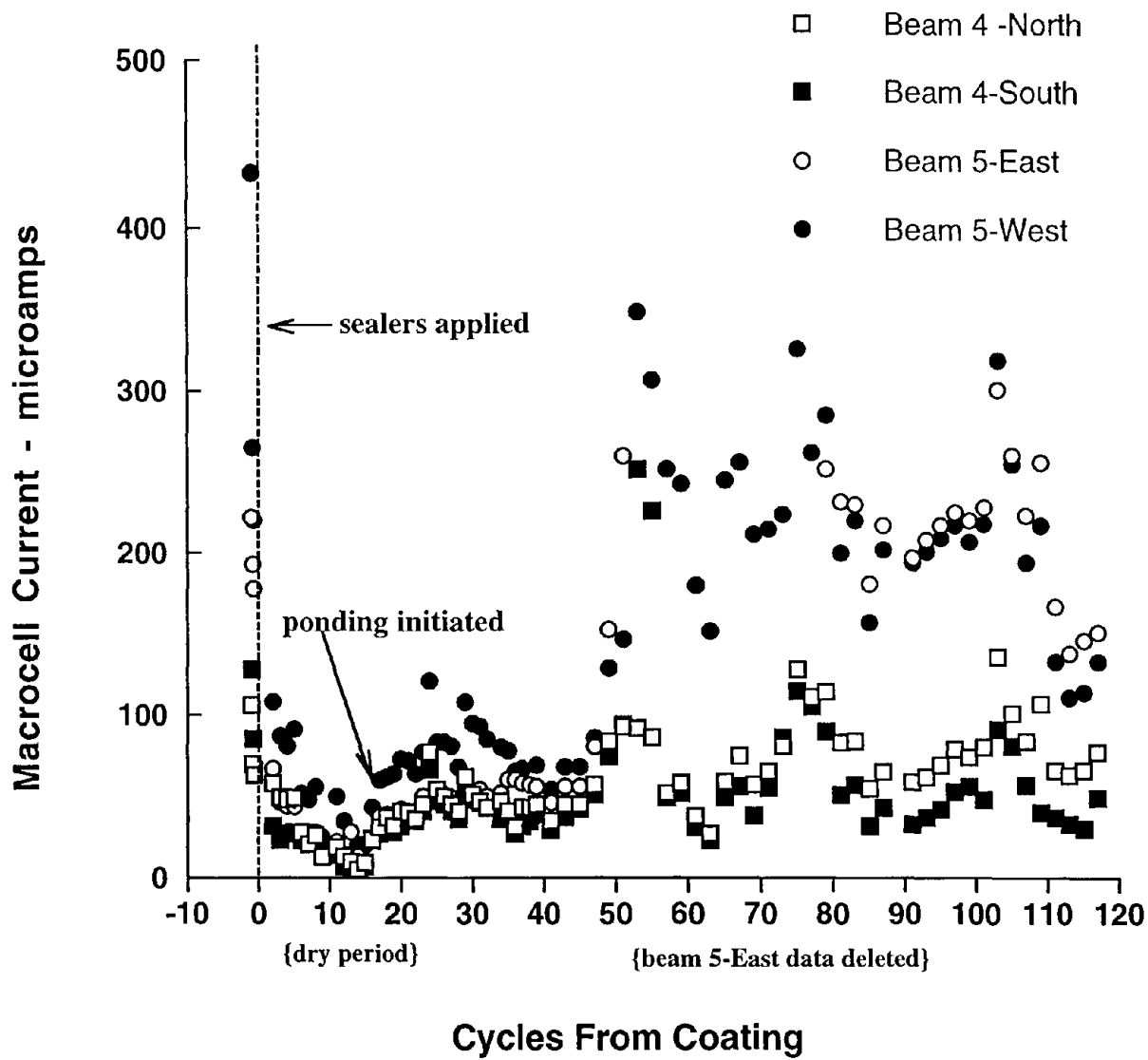


Figure 72. Macrocell currents in coated beam specimens over 118 cycles of testing.

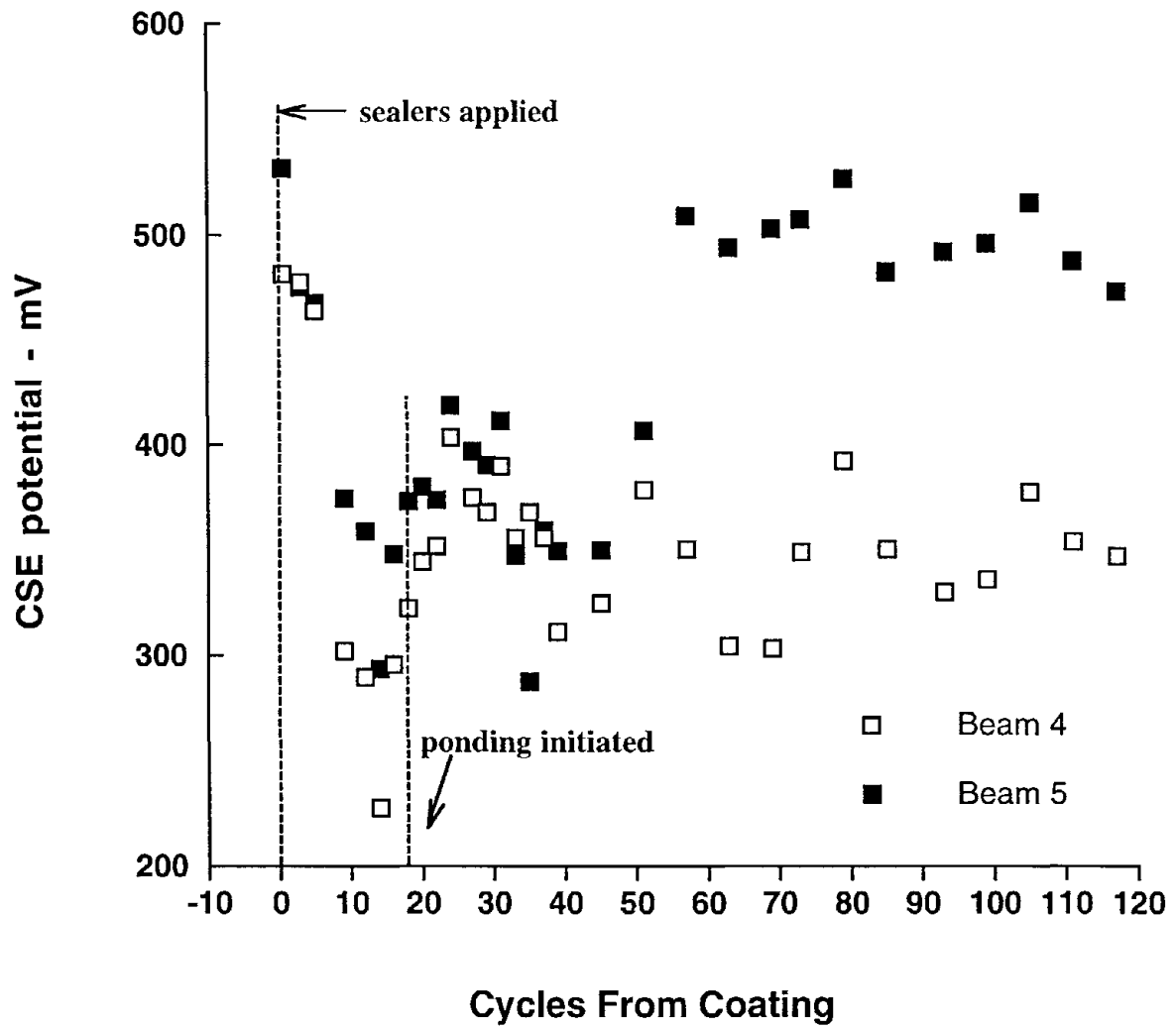


Figure 73. Half-cell potentials in coated beam specimens over 118 cycles of testing.

for the macrocell current measurements, half-cell readings were similar for both beams up to about 50 cycles, then they diverged. Potentials for beam 4 varied between 300 and 400 mV, whereas those for beam 5 returned to a more electro-negative potential near 500 mV. As for the macrocell currents, beam 5 potentials after 50 cycles approached those for initial (uncoated) conditions.

Visual appearance of the beams after the 118 cycles of exposure is shown in Figures 74 A and B (beam 4, north and south halves) and Figures 75 A and B (beam 5, east and west halves). The considerable amounts of rust staining on the surfaces of the specimens are associated with the feet of chairs used to support the embedded steel reinforcing bars. Although plastic-coated, the coating appears to have limited utility in such a corrosive environment. When these stains are discounted, the only other distresses observable are some surface cracks filled with an efflorescence presence on the surface of beam 5.

Drill samples were obtained from two locations on each beam over a single tendon. Samples were taken at 12-mm (0.5-in) increments and chemically analyzed for total chloride ions. Results are shown in Figure 76 and are compared with chloride profiles for these same beams taken after acceleration of chloride ingress but prior to application of coatings. It can be seen that at most depths, considerably more chloride had penetrated into the slabs during the exposure period. As for the slabs, it is apparent that these coatings also did not fully prevent additional chloride ions from entering the concrete.

Pretensioned Piles

After treatment with sealers, Category B pretensioned piles were returned to the polyethylene tanks and the 24-hour tidal cycle was re-initiated. The piles remained in this cycle throughout the course of monitoring (220 weeks) for a total of 3080 tidal cycles. In contrast to the slabs and beams, no macrocell currents were measured on the pilings. This is because conditions were not uniform from bottom to top of the pilings — there being submerged, tidal, and atmospheric zones as previously described. Half-cell measurements were carried out on two opposing faces of each piling at elevations of 305, 610, 915, 1065, 1220, and 1525 mm (12, 24, 36, 42, 48, and 60 in). Measurements were made over the middle tendon on each face. These measurements were made after temporarily draining the tanks each time. Results are shown in Figures 77 through 80. On each piling, potential becomes less electro-negative as the elevation from the bottom of the tank increases. This is not unexpected, as the saturated conditions at the bottom of the tank would reduce cathodic reactions and shift the potential into a more anodic zone. In this zone, potentials at first became somewhat more electro-negative, then appeared to stabilize near -600 to -700 mV.



Figure 74 A. Appearance of surface of north half of beam 4 after 118 weekly salt ponding cycles.

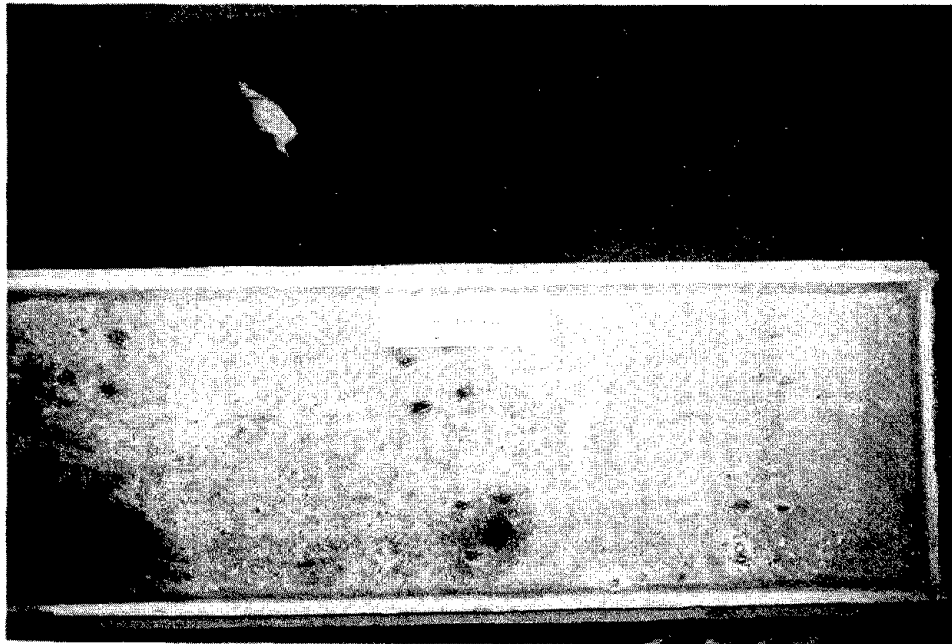


Figure 74 B. Appearance of surface of south half of beam 4 after 118 weekly salt ponding cycles.

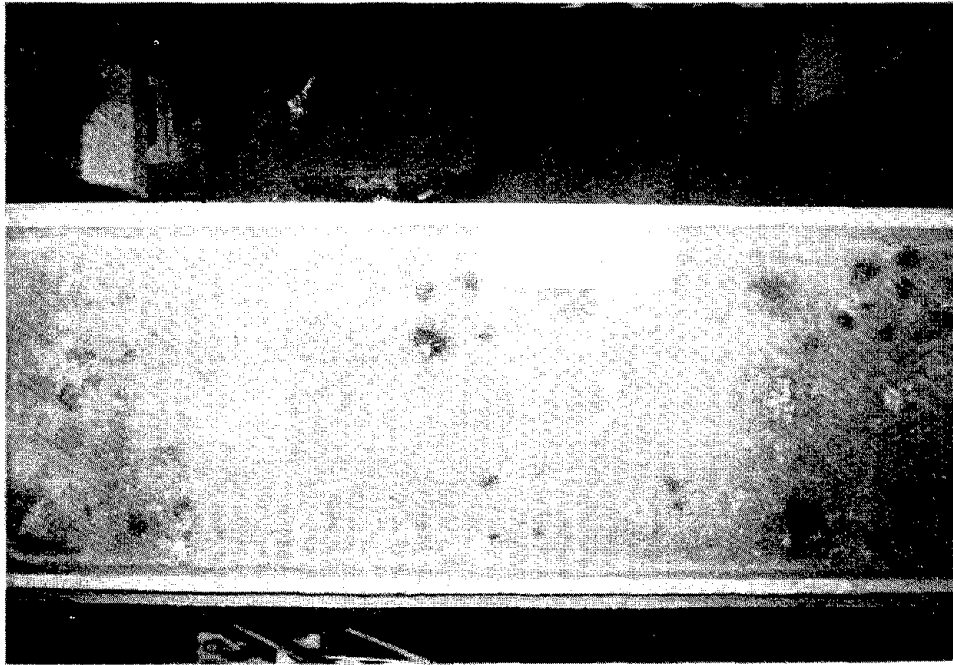


Figure 75 A. Appearance of surface of north half of beam 5 after 118 weekly salt ponding cycles.

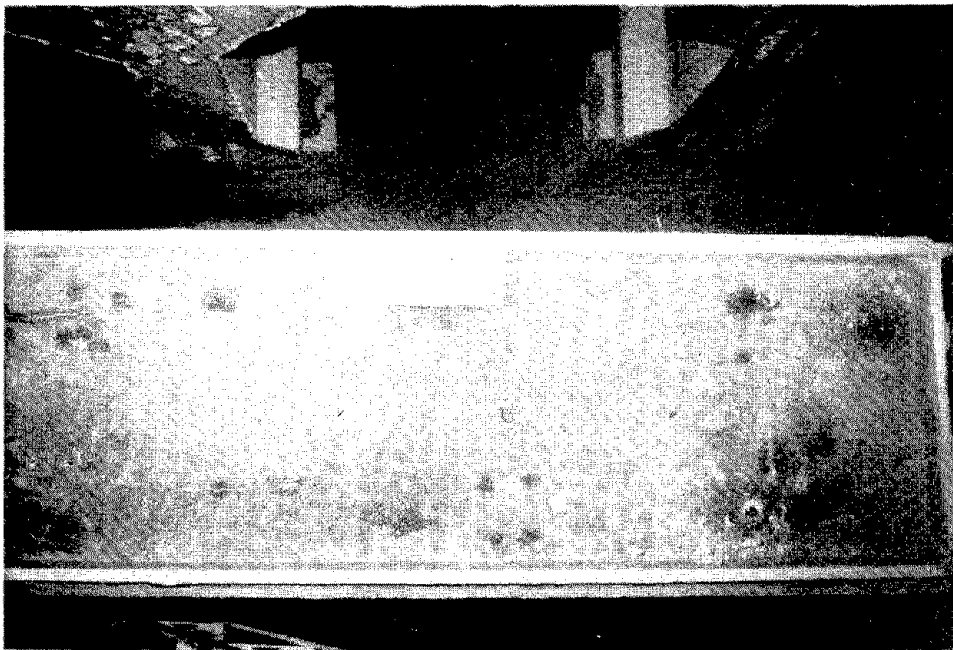


Figure 75 B. Appearance of surface of south half of beam 5 after 118 weekly salt ponding cycles.

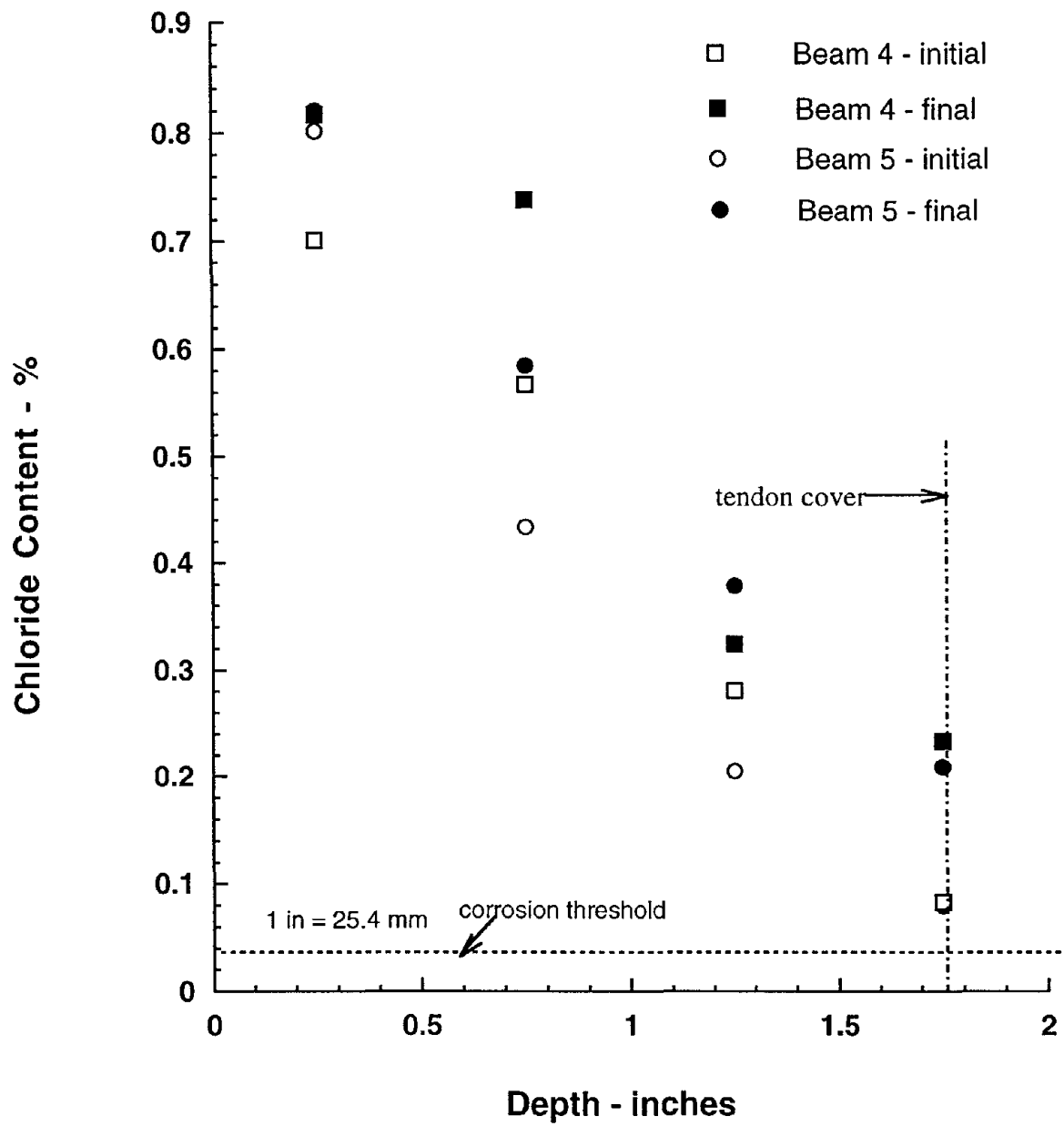


Figure 76. Chloride contents measured on beam specimens prior to and after 118 weeks of exposure.

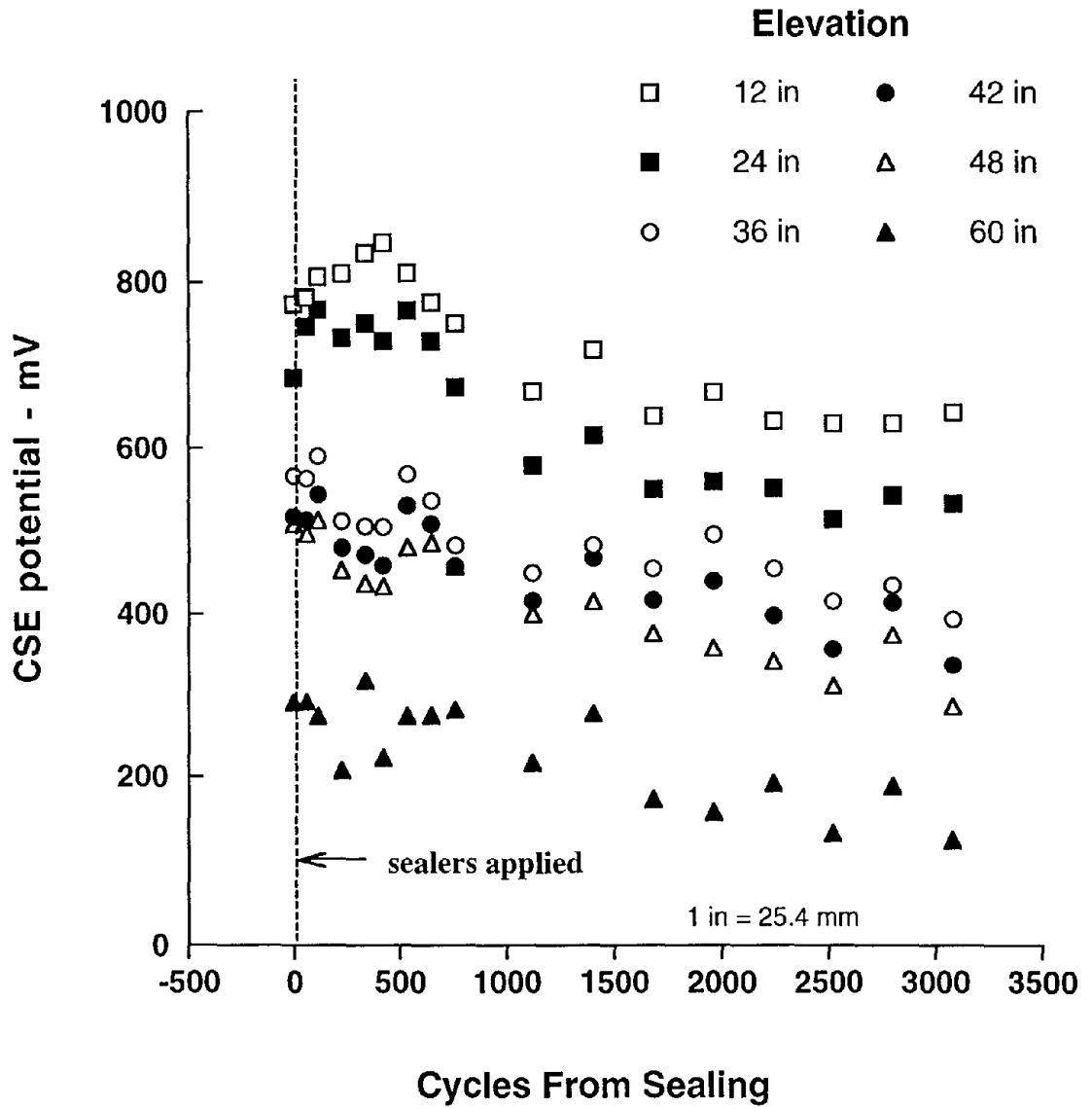


Figure 77. Half-cell potentials measured on north face of piling no. 4.

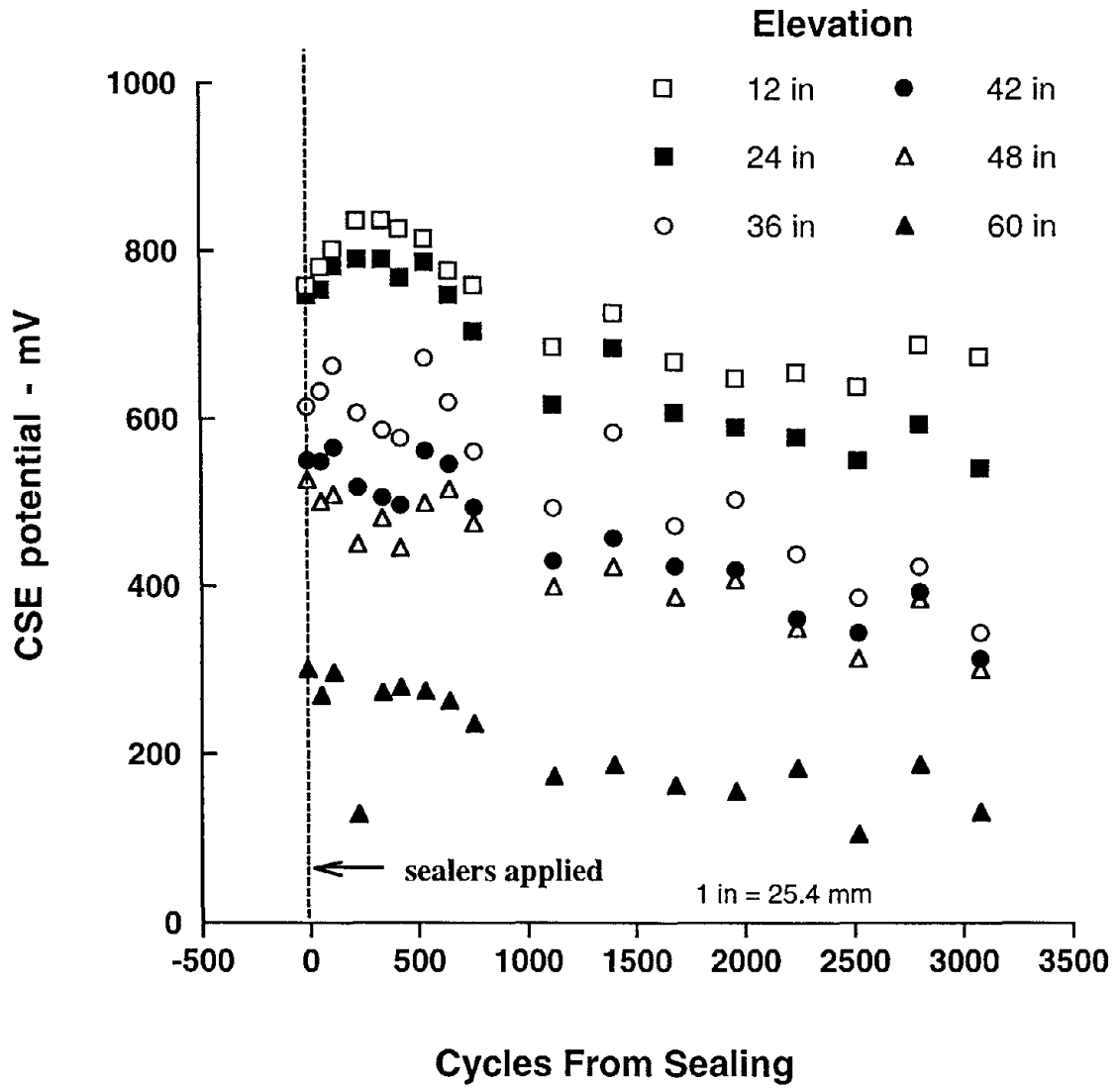


Figure 78. Half-cell potentials measured on south face of piling no. 4.

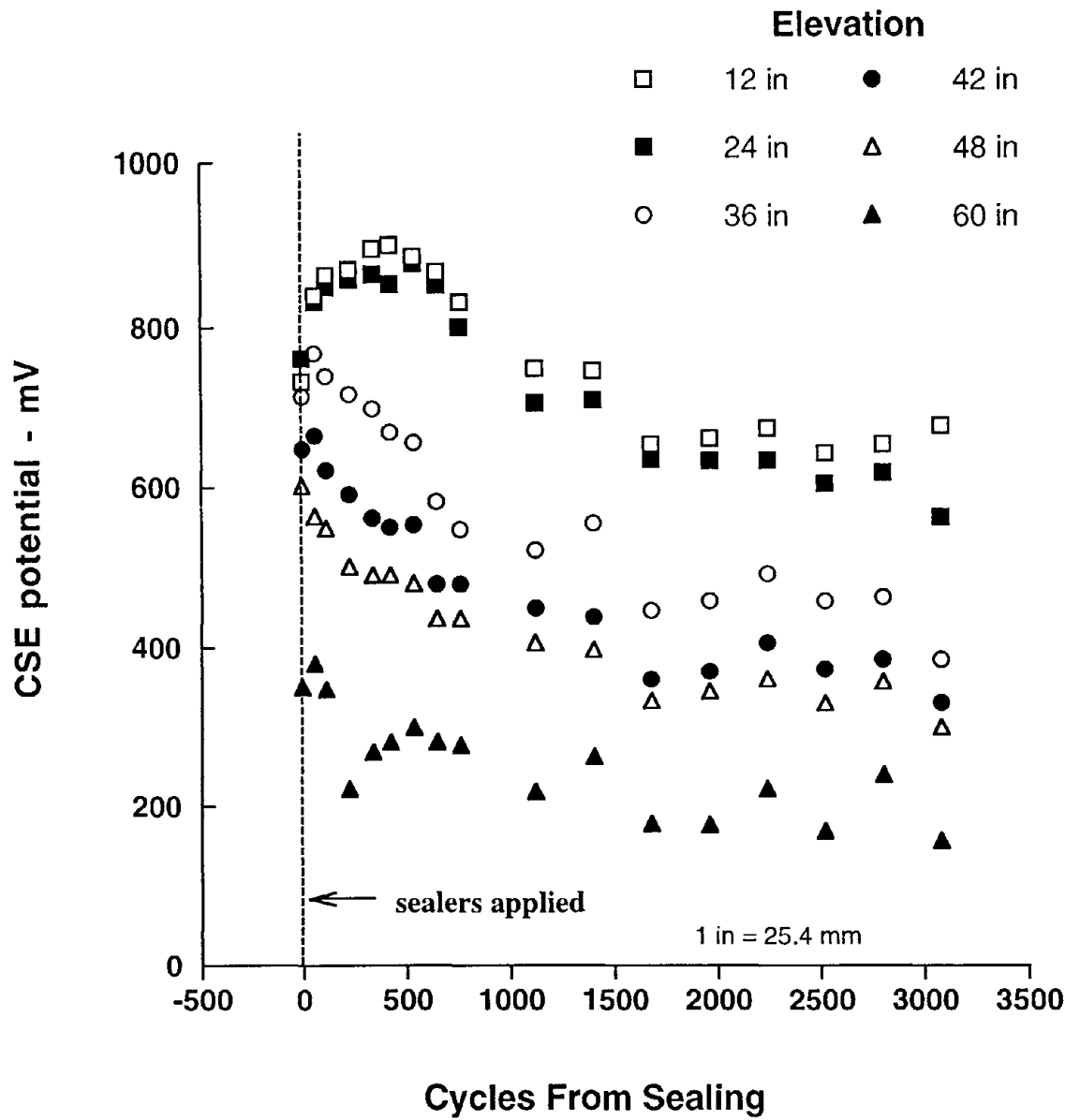


Figure 79. Half-cell potentials measured on north face of piling no. 5.

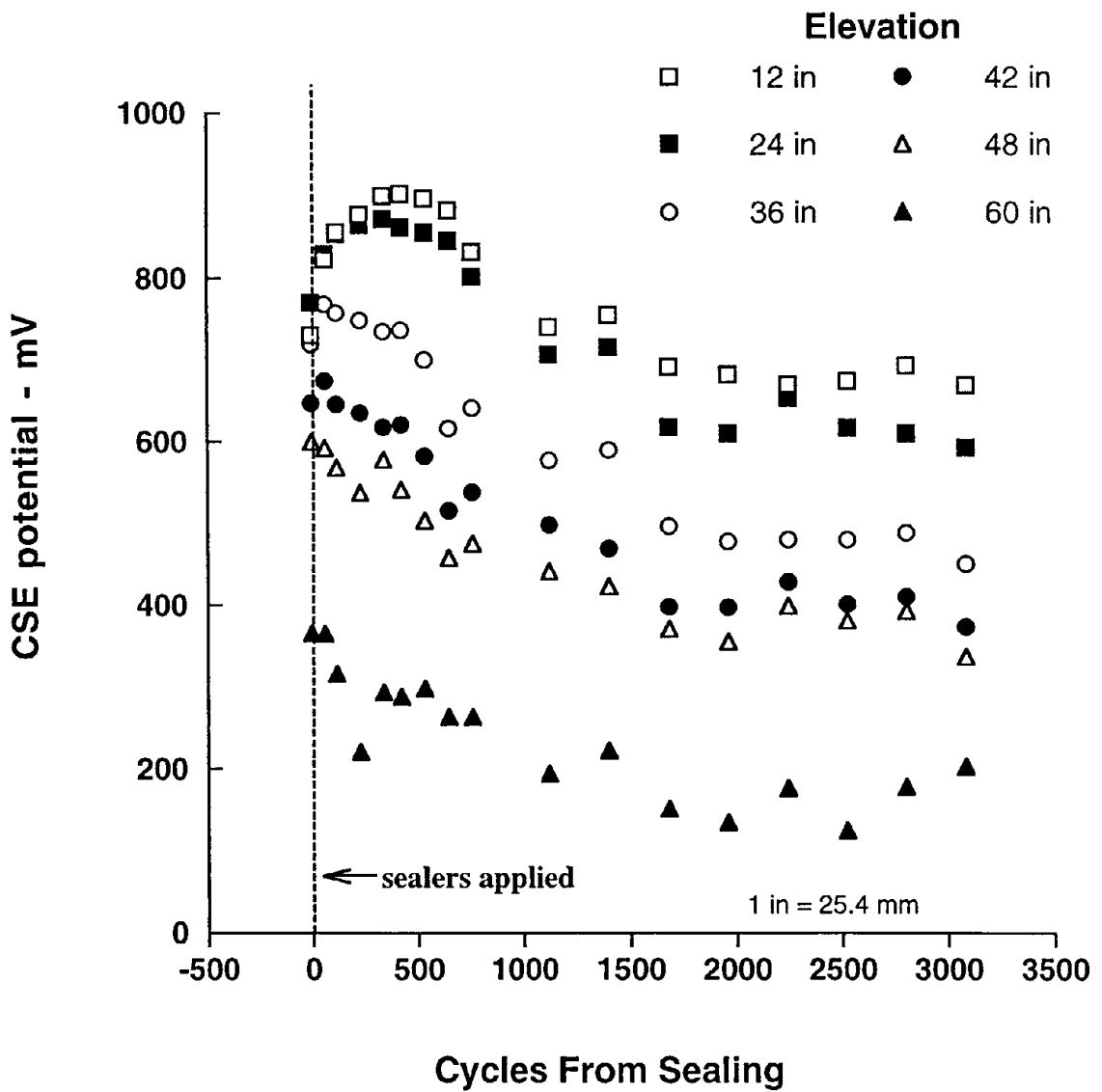


Figure 80. Half-cell potentials measured on south face of piling no. 5.

Within the tidal zone, extending from 710 to 1110 mm (28 to 44 in), potentials appeared to shift slightly more electro-positive with time; this is more apparent for pile 4 (alkyltrialkoxo silane) than for pile 5 (alkyl-alkoxy siloxane). Within the atmospheric zone at 1525 mm (60 in), potentials initially drop, then stabilize in the vicinity of - 200 mV.

Visual appearance of the surfaces of the piles after 3080 tidal cycles is shown in Figures 81 through 84. The rust staining seen on the north faces of piles 4 and 5 is associated with holes drilled for initial concrete samples and subsequently filled with epoxy. It is likely that some reinforcing steel was close to the holes, and corrosion was initiated during the course of monitoring. A crack over the middle tendon can be seen on both faces of pile 5, but the lack of rust staining indicates that this crack has not penetrated to the tendon. Again, as for the treated slabs and beams, any corrosion-induced damage appears to be associated with artifacts, and not corrosion of embedded tendons and reinforcing steel.

Drill samples were obtained from one location on the face of each pile over the middle tendon. Chloride profiles are shown in Figure 85. As compared with chloride levels just prior to coating, considerably more chloride had penetrated the piles, especially at depths less than 40 mm (1.5 in). In some cases, there appears to have been a decrease in chloride constants at depths greater than 50 mm (2 in). It would be expected that if the sealer were able to screen out a certain amount of chloride, the chloride levels initially present would readjust themselves and result in a steeper profile as chloride continued to diffuse further into the center of the pile.

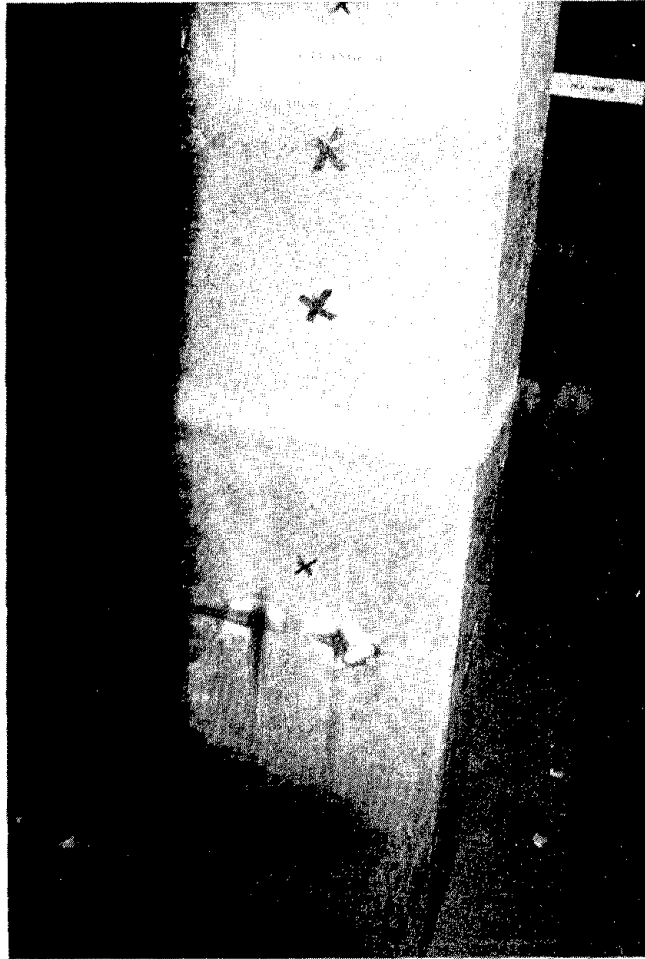


Figure 81. Appearance of surface of north face of pile 4 after 3080 tidal cycles.

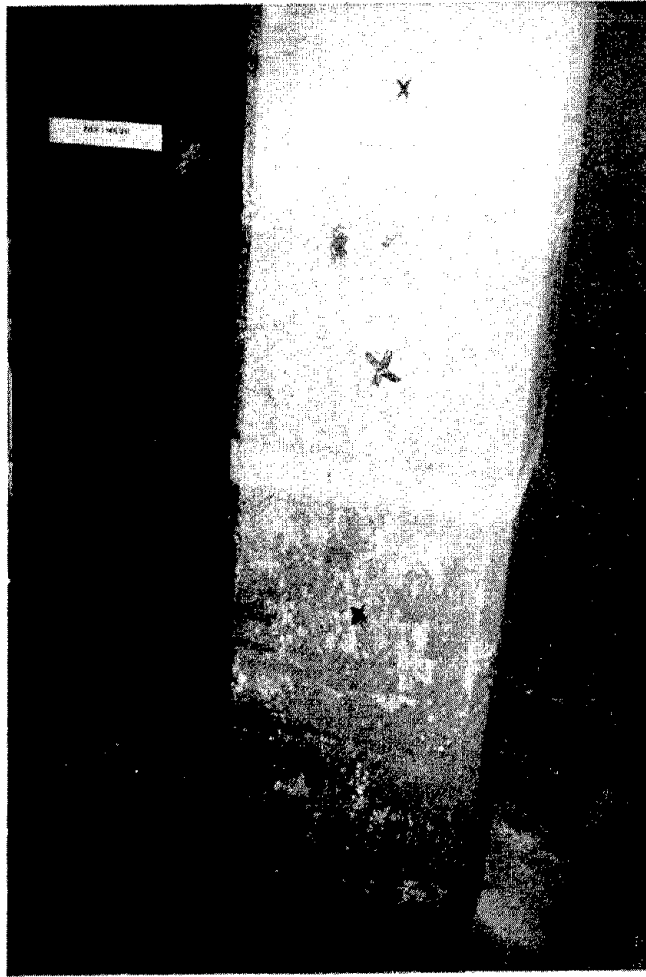


Figure 82. Appearance of surface of south face of pile 4 after 3080 tidal cycles.

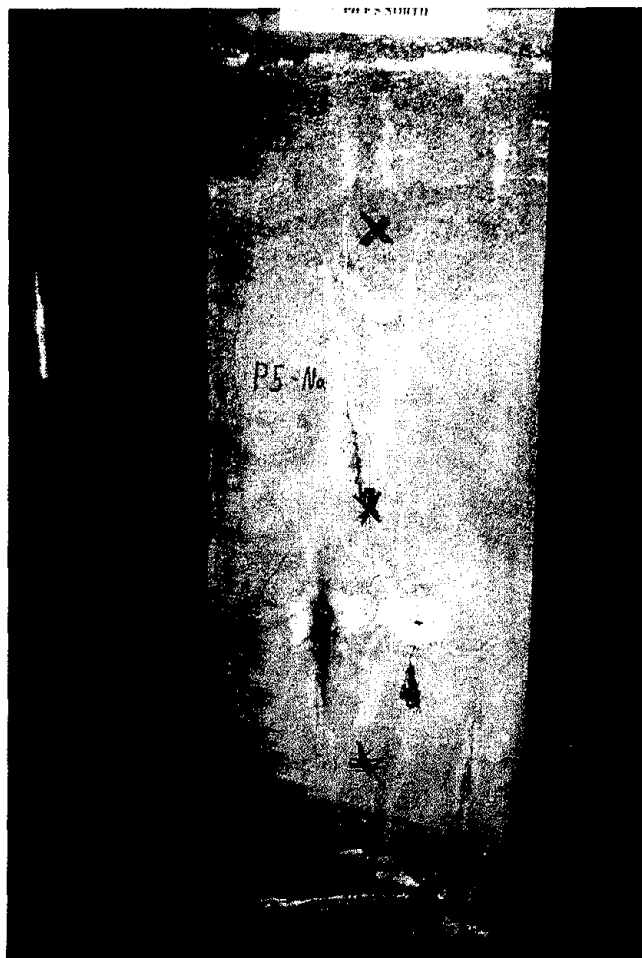


Figure 83. Appearance of surface of north face of pile 5 after 3080 tidal cycles.

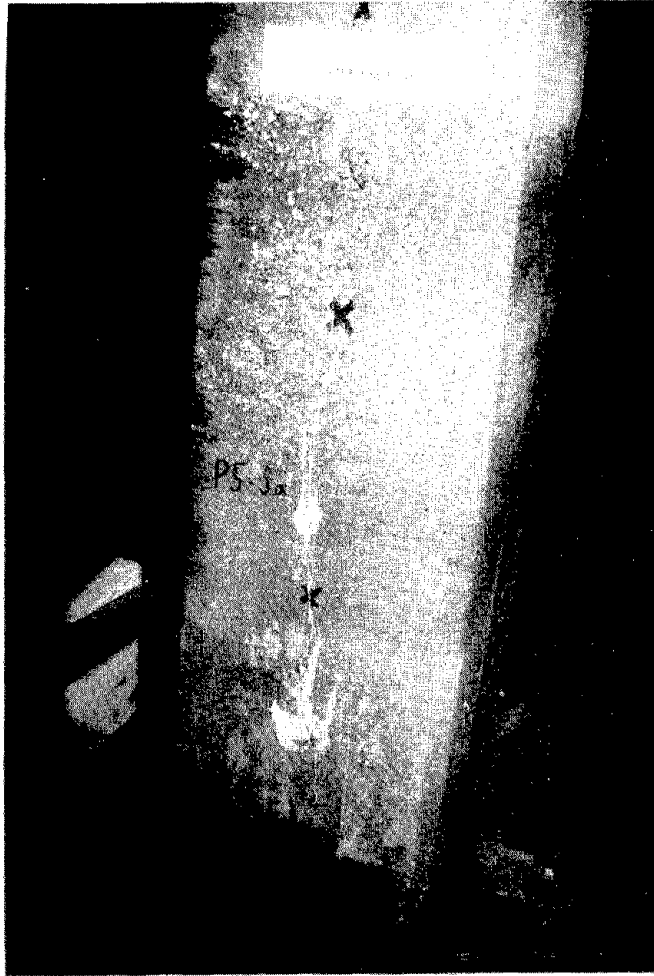


Figure 84. Appearance of surface of south face of pile 5 after 3080 tidal cycles.

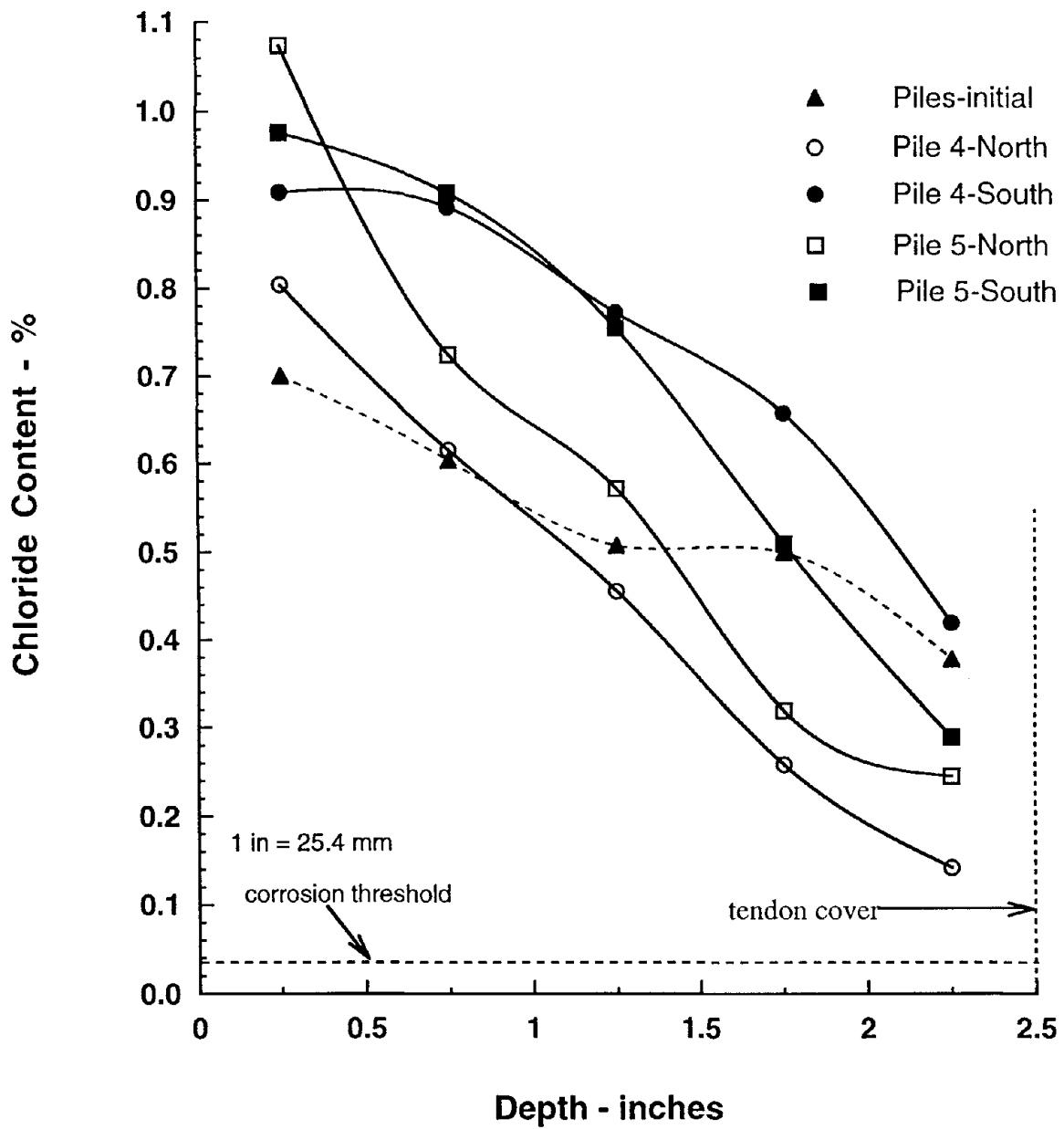


Figure 85. Chloride contents measured on pile specimens prior to and after 3080 tidal cycles.

CHAPTER 5. SUMMARY, CONCLUSIONS, AND RECOMMENDATIONS

SUMMARY

The present study encompassed a literature review of corrosion of prestressed concrete (PS/C) members; field surveys of 12 PS/C bridges of different types located in a variety of environments; and laboratory studies of the corrosion performance of patching materials, sealers, and coatings applied to model PS/C elements. Both pretensioned and post-tensioned systems were considered in all phases of the work. The ability of portland cement concrete to protect prestressing steel, both in new construction and rehabilitation, was the primary focus of this study.

In the technology review, types of corrosion and recent theories explaining stress corrosion and hydrogen embrittlement were discussed. Factors such as concrete materials, prestressing steel, and environments that may influence corrosion were categorized, and laboratory and field studies dealing with a variety of corrosion issues were summarized and presented. These issues included the development and improvement of grout materials for bonded tendons in post-tensioned concrete members, use of epoxy-coated prestressing wires, and corrosion of unbonded tendons under severe exposure. Selected case histories and field evaluation of concrete bridges subjected to corrosion were also included.

In the field surveys, 12 pre- and post-tensioned bridges built between 1954 and 1967 were examined to determine overall condition and exposure to corrosive environments. Bridges were located across the United States in marine and inland exposure areas. The 12 structures surveyed were grouped into 3 categories for the purposes of defining exposure conditions, causes of distress, and recommendations for avoiding similar distress in structures representative of these types. The categories are listed below and include:

- Pre- and post-tensioned beams exposed to marine environments.
- Pre-tensioned I- beams exposed to deicing environments.
- Pre-tensioned box beams exposed to deicing environments.
- Post-tensioned beams (and other elements) exposed to deicing environments.

In temperate marine climates away from direct sea spray, there is a slow accumulation of chloride within the concrete. In post-tensioned structures, attack on the strands themselves in this type of environment is rare. Provided that ducts and grout are intact, there is little likelihood of corrosion of post-tensioned members in this type of environment. For pretensioned members, the production of

high-quality concrete of low w/c ratio and permeability should significantly reduce the ingress of atmospheric chloride into these members.

Tropical marine environments represent a much more severe type of exposure. Year-round warm temperatures help foster both the rate of ingress of the chlorides as well as the rate of corrosion itself. For pretensioned members to be durable over the long term in such environments, it may be necessary to invest in high-quality concretes having low permeability to chloride ions. For post-tensioned members, use of non-corroding ducts (such as polyethylene ducts) would help to halt the progress of chlorides toward the strand. Care must also be taken to protect the anchorage areas, such as encapsulation of the anchorage in impermeable material.

In deicing environments, pre- and post-tensioned structures show susceptibility to corrosion at localized points on the structure. This can be at end expansion joints separating the deck slab from the approach slab, at joints separating the spans along the length of the bridge, through longitudinal spaces between box beams, and at anchorage zones in post-tensioned members. The actions of traffic and environment lead to joint failure, which allows deicer solutions to pass through the joint onto the pier caps and beam ends in I-beams, and onto the sides of box beams. Installation of gutters and downspouts to carry deicer solutions safely off the deck, and careful joint inspection and maintenance can help to reduce the potential for corrosion in these structures. For post-tensioned elements, it is very important that the grout fully encapsulate the tendons within the ducts, and that no potentially corrosive substances be added to the grouts.

Subsequent to completion of the field surveys, a laboratory program designed to evaluate corrosion performance of conventional concrete repair materials was initiated. A series of near full-scale prestressed concrete specimens were cast and subjected to accelerated corrosive conditions. Specimens included pretensioned AASHTO I-beams, pretensioned concrete repair slabs, pretensioned concrete piles, and post-tensioned beams using threadbar and multiple-strand post-tensioning systems. Exposures to salt solution were designed to simulate both deicer applications and marine exposures. Electrical current was applied to specimens during the early stages of exposure in order to accelerate the ingress of chloride ions toward the prestressing strands. In order to study conventional concrete repairs, it was necessary to remove concrete from preselected areas on each test specimen and replace the original concrete with repair materials. Materials evaluated included conventional portland cement concrete, latex-modified fiber-reinforced patching mortar, and silica fume concrete containing either organic or inorganic corrosion inhibitors. Prior to placement of repair materials, exposed prestressing and reinforcing steel in the repair areas was cleaned and coated with either a liquid epoxy-based or zinc-rich coating system. Specimens where concrete was not removed were used to study the effects of

sealers and coatings. These included application of a two-part epoxy system, and silane and siloxane-based penetrating sealers to the surfaces of the concrete specimens.

All specimens were exposed for approximately 200 weeks to a 15% solution of sodium chloride. Beams and slabs were exposed to a bi-weekly wet/dry ponding cycle. Piles were exposed to a 24-h immersion cycle simulating piles in a marine environment. The monitoring program consisted of macrocell current measurements, surface half-cell measurements, and visual observations. In some cases, such as the beams and slabs repaired with patching materials, these non-destructive measurements offered useful insight into performance, which was confirmed in subsequent dissection of specimens. In other cases, such as the piles exposed to a tidal cycle, measurements were more reflective of zones set up in the specimens by the tidal immersions, rather than performance of steel in the patches. There was only minor surface distress on the specimens during the exposure period, confined to limited amounts of cracking and efflorescence on beam and slab repair specimens. At the conclusion of monitoring, patches were removed from repair specimens, and the steel and coatings were examined.

In many of the specimens, significant deterioration of the coatings had occurred over the 4 years of severe exposure. The distress was greater for steel coated with liquid epoxy than for steel coated with the zinc-rich liquid coating. Typically, there was more disruption of coating and corrosion of base steel in areas where latex-modified mortar had been used as repair material than where conventional concrete or silica fume concretes were used. Coating distress and corrosion were greater on slabs and beams, where covers ranged from 38 to 44 mm (1.5 to 1.75 in), than on prestressed piles, where covers averaged 64 mm (2.5 in). Although only two specimens were available for comparison, an inorganic corrosion inhibitor appeared to be more effective in reducing the extent of corrosion than an organic-based product.

While significant amounts of chloride ion penetrated into all repair materials over the exposure period, the content of chloride ion that penetrated to the level of the prestressing steel did little to explain ultimate behavior. Corrosion was observed in repair areas where bulk chloride ion contents in the concrete surrounding prestressing steel were below commonly accepted threshold levels. Conversely, in the case of the repair slab specimens, the least corrosion was observed for those patches showing the highest amount of chloride at the level of the prestressing strands. At repair area edges, however, coating failure and corrosion were, in general, greater than in the bulk of the repair, and testing demonstrated that chloride ions moved laterally into the concrete, raising the concentration at patch edges.

When tendon bundles were cut and pulled apart, corrosion was observed on the interior surfaces of the individual strands. As specimens were pre-corroded (equivalent to the condition existing in actual structures prior to repairs), it is likely that chloride ions penetrated into the interstices of the strand bundles and initiated corrosion prior to repairs. Simple sandblasting of the exterior of the strands during repair preparation will not remove this residual chloride contamination, and when concrete is placed and a moist environment recreated, corrosion may re-initiate.

Penetrating sealers and coatings were of limited effectiveness when applied to specimens undergoing active corrosion. In most cases, chloride continued to penetrate into the concrete, though most probably at a reduced rate. While half-cell and macrocell measurements indicate that corrosion activity may have been initially reduced after application of sealers, long-term trends suggested that corrosion activity may slowly increase back towards initial levels over many years. Previous studies have recommended that sealers be reapplied at intervals ranging from 5 to 8 years in order to maintain effectiveness of these protective systems. This maintenance strategy will be most effective if the sealers are applied before initial exposure of the concrete to chloride ions.

CONCLUSIONS

Based on the results of the technology review, field surveys, and laboratory investigation of the performance of conventional prestressed concrete repair systems, the following conclusions may be drawn:

- Both within the United States and overseas, corrosion-based deterioration of PS/C highway structures has been relatively minor compared to corrosion of reinforced concrete bridge decks and support elements in deicing and marine environments. The generally higher quality of factory-produced precast elements and the additional protection offered by ducted and grouted post-tensioning systems may explain the low incidence of failure for these systems. However, care must be taken in design and construction of prestressed concrete structures in order to sustain this overall good performance record.
- Where corrosion problems are observed in PS/C structures, they can be attributed to long-term exposure to severely corrosive marine environments, or to localized exposure to deicing salts such as occurs below drains and joints that leak deicing solution onto the ends of prestressed AASHTO girders and box beams. The latter exposures may be minimized by proper drain and joint maintenance, installation of improved deck drainage and protection systems, and changes in bridge design to reduce the number and location of joints in a

structure. Anchorage areas can be further protected by encapsulation of strand ends and use of low-permeability materials in anchorage pockets. Tropical marine environments represent the greatest challenge and may require the use of very low-permeability high-performance concretes, corrosion inhibitors, or cathodic protection.

- Laboratory studies of the performance of conventional concrete repair materials suggest that these systems may not offer long-term protection to rehabilitated PS/C members. Even in low-permeability patches (such as those based on silica fume concrete), chloride ions may penetrate both vertically from the surface of the members and laterally from the adjoining unrepaired concrete. Field-applied coatings lose their effectiveness over time and deteriorate, exposing the underlying steel to corrosive agents. A more insidious problem exists with respect to the interior of the strand bundles, where chloride ions may become trapped during initial exposure and are not removed during conventional repair preparations. These ions then become available to foster additional corrosion over time after repair concretes have been applied.

RECOMMENDATIONS

Based on the results of the field and laboratory investigations, long-term performance of PS/C highway structures in corrosive environments can best be ensured by proper design in new construction. Corrosive agents, such as deicing salt solutions, should be directed away from PS/C elements by proper design and maintenance of drain systems and joints. Consideration should be given to encapsulation of anchorages in corrosion-resistant materials, use of corrosion inhibitors in surrounding concrete, and use of very low-permeability, high-performance concrete mixtures. Sealers may be applied to new structures to reduce, but not totally eliminate, ingress of chlorides. In structures where these precautions have not been taken, corrosion may occur and significant concrete distress in the form of cracking and spalling may develop. Conventional concrete repairs, as observed in field and laboratory investigations, are a temporary measure and do not appear to ensure long-term protection of the prestressing steel and associated conventional reinforcement. Periodic repair and reapplication of protective systems may be necessary to maintain such structures. Where such periodic repairs are difficult to carry out, complete replacement of distressed members may be a long-term cost-effective alternative.

REFERENCES

1. D. Whiting, B. Stejskal, and M. Nagi, *Condition of Prestressed Concrete Bridge Components: Technology Review and Field Surveys*, Report No. FHWA-RD-93-037, Federal Highway Administration, Washington, DC, 1993, 286 pp.
2. M. Nagi and D. Whiting, "Corrosion of Prestressed Reinforcing Steel in Concrete Bridges: State-of-the-Art," *Concrete Bridges in Aggressive Environments*, ACI SP-151, R.E. Weyers, Ed., American Concrete Institute, Farmington Hills, MI, 1994, pp. 17-42.
3. D. Whiting and B.G. Stejskal, "Field Studies of Corrosion in Prestressed Concrete Bridges," *Concrete Bridges in Aggressive Environments*, ACI SP-151, R.E. Weyers, Ed., American Concrete Institute, Farmington Hills, MI, 1994, pp. 73-94.
4. D. Whiting, *Rapid Determination of the Chloride Permeability of Concrete*, Report No. FHWA/RD-81/119, Federal Highway Administration, Washington, DC, 1981, 174 pp.
5. J. Bennett, K.F. Fong, and T.J. Schue, *Electrochemical Chloride Removal and Protection of Concrete Bridge Components: Field Trials*, Strategic Highway Research Program Report SHRP-S-669, National Research Council, Washington, DC, 1993, 149 pp.
6. D.W. Whitmore, "Electrochemical Chloride Extraction From Concrete Bridge Elements: Some Case Studies," CORROSION/96, Paper No. 299, National Association of Corrosion Engineers, Houston, Texas, 1996.
7. K.C. Clear and R.E. Hay, *Time-to-Corrosion of Reinforcing Steel in Concrete Slabs, Volume 1: Effect of Mix Design and Construction Parameters*, Report No. FHWA-RD-73-32, Federal Highway Administration, Washington, DC, 1973, 103 pp.
8. American Concrete Institute, *Corrosion of Metals in Concrete*, ACI 222R-96, ACI, Farmington Hills, MI, 1997, 30 pp.
9. D. Whiting, B. Ost, and M. Nagi, *Condition Evaluation of Concrete Bridges Relative to Reinforcement Corrosion - Volume 5: Methods for Evaluating the Effectiveness of Penetrating Sealers*, Strategic Highway Research Program Report SHRP-S-327, National Research Council, Washington, DC, 1992, 59 pp.
10. D.W. Pfeiffer and M.J. Scali, *Concrete Sealers for Protection of Bridge Structures*, NCHRP Report 244, Transportation Research Board, Washington, DC, 1981, 138 pp.

